



# BISON Capability to Account for Dopant Sensitivity in Relevant $\text{UO}_2$ Material Models

August 2022

## *Technical Report*

Aysenur Toptan<sup>1</sup>, Fernando Angulo Barba<sup>1</sup>, Yifeng Che<sup>1</sup>, Kyle A. L. Gamble<sup>1</sup>, Gyanender Singh<sup>1</sup>, Conor O. T. Galvin<sup>2</sup>, and Michael W. D. Cooper<sup>2</sup>

<sup>1</sup>Idaho National Laboratory

<sup>2</sup>Los Alamos National Laboratory



#### **DISCLAIMER**

This information was prepared as an account of work sponsored by an agency of the U.S. Government. Neither the U.S. Government nor any agency thereof, nor any of their employees, makes any warranty, expressed or implied, or assumes any legal liability or responsibility for the accuracy, completeness, or usefulness, of any information, apparatus, product, or process disclosed, or represents that its use would not infringe privately owned rights. References herein to any specific commercial product, process, or service by trade name, trade mark, manufacturer, or otherwise, does not necessarily constitute or imply its endorsement, recommendation, or favoring by the U.S. Government or any agency thereof. The views and opinions of authors expressed herein do not necessarily state or reflect those of the U.S. Government or any agency thereof.

# **BISON Capability to Account for Dopant Sensitivity in Relevant UO<sub>2</sub> Material Models**

## **Technical Report**

Aysenur Toptan<sup>1</sup>, Fernando Angulo Barba<sup>1</sup>, Yifeng Che<sup>1</sup>, Kyle A. L. Gamble<sup>1</sup>, Gyanender Singh<sup>1</sup>, Conor O. T. Galvin<sup>2</sup>, and Michael W. D. Cooper<sup>2</sup>

<sup>1</sup>Idaho National Laboratory

<sup>2</sup>Los Alamos National Laboratory

**August 2022**

**Idaho National Laboratory  
Computational Mechanics and Materials Department  
Idaho Falls, Idaho 83415**

**<http://www.inl.gov>**

**Prepared for the  
U.S. Department of Energy  
Office of Nuclear Energy  
Under U.S. Department of Energy-Idaho Operations Office  
Contract DE-AC07-05ID14517**

*Page intentionally left blank*

## ABSTRACT

The U.S. Department of Energy's Nuclear Energy Advanced Modeling and Simulation program aims to develop predictive capabilities using computational methods for the analysis and design of advanced reactor and fuel cycle systems. This program has been supporting the development of BISON, a high-fidelity and high-resolution fuel performance tool at the engineering scale.

Incorporation of more physics-based models in BISON for the accident tolerant fuel applications motivated this study. This document details integration of new modeling capabilities in BISON, including: a tensile strength model for uranium dioxide ( $\text{UO}_2$ ) fuel to incorporate the microstructural effects (e.g., grain size, fabrication pore size, and porosity), and atomistic-informed creep model for  $\text{UO}_2$  fuel that is developed by Los Alamos National Laboratory. Sensitivity analyses are conducted on these models separately as well as a two-dimensional full rod application under normal operating conditions. Lastly, these new modeling capabilities in BISON are exercised in Halden IFA-677.1 and IFA-716.1 assessment cases.

#### ACKNOWLEDGMENT

This report was authored by a contractor of the U.S. Government under Contract DE-AC07-05ID14517. Accordingly, the U.S. Government retains a non-exclusive, royalty-free license to publish or reproduce the published form of this contribution, or allow others to do so, for U.S. Government purposes.

This research made use of the resources of the High Performance Computing Center at Idaho National Laboratory, which is supported by the Office of Nuclear Energy of the U.S. Department of Energy and the Nuclear Science User Facilities under Contract No. DE-AC07-05ID14517.

#### DECLARATION OF COMPETING INTEREST

The authors declare that they have no known competing financial interests or personal relationships that could appear to have influenced the work reported in this technical report.

#### ORCID

Fernando Angulo Barba		0000-0001-7549-2351
Yifeng Che		0000-0003-1841-9937
Kyle A. L. Gamble		0000-0002-8487-8077
Gyanender Singh		0000-0003-1828-4438
Aysenur Toptan		0000-0003-4250-6336

## CONTENTS

<b>ABSTRACT</b>	iv
<b>LIST OF FIGURES</b>	vii
<b>LIST OF TABLES</b>	vii
<b>ACRONYMS</b>	1
<b>I INTRODUCTION</b>	2
<b>II NEW MODELING CAPABILITIES</b>	2
II-A Tensile Strength Model . . . . .	2
II-B LLS-informed Creep Model . . . . .	3
<b>III DEMONSTRATION: 2D-RZ RODLET APPLICATION</b>	4
III-A Impact of Tensile Strength on the Predictions . . . . .	5
III-B Impact of Creep Modeling on the Predictions . . . . .	9
<b>IV SENSITIVITY ANALYSIS</b>	10
IV-A Sensitivity Analysis Techniques . . . . .	11
IV-B Applications . . . . .	15
IV-C Results & Discussion . . . . .	15
<b>V HALDEN IFA-677.1 AND IFA-716.1</b>	34
V-A Halden IFA-677.1 Rods 1 and 5 . . . . .	34
V-B Halden IFA-716.1 Rods 1 and 6 . . . . .	38
<b>VI CONCLUSION</b>	43
<b>REFERENCES</b>	48
<b>Appendix A: MATPRO CREEP MODEL</b>	51

## LIST OF FIGURES

1	Effect of grain size, pore size, and porosity on the $\text{UO}_2$ fracture strength . . . . .	3
2	Predicted MATPRO and atomistic-informed creep rates as a function of inverse temperature and fission rate density . . . . .	4
3	Predicted atomistic-informed creep rates as a function of inverse temperature and fission rate density under various microstructural conditions . . . . .	5
4	Contours of crack damage indices from the BISON simulations using constant tensile strength values for the undoped and doped fuel rodlets . . . . .	6
5	Tensile strength evolution as a function of rod average burnup for the undoped $\text{UO}_2$ fuel . .	7
6	Contours of crack damage indices and residuals between the BISON simulations using the tensile strength model and constant tensile strengths for the undoped fuel rodlets . . . . .	7
7	Tensile strength evolution as a function of rod average burnup for the doped $\text{UO}_2$ fuel . . .	8
8	Contours of crack damage indices and residuals between the BISON simulations using the tensile strength model and constant tensile strengths for the doped fuel rodlets . . . . .	8
9	Contours of crack damage indices and residuals between the BISON simulations using LLS-informed and MATPRO creep models for the undoped fuel rodlets . . . . .	9
10	Contours of crack damage indices and residuals between the BISON simulations using LLS-informed and MATPRO creep models for the doped fuel rodlets . . . . .	10
11	Sobol' indices versus the sample size for the tensile-strength model . . . . .	16
12	Pearson correlation coefficients between the tensile strength and its model parameters . . . .	17
13	Pearson correlation coefficients between the LLS-informed creep rate and its model parameters	18
14	Morris measures for the LLS-informed creep model . . . . .	18
15	Sobol' indices versus the sample size for the LLS-informed creep model . . . . .	19
16	Sobol' indices for different temperatures or fission rates using the LLS-informed model . . .	19
17	The combination of perturbed input parameters and the corresponding simulation results using the perturbed input parameters for the undoped fuel . . . . .	21
18	The combination of perturbed input parameters and the corresponding simulation results using the perturbed input parameters for the doped fuel . . . . .	22
19	Pearson correlation coefficients between QoIs and the selected input parameters at various rod average burnups for the undoped fuel rodlets. . . . .	23
20	Pearson correlation coefficients between QoIs and the selected input parameters at various rod average burnups for the doped fuel rodlets. . . . .	24
21	Average LHR history used as input for the simulation of IFA-677.1 Rods 1 and 5 . . . . .	36
22	Comparison of predicted and measured data for Halden IFA-677.1 Rod 1 . . . . .	38
23	Comparison of predicted and measured data for Halden IFA-677.1 Rod 5 . . . . .	39
24	Integral response residuals between the BISON predictions using LLS-informed and MATPRO creep models for the Halden IFA-677.1 Rods 1 and 5 . . . . .	40
25	Average LHR history used as input for the simulation of IFA-716.1 Rods 1 and 6 . . . . .	42
26	Comparison of predicted and measured data for Halden IFA-716.1 Rod 1 . . . . .	43
27	Comparison of predicted and measured data for Halden IFA-716.1 Rod 6 . . . . .	44
28	Integral response residuals between the BISON predictions using LLS-informed and MATPRO creep models for the Halden IFA-716.1 Rods 1 and 6 . . . . .	45



## LIST OF TABLES

I	Fitting parameters used in the LLS-informed creep model. . . . .	3
II	Rodlet specifications under normal operation. . . . .	5
III	Properties of the uncertainty importance measure from the delta moment-independent analysis	14
IV	Parameter ranges for the tensile-strength model . . . . .	15
V	Parameter ranges for the LLS-informed creep model . . . . .	15
VI	Parameter uncertainties for the combined 2D RZ application . . . . .	16
VII	Comparison of first-order and total sensitivity indices between STM, Dakota and SALib . .	17
VIII	Delta moment-independent analysis for the crack damage in axial direction . . . . .	26
IX	Delta moment-independent analysis for the crack damage in hoop direction . . . . .	27
X	Delta moment-independent analysis for the crack damage in radial direction . . . . .	28
XI	Delta moment-independent analysis for the fission gas release . . . . .	29
XII	Delta moment-independent analysis for the fuel elongation . . . . .	30
XIII	Delta moment-independent analysis for the maximum fuel centerline temperature . . . . .	31
XIV	Delta moment-independent analysis for the maximum hoop stress . . . . .	32
XV	Delta moment-independent analysis for the plenum pressure . . . . .	33
XVI	Fabrication characteristics of IFA-677.1 Rods 1 and 5 . . . . .	35
XVII	Fabrication characteristics of IFA-716.1 Rods 1 and 6 . . . . .	41
A.1	Parameters used in the UO <sub>2</sub> thermal creep model . . . . .	51

## ACRONYMS

<b>AFC</b>	Advanced Fuels Campaign
<b>ATF</b>	accident tolerant fuel
<b>BOL</b>	beginning of life
<b>Cr<sub>2</sub>O<sub>3</sub></b>	chromia
<b>DOE</b>	U.S. Department of Energy
<b>EOL</b>	end of life
<b>FGR</b>	fission gas release
<b>HBWR</b>	Halden Boiling Water Reactor
<b>IFA</b>	Integrated Fuel Assembly
<b>INL</b>	Idaho National Laboratory
<b>INEL</b>	Idaho National Engineering Laboratory
<b>LANL</b>	Los Alamos National Laboratory
<b>LHR</b>	linear heat rate
<b>LHS</b>	Latin hypercube sampling
<b>LLS</b>	lower-length scale
<b>LWR</b>	light-water reactor
<b>MC</b>	Monte Carlo
<b>MOOSE</b>	Multiphysics Object-Oriented Simulation Environment
<b>NEAMS</b>	Nuclear Energy Advanced Modeling and Simulation
<b>OAT</b>	one-at-a-time
<b>OECD</b>	Organisation for Economic Co-operation and Development
<b>O/M</b>	oxygen-to-metal ratio
<b>PCMI</b>	pellet-clad mechanical interaction
<b>QoI</b>	quantity of interest
<b>SA</b>	sensitivity analysis
<b>SALib</b>	Sensitivity Analysis Library
<b>SNL</b>	Sandia National Laboratories
<b>STM</b>	Stochastic Tools Module
<b>TC</b>	thermocouple
<b>UO<sub>2</sub></b>	uranium dioxide
<b>VBD</b>	variance-based decomposition
<b>XFEM</b>	extended finite element method
<b>2D</b>	two-dimensional

## I. INTRODUCTION

This report presents two new modeling capabilities incorporated into BISON: (1) a tensile strength model for  $\text{UO}_2$  fuel, developed by Oguma (1982), as a function of average grain size, fabrication pore size, and porosity; and (2) a physics-based, lower-length scale (LLS)-informed creep model, developed at Los Alamos National Laboratory (LANL) by Galvin et al. (2022). Both capabilities are described in Section II. The impact of the inclusion of the aforementioned models on BISON (Williamson et al., 2021) predictions is investigated in Section III with a two-dimensional (2D)-RZ application under normal operating conditions for both undoped and doped fuel rodlets. We conduct sensitivity analysis (SA) exercises on these models as well as the 2D full rod application under normal operating conditions in Section IV. Later, new modeling capabilities are exercised in Halden IFA-677.1 and IFA-716.1 assessment cases in Section V. Lastly, the report is concluded with a discussion and outline of future work in Section VI.

## II. NEW MODELING CAPABILITIES

### A. Tensile Strength Model

Ceramic fuel fractures during normal operation, due to the large thermal gradients caused by the fuel's low thermal conductivity. Adding ceramic dopants (e.g., alumina and chromia) is expected to minimally affect the thermal conductivity and specific heat properties of the material. Large temperature gradients are still expected. The difference in fracture behavior stems from differences in the fracture toughness of the fuel, due to the larger grain size in doped fuel. Oguma (1982) proposed Equation 1 to model the tensile strength<sup>a</sup> of  $\text{UO}_2$ .

$$\sigma_{\text{TS}} = \frac{626e^{-0.057p}}{\sqrt{0.5G + P}} \quad (1)$$

where  $p$  is the porosity of the fuel (%),  $G$  is the average grain size ( $\mu\text{m}$ ), and  $P$  is the fabrication pore size ( $\mu\text{m}$ ) that corresponds to the largest pore.

Figure 1 shows the effects of grain size, pore size, and porosity on the  $\text{UO}_2$  fracture strength. The fracture strength decreases as the grain size, pore size, and porosity increase. The Advanced Fuels Campaign (AFC) measurements agree reasonably with the model predictions from Equation 1 at a fuel porosity of  $\sim 10\%$  and for small values of the grain radii and pore sizes.

BISON offers three primary ways of incorporating the effects of fracture into an analysis: isotropic, discrete, and smeared. The applicability of each approach depends on the level of complexity and accuracy needed for the given analysis. (1) In the *isotropic approach*, the fuel's elastic properties (Young's modulus and Poisson's ratio) continue to degrade with the formation of each new crack. This degradation is applied uniformly throughout the fuel (Barani et al., 2019). The degradation is not a function of grain size and would thus yield the same results for both doped and undoped  $\text{UO}_2$ . (2) The *discrete approach* to modeling fracture involves coupling to the extended finite element method (XFEM) and observing the actual fracture-related discontinuities in the mesh (Spencer et al., 2014; Gamble et al., 2021). At present,

<sup>a</sup>According to Oguma (1982), Equation 1 predicts the  $\text{UO}_2$  pellet strength within the approximate ranges of a porosity of 10%, the largest pore size of 100  $\mu\text{m}$ , and the average grain size of 80  $\mu\text{m}$ , to within errors of  $\pm 10\%$ . Beyond the suggested applicability ranges, the model predictions from Equation 1 are limited to aforementioned upper limits for grain size, pore size, and porosity in the code. Note that the fabrication pore size is assumed to be 4  $\mu\text{m}$  by default in the code.

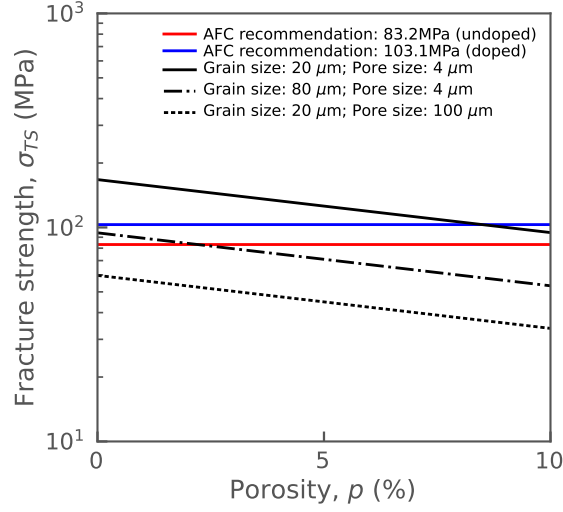


Fig. 1. Effect of grain size, pore size, and porosity on the UO<sub>2</sub> fracture strength.

the discrete approach is limited to modeling radial crack formation, and is typically done on a cross-sectional slice—or multiple cross-sectional slices stacked along the axial direction of the fuel rod. The discrete approach is not within the scope of the present study. (3) In a *smear cracking approach* to fracture, the local material point becomes degraded over time once a critical stress is reached. In previous analyses, this value was the tensile strength of the fuel. The rate at which the properties degrade depends on which type of softening model is selected: abrupt, exponential, or power law.

#### B. LLS-informed Creep Model

The LLS-informed creep model, developed at LANL, is given by (Galvin et al., 2022) as:

$$\dot{\epsilon}_{\text{Coble},x} = \frac{42\pi\delta}{k_B T G^3} \sigma_v \left[ A_1 \exp\left(-\frac{B_1}{k'_B T}\right) + A_2 \exp\left(-\frac{B_2}{k'_B T}\right) \dot{F}^{0.3} + A_3 \dot{F}^{0.6} \right] \quad (2)$$

where  $A_1$ ,  $A_2$ ,  $A_3$ ,  $B_1$ , and  $B_2$  are fitting parameters (see Table I for the numerical values),  $\dot{F}$  is the fission rate density (fissions/m<sup>3</sup>s),  $\sigma_v$  is the von-Mises stress (Pa),  $G$  is the grain size (m),  $\delta$  is the grain boundary thickness (m),  $T$  is the temperature (K), and  $k_B$  and  $k'_B$  are the Boltzmann constants in J/K ( $1.380649 \times 10^{-23}$ ) and eV/K ( $8.617333262 \times 10^{-5}$ ), respectively.

TABLE I. Fitting parameters used in the LLS-informed creep model (Equation 2) from Galvin et al. (2022).

$A_1$	$1.20 \times 10^{-35}$	$B_1$	2.46
$A_2$	$4 \times 10^{-45}$	$B_2$	1.25
$A_3$	$2.5 \times 10^{-56}$		

Figure 2 shows the model-predicted atomistic-informed creep rates (from Equation 2) as a function of inverse temperature and fission rate density, for a grain size of 27 μm, grain boundary thickness of 1 nm,

and stress of 30 MPa. The creep rate increases with increasing fission rate density, proportionally increases with the grain boundary thickness, and inversely proportional to the grain size (see Figure 3). Note that the default value of the grain boundary thickness is assumed to be 1 nm in the code. Additionally, the MATPRO model behavior, for both low-temperature irradiation creep and MATPRO–Halden approaches, is included in Figure 2 at various fission rates. Details of the MATPRO model can be found in Appendix A. The MATPRO model does not take into account the grain boundary thickness, but takes into account fuel theoretical density and oxygen-to-metal ratio (O/M), which is different from Equation 2.

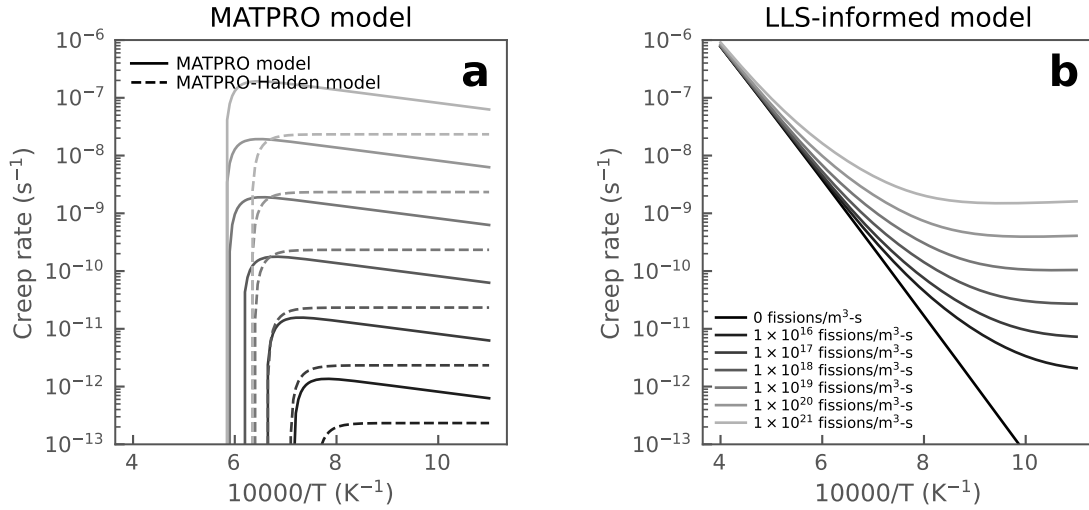


Fig. 2. Predicted (a) MATPRO and (b) atomistic-informed creep rates as a function of inverse temperature and fission rate density, for a grain size of 27  $\mu\text{m}$ , grain boundary thickness of 1 nm, and stress of 30 MPa.

### III. DEMONSTRATION: 2D-RZ RODLET APPLICATION

We chose the same 2D-RZ rodlet application under normal operating conditions from the previous year (Gamble and Cooper, 2021). Table II tabulates the rodlet specifications under normal operating conditions. We investigate the newly implemented tensile strength model and its effects on the code predictions for both undoped and doped fuel rodlets in Section III-A. Similarly, the effects of newly implemented creep model on the code predictions are presented in Section III-B for both undoped and doped fuel rodlets. The crack damage index is chosen as the quantity of interest (QoI) since both tensile strength and creep change the stress state and affect the cracking depending on the stress level.

In the current analyses, we employed a smeared cracking approach with a selection of the exponential softening law, in which the cracking is recorded in a vector material property that houses the damage in the axial, radial, and hoop directions. An exponential softening law degrades the elastic strength of the material upon reaching the tensile strength, following an exponential decay rather than an abrupt reduction in strength. The crack damage in the axial, radial, and hoop directions at the end of the simulation are presented for the undoped and doped fuel rodlets. The crack damage varies between zero and one (i.e., [0,1]), and is a measure of the reduced strength of the material point in the direction specified. A value

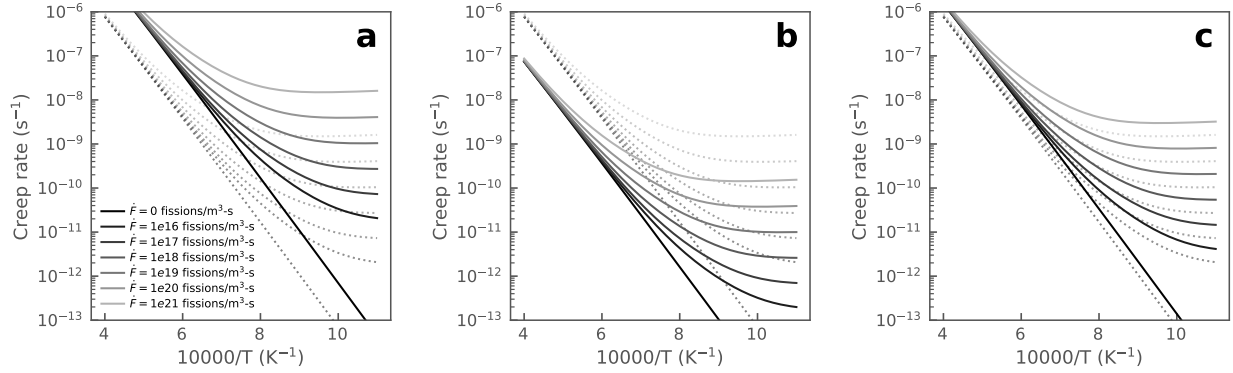


Fig. 3. Predicted atomistic-informed creep rates as a function of inverse temperature and fission rate density, for (a)  $G = 27 \mu\text{m}$ ,  $\delta = 10 \text{ nm}$ , and  $\sigma_v = 30 \text{ MPa}$ , where the grain boundary thickness  $\delta$  is changed from 1 to 10 nm, (b)  $G = 59 \mu\text{m}$ ,  $\delta = 1 \text{ nm}$ , and  $\sigma_v = 30 \text{ MPa}$ , where the grain size  $G$  is changed from 27 to 59  $\mu\text{m}$ , and (c)  $G = 27 \mu\text{m}$ ,  $\delta = 1 \text{ nm}$ , and  $\sigma_v = 60 \text{ MPa}$ , where the stress  $\sigma_v$  is changed from 30 to 60 MPa. Note that the dashed line corresponds to the results in Figure 2(b) for  $G = 27 \mu\text{m}$ ,  $\delta = 1 \text{ nm}$ , and  $\sigma_v = 30 \text{ MPa}$ , to emphasize the variation in model predictions with varying state parameters. The LLS-informed creep rate (from Equation 2) increases with increasing grain boundary thickness and stress (a,c), while it decreases with increasing grain size (b).

TABLE II. Rodlet specifications under normal operation.

	Value		Value
Number of pellets	10	Initial fill gas	helium
Fuel enrichment	5%	Plenum height	26 mm
Pellet length	9.83 mm	Initial undoped fuel grain diameter	20 $\mu\text{m}$
Pellet outer diameter	8.2 mm	Initial doped fuel grain diameter	58 $\mu\text{m}$
Radial gap width	100 $\mu\text{m}$	Coolant inlet mass flux	3800 kg/m-s
Clad thickness	0.56 mm	Coolant inlet temperature	580 K
Rodlet diameter	9.52 mm	Coolant pressure	15.5 MPa
Initial fill pressure	2 MPa	Tensile strength <sup>‡</sup>	undoped <sup>‡</sup> : 83.2 MPa doped <sup>‡</sup> : 103.1 MPa

<sup>‡</sup> Compared the results to investigate the impact of new tensile strength model.

<sup>†</sup> Provided by Josh White of LANL as part of AFC.

of zero indicates an intact material point, a value of one indicates complete damage, and an intermediate value indicates partial damage.

#### A. Impact of Tensile Strength on the Predictions

We use the same 2D-RZ rodlet application from Table II under normal operating conditions. Based on the AFC-recommendation,  $\sigma_{\text{TS}} = 83.2 \text{ MPa}$  is used for the undoped fuel, and  $\sigma_{\text{TS}} = 103.1 \text{ MPa}$  is used for the doped fuel. Code predictions of the crack damage indices at various rod average burnups are provided in Figure 4. More cracking is observed for the undoped fuel than the doped fuel, particularly towards the

center of the fuel rod as the fuel burns out, due to the use of lower tensile strength in the simulations. Impact of the new tensile strength model on the code predictions are provided in the following sections; Section III-A1 for the undoped fuel and Section III-A2 for the doped fuel.

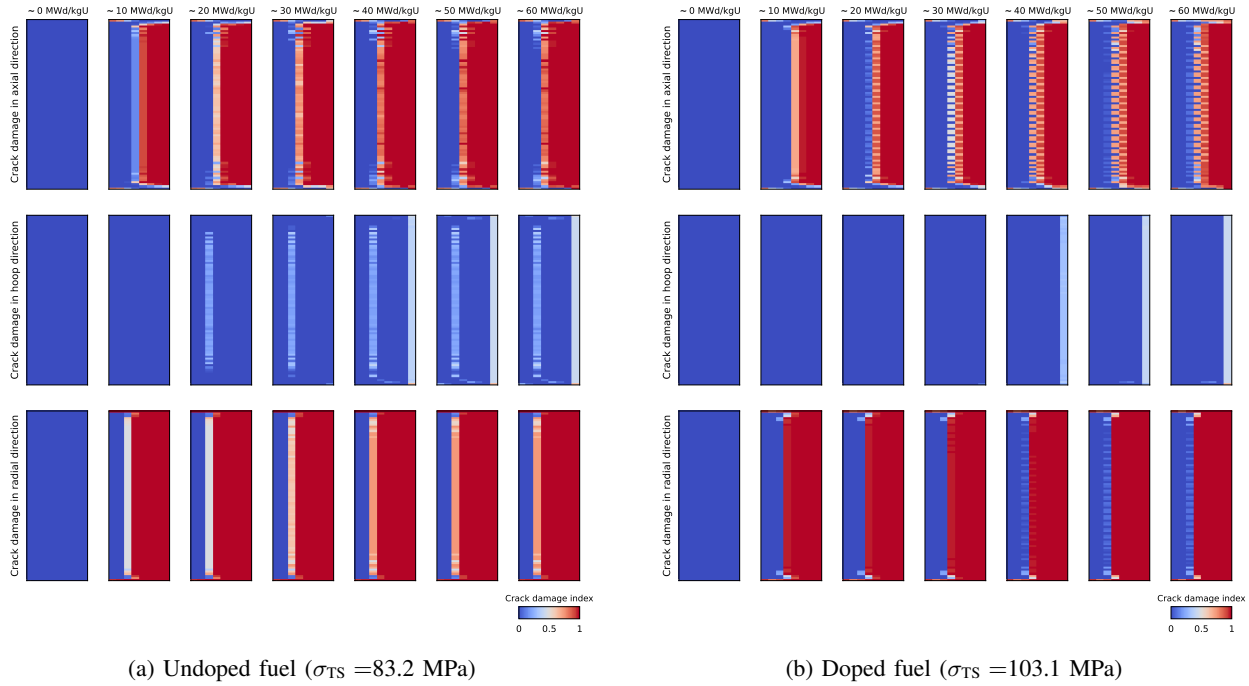


Fig. 4. Contours of the crack damage in axial, hoop, and radial directions for the undoped and doped  $\text{UO}_2$  fuels at various rod average burnups under the normal operation conditions, using a constant tensile strength of (a) 83.2 MPa for the undoped fuel and (b) 103.1 MPa for the doped fuel based on the AFC recommendation (Gamble and Cooper, 2021).

### 1) Undoped $\text{UO}_2$ Fuel

The tensile strength contours at various rod average burnups are shown in Figure 5 for the undoped fuel rodlets. The tensile strength decreases as the fuel burns out, mainly due to microstructural evolution. The resulting tensile strength from the code predictions varies between 90 and 120 MPa using Equation 1 from the BISON simulations, which is slightly larger at the beginning of life (BOL) than the AFC-measured value and approaches this value towards the end of life (EOL). The crack damage predictions using the tensile strength model (Equation 1) are shown for the undoped  $\text{UO}_2$  fuel in Figure 6a and corresponding residuals between the numerical solutions using Equation 1 and  $\sigma_{\text{TS}} = 83.2$  MPa are plotted in Figure 6b. The results indicate that significant fracture occurs in the radial and axial directions during a hold at power without any power down. Circumferential cracking tends to form during power downs after a duration at power. Slightly less damage is observed in Figure 6a for the undoped  $\text{UO}_2$  due to its higher tensile strength as shown in Equation 1 for given microstructural conditions.

### 2) Doped $\text{UO}_2$ Fuel

The tensile strength contours at various rod average burnups are shown in Figure 7 for the doped fuel rodlets. The tensile strength decreases as the fuel burns out, mainly due to the evolution of microstructural

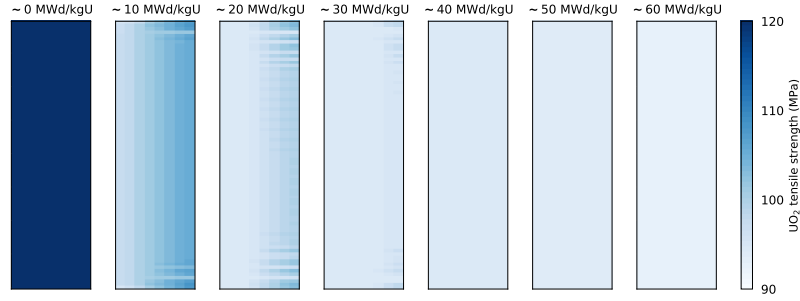


Fig. 5. Tensile strength evolution as a function of rod average burnup for the undoped  $\text{UO}_2$  fuel.

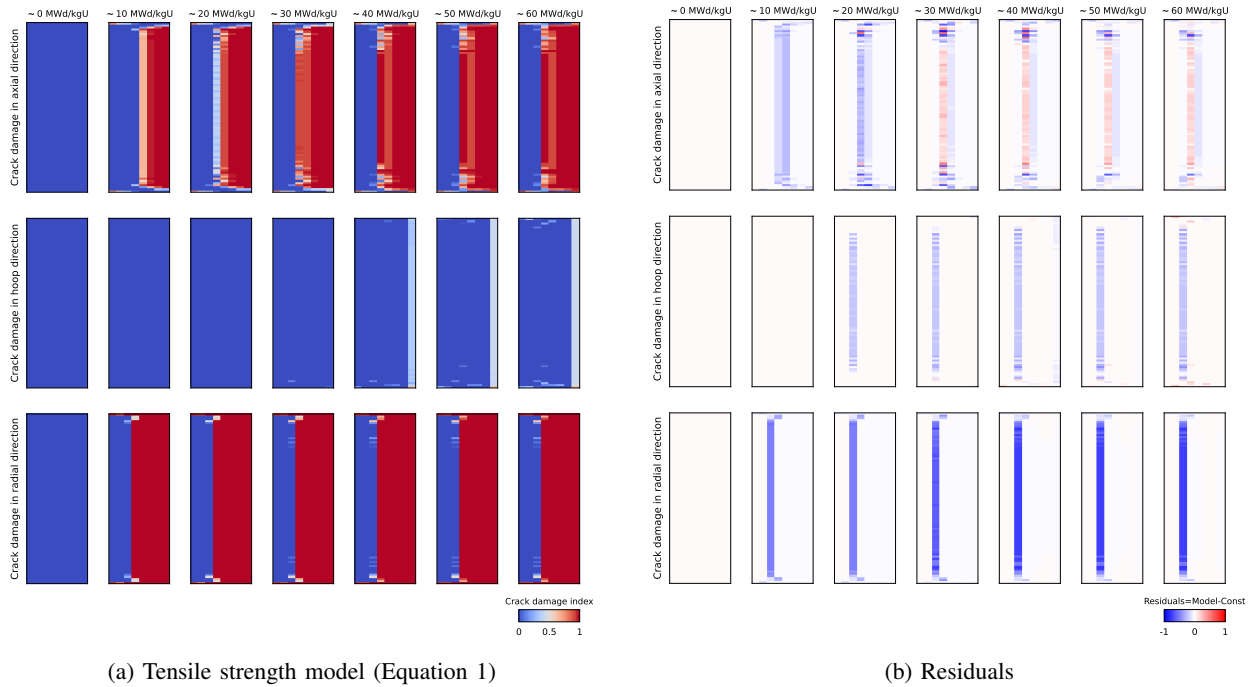


Fig. 6. Contours of (a) the crack damage and (b) crack damage residuals in axial, hoop, and radial directions for the undoped  $\text{UO}_2$  fuel at various rod average burnups under the normal operation conditions. The residuals are computed between the predictions using Equation 1 (see Figure 6a) and  $\sigma_{\text{TS}} = 83.2$  MPa (see Figure 4a). The default MATPRO creep model is employed in this exercise.

effects. The code-predicted tensile strength varies between 60 and 80 MPa using Equation 1 from the BISON simulations, which is significantly lower than the AFC-measured value of 103.1 MPa at the BOL. As the fuel burns out, the  $\text{UO}_2$  tensile strength degrades even more and approaches 60 MPa at the EOL for the doped fuel.

The tensile strength in doped fuel is lower than that in undoped fuel due to the large grain size as shown in Figure 1. The crack damage predictions using Equation 1 are shown for the doped  $\text{UO}_2$  fuel



in Figure 8a and corresponding residuals between the numerical solutions using the tensile strength model and  $\sigma_{TS} = 103.1$  MPa are shown in Figure 8b. The results indicate that significant fracture occurs in the radial and axial directions during a hold at power without any power down. Circumferential cracking tends to form during power downs after a duration at power. Slightly more damage is observed in Figure 8a for the doped  $\text{UO}_2$  case due to its lower tensile strength resulted from the Equation 1 at given microstructural conditions than 103.1 MPa.

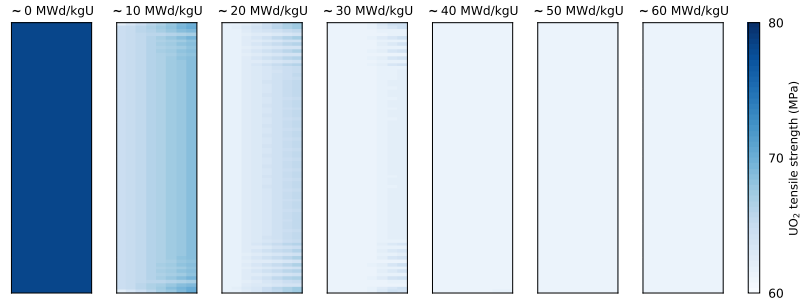


Fig. 7. Tensile strength evolution as a function of rod average burnup for the doped  $\text{UO}_2$  fuel.

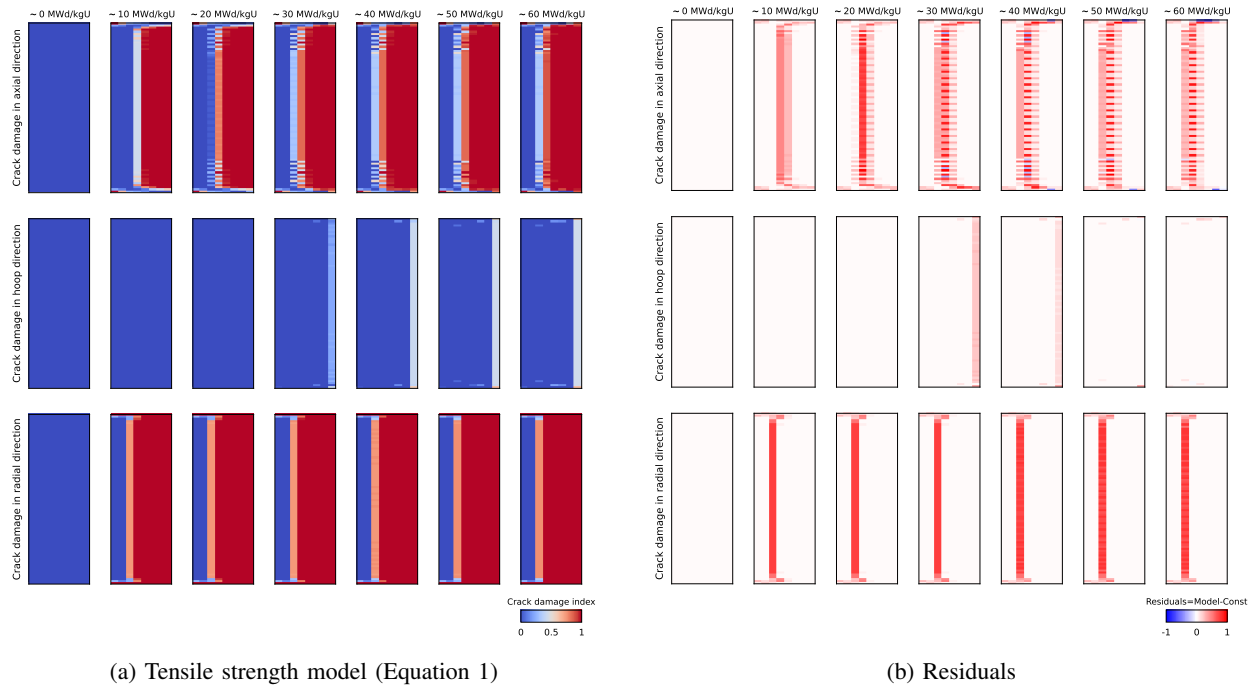


Fig. 8. Contours of (a) the crack damage and (b) crack damage residuals in axial, hoop, and radial directions for the doped  $\text{UO}_2$  fuel at various rod average burnups under the normal operation conditions. The residuals are computed between the predictions using Equation 1 (see Figure 8a) and  $\sigma_{TS} = 103.1$  MPa (see Figure 4b). The default MATPRO creep model is employed in this exercise.

### B. Impact of Creep Modeling on the Predictions

The same 2D-RZ rodlet application from Table II under normal operating conditions is used to study the impact of creep modeling. Previous code predictions using the MATPRO creep model are provided in Appendix A; therefore, the MATPRO predictions are not repeated here and only used in the residual computations between the two creep models.

#### 1) Undoped $\text{UO}_2$ Fuel

The code predictions using the MATPRO creep model are provided for the undoped fuel rodlets in Figure 6a and using the LLS-informed creep model in Figure 9a for the same exercise. The crack damage residuals are computed between the code predictions using LLS-informed and MATPRO creep models and its contours are provided in Figure 9b. For the undoped fuel, local crack damage behavior differentiates significantly depending on the rod average burnup: (i) in the axial direction, simulation using Equation 2 yields less cracking at 10 MWd/kgU, and more cracking as the fuel burns out; (ii) in the hoop direction, differences are insignificant except towards the upper center of fuel rod where the simulation using Equation 2 yields more damage as compared to the default settings; and (iii) in the radial direction, less cracking is observed at the top and bottom sections of the fuel rod while more cracking is observed through the center fuel rod using Equation 2.

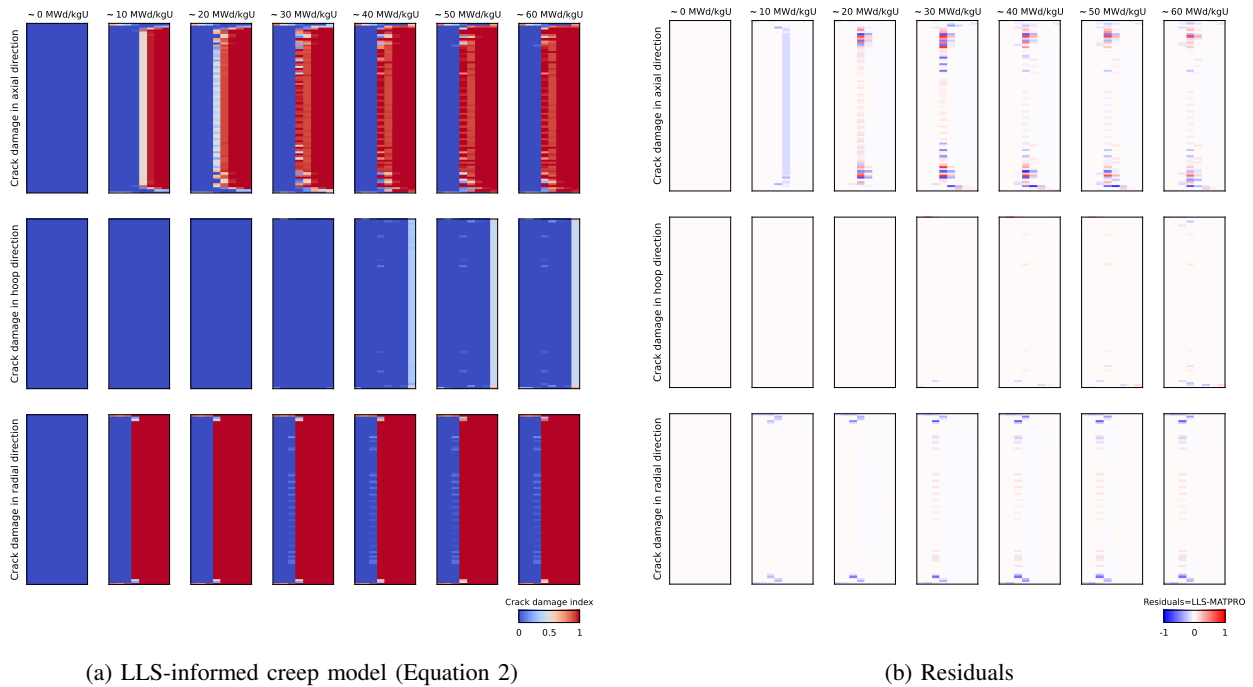


Fig. 9. Contours of (a) the crack damage and (b) its residuals in axial, hoop, and radial directions for the undoped  $\text{UO}_2$  fuel at various rod average burnups under the normal operation conditions. The residuals are computed between the predictions using Equation 2 (see Figure 9a) and MATPRO model (see Figure 6a). The tensile strength model given in Equation 1 is employed in this exercise.

## 2) Doped $UO_2$ Fuel

The code predictions using the MATPRO creep model are provided for the doped fuel rodlets in Figure 8a and using the LLS-informed creep model in Figure 10a for the same exercise. The crack damage residuals are computed between the code predictions using LLS-informed and MATPRO creep models and its contours are provided in Figure 10b. For the doped fuel, significant differences in the crack damage indices are only observed in the axial direction. Depending on the rod average burnup, the differences in the axial direction are as follows: (i) more damage occurs towards the center of the fuel rod at 10 MWd/kgU using Equation 2 as compared to the simulation with the default creep model; (ii) as the fuel burns out, local crack damage differences are more pronounced at top and bottom fuel pellet locations towards the center.

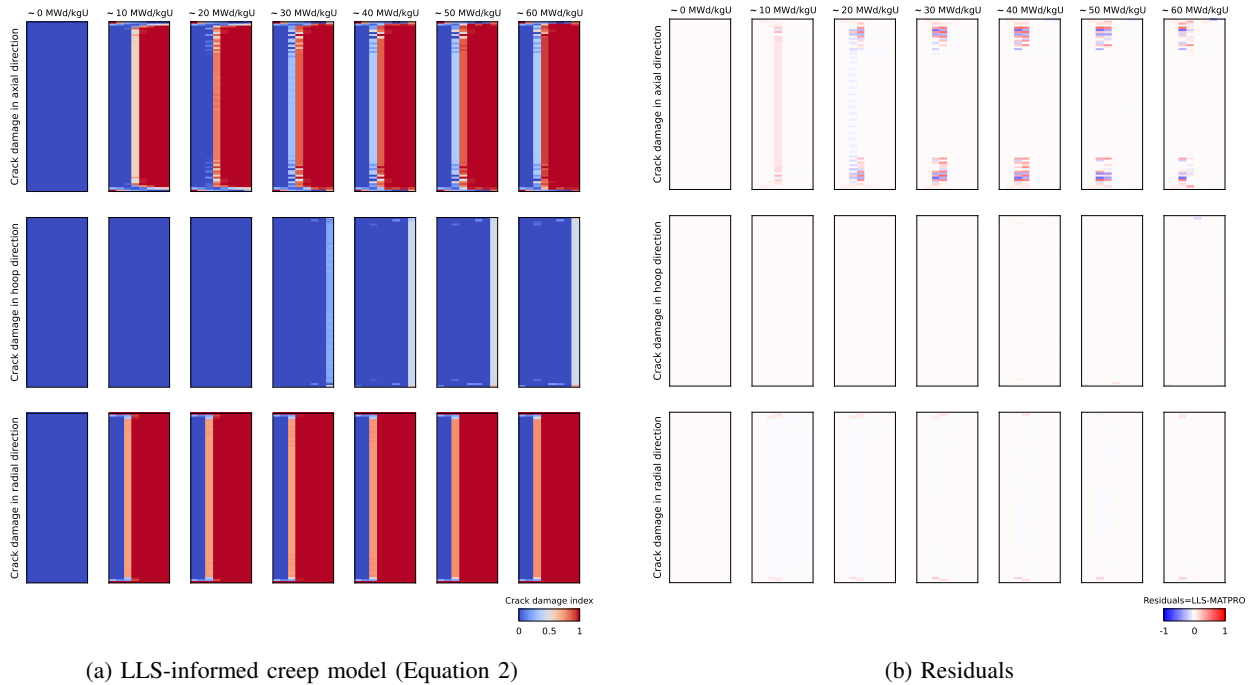


Fig. 10. Contours of (a) the crack damage and (b) its residuals in axial, hoop, and radial directions for the doped  $UO_2$  fuel at various rod average burnups under the normal operation conditions. The residuals are computed between the predictions using Equation 2 (see Figure 10a) and MATPRO model (see Figure 8a). The tensile strength model given in Equation 1 is employed in this exercise.

## IV. SENSITIVITY ANALYSIS

This section covers the theory behind the SA techniques used in this study and our results. To perform these studies, we use the Stochastic Tools Module (STM) in the Multiphysics Object-Oriented Simulation Environment (MOOSE) (Permann et al., 2020) developed by Idaho National Laboratory (INL), an uncertainty quantification software, Dakota (Adams et al., 2014), developed by Sandia National Laboratories (SNL), and Sensitivity Analysis Library (SALib) (Herman and Usher, 2017), which is

available in the Python. Results from these software tools are compared to establish credibility in our results. The sensitivity measures that will be covered are the Pearson correlation coefficients, the Morris sensitivity measures, the Sobol' indices, and the delta moment-independent sensitivity indicator (see Section IV-A). Then, we conduct SA on the tensile-strength model and the LLS-informed creep model prior to performing an SA on the 2D full rod application. Details of the problem settings are provided in Section IV-B. Lastly, SA results are discussed in Section IV-C.

#### A. Sensitivity Analysis Techniques

##### 1) Pearson Correlation Coefficient

To establish relationships between model inputs and outputs we use the Pearson's correlation coefficient,  $r$ , which is defined as below for the selected input parameter  $x$  and integral response parameter  $y$ :

$$r = \text{Corr}(x, y) = \frac{\sum_{i=1}^N (x_i - \bar{x})(y_i - \bar{y})}{\sqrt{\sum_{i=1}^N (x_i - \bar{x})^2} \sqrt{\sum_{i=1}^N (y_i - \bar{y})^2}} \quad (3)$$

where  $x = \{x_i\}_{i=1}^N$ ,  $\bar{x} = \frac{1}{N} \sum_{i=1}^N x_i$ ,  $y = \{y_i\}_{i=1}^N$ ,  $\bar{y} = \frac{1}{N} \sum_{i=1}^N y_i$ , and  $N$  is the sample size.

Three possible states of the Pearson's correlation coefficient  $r$  are: (i)  $r < 0$ , which indicates a negative correlation between  $x$  and  $y$ , (ii)  $r = 0$ , which indicates no correlation between  $x$  and  $y$ , and (iii)  $r > 0$ , which indicates positive correlation between  $x$  and  $y$ .

##### 2) Morris Method

Morris Method (Campolongo et al., 2007), a type of one-at-a-time (OAT) method, is a global sensitivity method that gives the relative influence of each parameter. The method fixes all but one of the  $k$  parameters,  $X_i$  for  $i \in \{1, 2, \dots, k\}$ , at their nominal values and allows for  $X_i$  to vary after the sample space is discretized into  $p$  levels. The changed value is kept the same and this process is repeated many times to better sample the parameter space. The elementary effect for the  $i^{\text{th}}$  parameter  $EE_i$  is calculated as:

$$EE_i = \frac{Y(X_1, \dots, X_i + \Delta, \dots, X_k) - Y(X_1, \dots, X_k)}{\Delta}, \quad (4)$$

where  $\Delta$  is the change of the parameter between two adjacent levels of the grid.  $EE_i$ 's can be identified with a distribution  $F_i$ , which gives us a measure of sensitivity through its mean  $\mu_i$  and standard deviation  $\sigma$ . One can also consider the average of the absolute values of the elementary effect  $\mu_i^*$  to avoid canceling out of the elementary effects in non-monotonic distributions. In practice, the Morris Method can be used as a screening procedure to make computationally expensive analyses more manageable by identifying which parameters have little influence on the output before continuing with a variance-based analysis.

Most packages have a Morris sampling method sample from the  $[0, 1]$  uniform distribution, from which one can easily transform to another distribution. A *Box-Muller Transform* (Box and Muller, 1958) is used to transform a  $\mathcal{U}(0, 1)$  sample to a normally-distributed one. Given two uniform distributions,  $\mathcal{U}_1(0, 1)$

and  $\mathcal{U}_2(0, 1)$  over the unit interval  $[0, 1]$ , two standard normal distributions  $\mathcal{N}(\mu, \sigma)$ , where  $\mu$  is the mean and  $\sigma$  is the standard deviation, can be formed via

$$\mathcal{N}_1(0, 1) = \sqrt{-2 \ln \mathcal{U}_1} \cos(2\pi \mathcal{U}_2) \quad (5a)$$

and

$$\mathcal{N}_2(0, 1) = \sqrt{-2 \ln \mathcal{U}_1} \sin(2\pi \mathcal{U}_2). \quad (5b)$$

Then, all that needs to be done is scaling and shifting these normal distributions to the desired center and shape.

### 3) Sobol' Analysis

Variance-based decomposition (VBD) is a global sensitivity method that shows how the variance in the model output can be apportioned to variance in individual input variables. Two primary measures are considered in this study:

- 1) The first-order sensitivity index ( $S_i$ ) quantifies how much of the variance in an output is explained by the  $i^{th}$  input itself.

$$S_i = \frac{D_i(Y)}{Var(Y)}; \quad S_{ij} = \frac{D_{ij}(Y)}{Var(Y)}; \dots \quad (6)$$

where  $i \in \{1, 2, \dots, d\}$  and  $D_i(Y)$  is the first-order effect of the  $i^{th}$  parameter on  $Y$ .

- 2) The total sensitivity index ( $S_{T_i}$ ) quantifies how much of the variance of an output is explained by the  $i^{th}$  input parameter and its interactions with other uncertain parameters.

$$S_{T_i} = S_i + \sum_{j < i} S_{ij} + \sum_{\substack{j \neq i \\ k \neq i \\ j < k}} S_{ijk} + \dots = \sum_{l \in \#i} S_l, \quad (7)$$

where  $i \in \{1, 2, \dots, d\}$ .

In general, we are interested in models of the following form

$$Y = f(X_1, X_2, \dots, X_k),$$

with  $k$  variables and where each  $X_j$  for  $j \in \{1, 2, \dots, k\}$  represents a different variable of the model. In the sensitivity analysis, each  $X_j$  has its appropriate probability distribution and range of uncertainty and we are interested in how this uncertainty affects the uncertainty of the output. VBD takes  $Y, X_1, X_2, \dots, X_k$  to be probability distributions and decomposes the output variance into variances that can be attributed to the variance of particular variables (or combinations of variables).

When computing the sensitivity indices, sample sizes of the form  $N = 2^p$ ,  $p \in \mathbb{N}$ , are preferred for convergence purposes. Then, using a sampling scheme such as Monte Carlo (MC) or Latin hypercube sampling (LHS), two  $N \times k$  matrices are created (the elements are  $x_j^{(n)}$ , where the superscript denotes

the  $n^{\text{th}}$  sample and the subscript denotes the  $j^{\text{th}}$  variable)

$$A = \begin{bmatrix} x_1^{(1)} & x_2^{(1)} & \dots & x_j^{(1)} & \dots & x_k^{(1)} \\ x_1^{(2)} & x_2^{(2)} & \dots & x_j^{(2)} & \dots & x_k^{(2)} \\ \vdots & \vdots & \vdots & x_j^{(n)} & \vdots & \vdots \\ x_1^{(N-1)} & x_2^{(N-1)} & \dots & x_j^{(N-1)} & \dots & x_k^{(N-1)} \\ x_1^{(N)} & x_2^{(N)} & \dots & x_j^{(N)} & \dots & x_k^{(N)} \end{bmatrix}, \quad (8a)$$

and

$$B = \begin{bmatrix} x_{k+1}^{(1)} & x_{k+2}^{(1)} & \dots & x_{k+j}^{(1)} & \dots & x_{2k}^{(1)} \\ x_{k+1}^{(2)} & x_{k+2}^{(2)} & \dots & x_{k+j}^{(2)} & \dots & x_{2k}^{(2)} \\ \vdots & \vdots & \vdots & x_{k+j}^{(n)} & \vdots & \vdots \\ x_{k+1}^{(N-1)} & x_{k+2}^{(N-1)} & \dots & x_{k+j}^{(N-1)} & \dots & x_{2k}^{(N-1)} \\ x_{k+1}^{(N)} & x_{k+2}^{(N)} & \dots & x_{k+j}^{(N)} & \dots & x_{2k}^{(N)} \end{bmatrix}. \quad (8b)$$

We then define  $k$  matrices  $C_j$  for  $j = 1, 2, \dots, k$  where  $C_j$  is the matrix  $B$  with the  $j^{\text{th}}$  column replaced by the  $j^{\text{th}}$  column of  $A$ :

$$C = \begin{bmatrix} x_{k+1}^{(1)} & x_{k+2}^{(1)} & \dots & \mathbf{x}_j^{(1)} & \dots & x_{2k}^{(1)} \\ x_{k+1}^{(2)} & x_{k+2}^{(2)} & \dots & \mathbf{x}_j^{(2)} & \dots & x_{2k}^{(2)} \\ \vdots & \vdots & \vdots & \mathbf{x}_j^{(n)} & \vdots & \vdots \\ x_{k+1}^{(N-1)} & x_{k+2}^{(N-1)} & \dots & \mathbf{x}_j^{(N-1)} & \dots & x_{2k}^{(N-1)} \\ x_{k+1}^{(N)} & x_{k+2}^{(N)} & \dots & \mathbf{x}_j^{(N)} & \dots & x_{2k}^{(N)} \end{bmatrix}. \quad (8c)$$

Each of the  $N$  rows of these matrices corresponds to an element in our sample space, thus

$$y_A = f(A), \quad (9a)$$

$$y_B = f(B), \quad (9b)$$

and

$$y_{C_j} = f(C_j), \quad (9c)$$

correspond with the  $N(k+2)$  outputs generated by our sampling method. In doing so, the sensitivity indices can be computed in the following way:

$$S_i = \frac{D_i(Y)}{Var(Y)} = \frac{y_A \cdot y_{C_j} - f_0^2}{y_A \cdot y_A - f_0^2} = \frac{\frac{1}{N} \sum_{\ell=1}^N y_A^{(\ell)} y_{C_j}^{(\ell)} - f_0^2}{\frac{1}{N} \sum_{\ell=1}^N \left[ y_A^{(\ell)} \right]^2 - f_0^2}, \quad (10)$$

where

$$f_0^2 = \left[ \frac{1}{N} \sum_{\ell=1}^N y_A^{(\ell)} \right]^2. \quad (11)$$

Note that this method yields the first-order and total sensitivity indices, but using the method described in Saltelli (2002) the calculation of the first-order, second-order, and total sensitivity indices can be computed at the cost of  $N(2k + 2)$  runs.

#### 4) Delta Moment-independent Analysis

The delta moment-independent method as developed in Borgonovo (2007); Plischke et al. (2013) is first briefly summarized. Given a set of uncertain parameters,  $\underline{X} = (X_1, X_2, \dots, X_n)$ ,  $f_Y(y)$  is the probability density function corresponding to the cumulative distribution  $F_Y(y)$  of the model output, and  $f_{\underline{X}}(\underline{x})$  is the joint probability density function of the cumulative distribution of  $F_{\underline{X}}(\underline{x})$ , at a realization  $\underline{x} = (x_1, x_2, \dots, x_n)$  of  $\underline{X}$ . The conditional probability density function, denoted by  $f_{Y|X_i}(y)$ , is the conditional probability density of the output  $Y$  given that parameter  $X_i$  is set to a fixed value. This allows us to define the shift between  $f_Y(y)$  and  $f_{Y|X_i}(y)$  as

$$s(X_i) = \int |f_Y(y) - f_{Y|X_i}(y)| dy, \quad (12)$$

which itself is a random variable given its dependence on  $X_i$ . The expected shift of this random variable is

$$E_{X_i} = \int f_{X_i}(x) \left[ \int |f_Y(y) - f_{Y|X_i}(y)| dy \right] dx_i, \quad (13)$$

where  $f_{X_i}(x_i)$  is the marginal density of  $x_i$ . We can finally define the new uncertainty measure,  $\delta_i$ , which is given by

$$\delta_i = \frac{1}{2} E_{X_i} [s(X_i)]. \quad (14)$$

This is called the moment independent sensitivity indicator of  $X_i$  with respect to  $Y$ . Some key properties are given below in Table III. A benefit of this measure is that it is independent of the sampling scheme (according to Herman and Usher (2017)), which allows us to make use of a sampling scheme for other methods more than once. It agrees with other variance based indicators on which parameters are less relevant and have a cost independent of the number of parameters (Plischke et al., 2013).

TABLE III. Properties of the uncertainty importance measure  $\delta$  from the delta moment-independent analysis (Borgonovo, 2007, Table 1).

Property	Meaning
$0 \leq \delta_i \leq 1$	Bounds the possible values $\delta_i$ can assume
$\delta_i = 0$	If $Y$ is independent of $X_i$ , then $\delta = 0$
$\delta_{1,2,\dots,n} = 1$	The importance of all parameters equals unity
$\delta_{ij} = \delta_i$	If $Y$ is dependent on $X_i$ but independent of $X_j$ , then $\delta_{ij} = \delta_i$
$\delta_i \leq \delta_{ij} \leq \delta_i + \delta_{j i}$	Bounds the possible values $\delta_{ij}$ can assume

## B. Applications

### 1) Tensile-strength Model

To test this model, we use a simulation that calculates the fabrication pore size, grain size, and porosity-dependent tensile strength model given by Equation 1. The simulation models a  $\text{UO}_2$  sample that is heated linearly from 500 to 2000 K over a time period of  $1 \times 10^6$  seconds. For the SA, we model the three parameters as uniform distributions, with ranges given in Table IV.

TABLE IV. Parameter ranges for the tensile-strength model (Equation 1).

Parameter	Ranges	Reference	Distribution
Porosity ( $p$ )	5–10%	Oguma (1982)	Uniform
Fabrication pore size ( $P$ )	5–100 $\mu\text{m}$	Oguma (1982)	Uniform
Grain size ( $G$ )	10–80 $\mu\text{m}$	Oguma (1982)	Uniform

### 2) LLS-informed Model

For the LLS-informed model (Equation 2), we simulate the creep rate of a unit  $\text{UO}_2$  cube that is pulled in the  $y$ -direction at a constant and uniform temperature and fission rate density (fissions per  $\text{m}^3$  per s) with a pressure of 50 MPa and over a period of  $1 \times 10^5$  s. We also present results at fixed sample size of  $N = 8192$  at varying temperatures (e.g., 1500, 2000, 2500, and 3000 K; fixed fission rate of  $2.0 \times 10^{18}$  fissions/ $\text{m}^3\text{-s}$ ) and varying fission rates (e.g.,  $2.0 \times 10^{18}$ ,  $2.0 \times 10^{20}$ ,  $2.0 \times 10^{22}$ , and  $2.0 \times 10^{24}$  fissions/ $\text{m}^3\text{-s}$ ; fixed temperature of 1500 K). For the SA, we model the five parameters as uniform/normal distributions, with ranges given in Table IV according to Galvin et al. (2022).

TABLE V. Parameter ranges for the LLS-informed creep model (Equation 2).

Parameter	Ranges	Reference	Distribution
$A_1, A_2, A_3$	10 orders of magnitude		Uniform
$B_1, B_2$	$\pm 0.3$ eV		Normal

### 3) 2D-RZ Rodlet Application

For the full rod example, we combine all uncertainties in Table VI from the previous two sections as well as some additional input parameters. In total, a total number of ten input parameters are considered as shown in Table VI. For some input parameters whose uncertainty has not been reported in literature, the uncertainty is assumed based on the authors' judgment. The distribution types are either (a) uniform,  $\mathcal{U}(\mu - \sigma, \mu + \sigma)$  or (b) normal,  $\mathcal{N}(\mu, \sigma)$  where  $\mu$  is the mean and  $\sigma$  is the standard deviation. Scale factors (or multipliers) are applied to the model predictions in the code for each QoI, e.g., for the Young's modulus (via `youngs_modulus_scale_factor`) in this case.

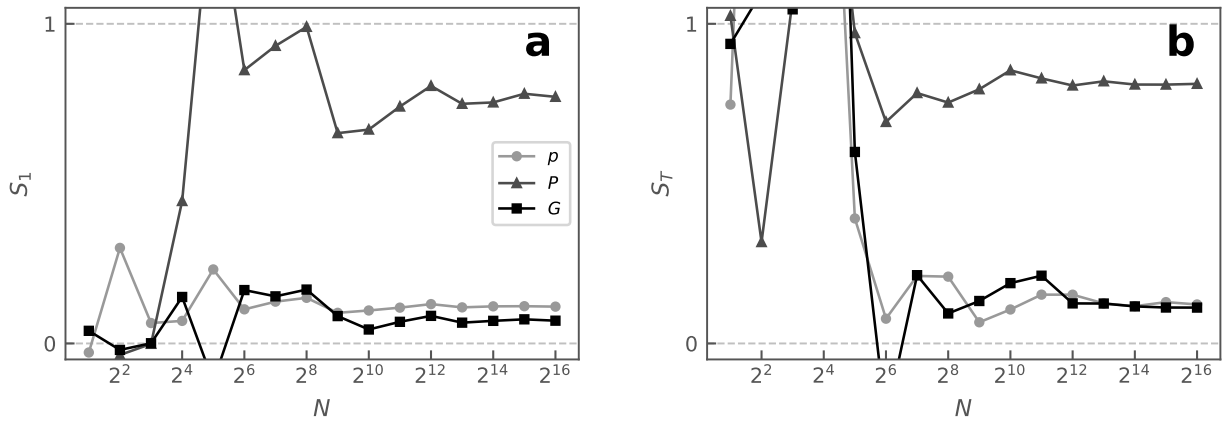
## C. Results & Discussion

Several SA techniques are applied on the models described in the previous sections. For convenience of the convergence analysis, sample sizes are restricted to the form  $N = 2^\ell$ , with  $\ell$  being an integer, as recommended by Herman and Usher (2017). For the tensile strength model, the Pearson correlation coefficients are calculated in addition to the Sobol' indices in Section IV-C1. For the LLS-informed model, the Morris Method is also incorporated, as shown in Section IV-C2. Lastly, combined analysis for



TABLE VI. Parameter uncertainties for the combined 2D RZ application

Parameter	Uncertainty	Reference	Distribution
Porosity	[5%, 10%]	Oguma (1982)	Uniform
Grain size	[10 $\mu\text{m}$ , 80 $\mu\text{m}$ ]	Oguma (1982)	Uniform
Fabrication pore size	[5 $\mu\text{m}$ , 100 $\mu\text{m}$ ]	Oguma (1982)	Uniform
Young's modulus	$\pm 10\%$	Hagman and Reymann (1979)	Normal
Grain boundary thickness	20%		Normal
$A_1, A_2, A_3$ of Equation 2	10 orders of magnitude		Uniform
$B_1, B_2$ of Equation 2	$\pm 0.3$ eV		Normal

Fig. 11. Sobol' indices versus the sample size for the tensile-strength model: (a) first-order sensitivity indices,  $S_1$  and (b) total sensitivity indices,  $S_T$ .

both doped and undoped fuel rodlets under normal operating conditions was performed in Section IV-C3 where the Pearson correlation coefficients, the delta moment-independent sensitivity indicators, and Sobol' indices are computed for several quantities of interest. For the full rod example, the computational run time is taken into consideration to select SA techniques.

#### 1) Tensile Strength Model

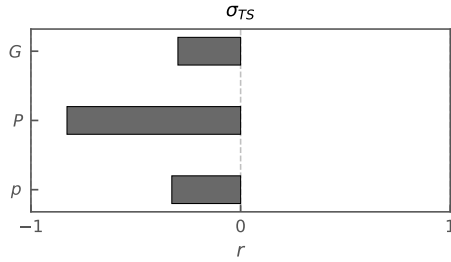
The parameter ranges for this analysis are displayed in Table IV. Figure 11(a) shows the different first-order indices as  $N$  increases. The fabrication pore size  $P$  has the greatest contribution to the variance of the tensile strength. The fabrication pore size also has the greatest total sensitivity index, while the porosity and grain size total sensitivity indices are about the same. It is noteworthy that if the sample size isn't large enough (see  $N < 128$  in Figure 11(b)), the resulting sensitivity indices are non-physical since they are out of  $[0, 1]$  bound. Convergence for all three indices begins to occur when  $N = 8192$  since the change in values from this point on becomes very small.

For reference, a table of indices computed across the three software packages, STM, Dakota, and SALib is provided in Table VII. Results from all three tools agree on the relative order of importance of parameters, although STM gives slightly different values compared to the other two packages. The Pearson correlation coefficients are also computed as shown in Figure 12. All three parameters have a

negative correlation with the tensile strength  $\sigma_{TS}$ , i.e. an increase in any of these parameters leads to a decrease in the tensile strength. Moreover, these coefficients are in agreement with the results of the Sobol' analysis.

TABLE VII. Comparison of first-order and total sensitivity indices between STM, Dakota and SALib ( $N = 8192$ ).

Software	1 <sup>st</sup> -order Sobol' indices, $S_1$			Total Sobol' indices, $S_T$		
	$p$	$P$	$G$	$p$	$P$	$G$
STM	0.113	0.750	0.065	0.125	0.820	0.125
Dakota	0.106	0.753	0.090	0.112	0.804	0.136
SALib	0.105	0.753	0.090	0.111	0.804	0.137



-	$p$	$P$	$G$	$\sigma_{TS}$
$p$	1.0000	-	-	-
$P$	-0.0004	1.0000	-	-
$G$	-0.0054	-0.0031	1.0000	-
$\sigma_{TS}$	-0.3281	-0.8280	-0.2989	1.0000

Fig. 12. Pearson correlation coefficients between the tensile strength and the selected model input parameters ( $N = 8192$ ). The strongest correlation lies in the fabrication pore size,  $P$ , and all parameters have inverse relationships with  $\sigma_{TS}$ .

## 2) LLS-informed Creep Model

In this analysis, the Pearson correlation coefficients and the Sobol' indices are computed, and the Morris method is performed as another measure of sensitivity. Typically, the Morris method is performed to identify the most influential parameters for including in further analyses, but for the number of parameters we have in this analysis, this method is done purely for assessing which parameters are the most influential. In Figure 14, we see that  $B_1$  and  $B_2$  are indeed the most influential according to this measure. This is confirmed by the Pearson correlation coefficients. The values shown in Figure 13 show that both methods attach similar importance to each parameter and also show that  $B_1$  and  $B_2$  are negatively correlated to the creep rate  $\dot{\epsilon}$ , while  $A_1, A_2$ , and  $A_3$  have a positive correlation with  $\dot{\epsilon}$ .

Based on the results from the previous model, we decided to start our Sobol' analysis with a sample size of  $N = 128$  (and keep the largest sample size of  $N = 2^{16}$ ). Figure 15(a) suggests that the parameters  $A_1, A_2$  and  $A_3$  have negligible effects on the output, and confirm that most of the sensitivity belongs to changes in  $B_1$  and  $B_2$ . On the other hand, Figure 15(b) shows that the total effect from  $A_1$  and  $A_2$  are relatively larger than their respective first-order indices, which suggests that there are higher-order interactions involving these parameters that influence the creep rate.

How the indices change with respect to temperature and fission rate is then investigated. Note that the sample size used is now  $N = 16384$  in order to arrive at more realistic Sobol' indices when using increased temperature and fission rate density. In Figure 16a, as the temperature increases,  $B_1$  becomes the most important parameter. The Sobol' indices corresponding to  $A_1$  increase slightly, indicating that

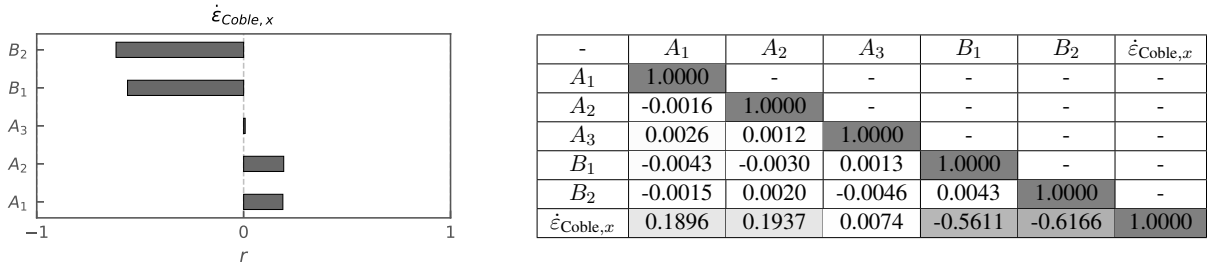


Fig. 13. Pearson correlation coefficients between the LLS-informed creep rate and the selected model input parameter (with  $N = 8192$ ).  $B_1$  and  $B_2$  have a negative correlation with the output  $\dot{\epsilon}$  while  $A_1, A_2$  and  $A_3$  are positively correlated with  $\dot{\epsilon}$ . This table shows that  $A_3$  will have negligible effect on the output, especially compared to the strongest parameters  $B_1$  and  $B_2$ .

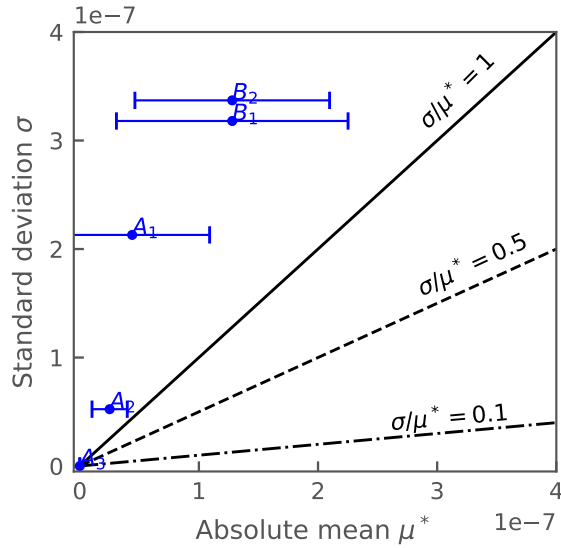


Fig. 14. Morris measures (standard deviation of elementary effect,  $\sigma$  and absolute mean of elementary effect,  $\mu^*$ ) for the LLS-informed creep model. Factors with small  $\mu^*$  can be considered non-influential, while factors with large  $\mu^*$  are important. The value of  $\sigma$  reveals a factors role interacting with other factors, with higher  $\sigma$  representing higher interactions.

this parameter becomes slightly more important as the temperature increases. On the other hand, when the fission rate is increased, the most sensitive parameter will be  $B_2$  while the indices related to the other parameters decrease.

### 3) Combined Analysis: 2D-RZ Rodlet Application

SAs are performed for both undoped and doped fuel rodlets under normal operating conditions (Table II). This 2D-RZ application is from the previous sections, refer to Section III for details of the problem settings as well as the operating conditions. In the SAs, the QoIs is chosen as the crack damage indices in

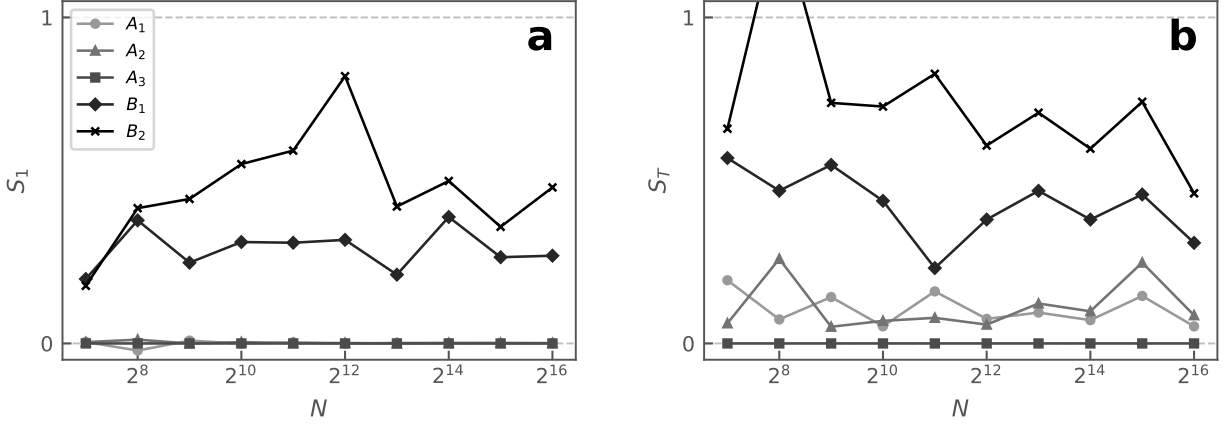


Fig. 15. Sobol' indices versus the sample size for the LLS-informed creep model: (a) first-order sensitivity indices,  $S_1$  and (b) total sensitivity indices,  $S_T$ .

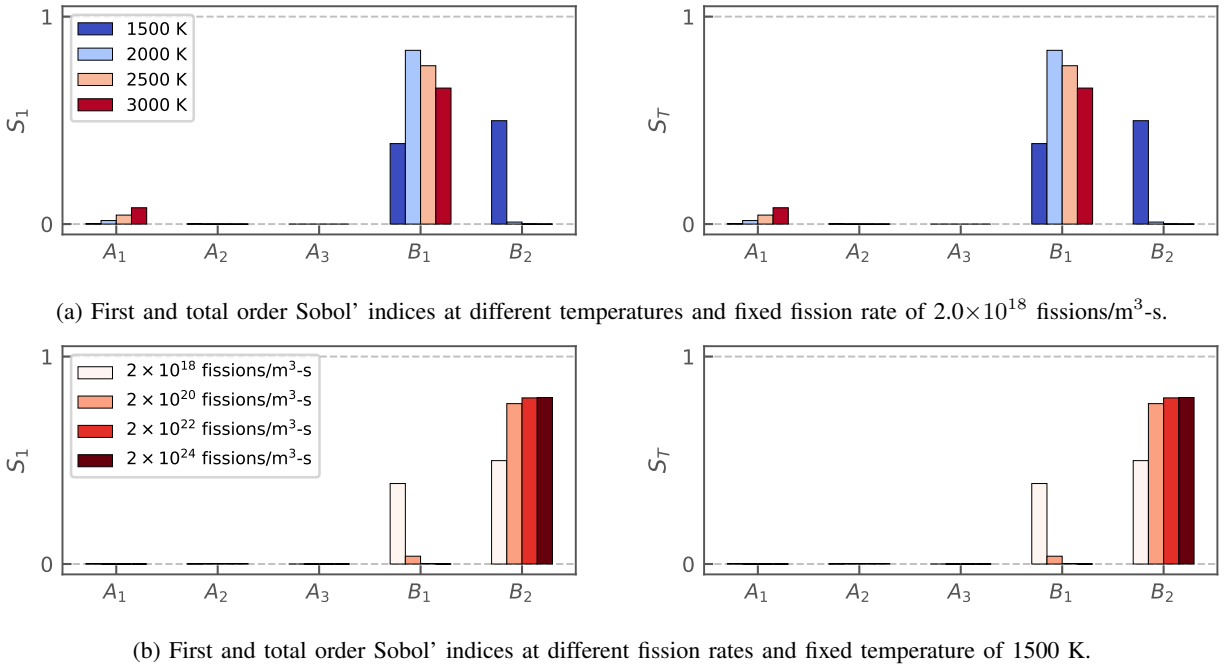


Fig. 16. Sobol' indices for different temperatures or fission rates using the LLS-informed model (Equation 2, with  $N = 16384$ ).

axial, hoop, and radial directions since both tensile strength and creep change the stress state and affect the cracking depending on the stress level. Contours of the local crack damage behavior at the nominal conditions have previously been shown in Figure 9a for the undoped fuel rodlets and Figure 10a for the doped fuel rodlets. In addition to the crack damage indices, five additional integral responses (e.g., fission gas release (FGR), fuel elongation, maximum fuel centerline temperature, maximum hoop stress, and rod internal pressure) are selected, which are typically measurable in experiments. Here, the volume integral values of the crack damage indices over the whole computational domain are considered for the SA purposes.

In this study, LHS samples are used to construct sensitivity indices for the Pearson correlation coefficients as well as the delta moment-independent analysis and first-order Sobol' indices (see Section IV-A for details). The perturbed input parameters are shown in Figure 17 for the undoped fuel rodlets and Figure 18 for the doped fuel rodlets using an LHS sampling with  $N = 1024$ . The perturbed input parameters are indicated in gray lines as well as the corresponding simulation results, while the nominal input parameters and corresponding results are indicated in black lines. The perturbed input parameters explore the parameter space well, as shown in Figures 17(a) and 18(a) in which the perturbed parameters are normalized between their maximum and minimum values.

Some combinations of the perturbed input parameters that yield the maximum (the limiting condition in this case) crack damage predictions are also investigated and indicated in different colors than gray in Figures 17 and 18. The corresponding contour plots of the crack damage indices at nominal and limiting conditions at EOL are also shown in Figures 17(c) and 18(c) as well as contour plots of the crack damage residuals between nominal and maximum cases. The crack damage indices vary between zero (i.e., no crack) and one (i.e., complete crack), as mentioned previously, while the crack damage residuals vary in  $[-1, 1]$ .

The SA results from the aforementioned techniques are provided for both undoped and doped fuel rodlets in the following. The results are given at various rod average burnups; 10, 20, 30, 40, 50, and 60 MWd/kgU, in which an interpolation scheme is generated to find the simulation results at the desired burnup values. We first start with the Pearson correlation coefficients to investigate the linear interactions between the QoI and selected input parameters listed in Table VI. Later, we present the results from delta moment-independent analysis, which also produces the first-order Sobol' sensitivity indices, to identify the most influential parameters on the QoI. Lastly, we provide a summary of findings from all SA techniques on this combined analysis. Note that selection of the delta moment-independent analysis is due to its compatibility with any samplers of choice and consideration of the computational run time. Therefore, we used the same 1024 LHS samples from the Pearson analysis for the delta moment-independent analysis.

The *Pearson correlation coefficients* are computed at various average burnup values (e.g., 10, 20, 30, 40, 50, and 60 MWd/kgU) to investigate the importance of input parameters on the selected QoI through-life. Figures 19 and 20 show the SA results for the selected QoIs for the undoped and doped fuel rodlets, respectively. The correlation coefficients ( $r$ ) vary between -1 and 1, which correspond to an inverse and proportional linear interactions, respectively. When  $r = 0$ , there is no relation between the QoI and input parameter. Here, we interpret correlation strength in terms of  $|r|$  as follows: 0.10 to 0.30 as a *weak* correlation, 0.30 to 0.50 as a *moderate* correlation and greater than 0.50 as a *strong* correlation (Gamble and Toptan, 2021).

The observations from the Pearson correlation coefficients are listed for each QoI as follows:

- The crack damage in axial and radial directions: A moderate positive correlation with  $B_2$  and grain

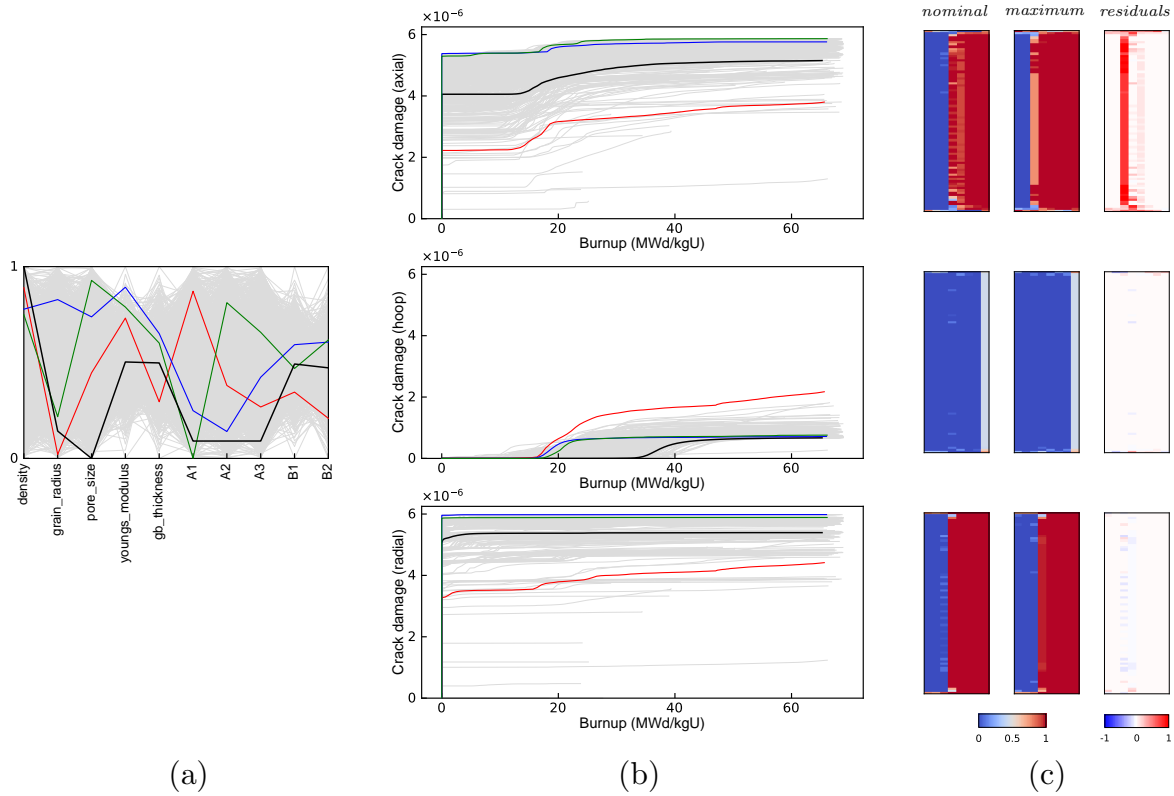


Fig. 17. The combination of perturbed input parameters (a) and the corresponding simulation results using the perturbed input parameters (b) for the undoped fuel (LHS with  $N = 1024$ ). Gray lines indicate the perturbations and corresponding simulation results using these perturbed input parameters. Solid lines indicate the nominal parameter conditions and simulation results. Some combinations of the perturbed input parameters that yield maximum crack damage predictions are indicated in different colors than the gray, whose contour plots are shown in (c) at the EOL.

radius, a weak-to-moderate positive correlation with the pore size depending on the rod average burnup, and weak relations with the rest of the parameters.

- The crack damage in hoop direction: Youngs modulus and pore size exhibit positive relations with varying strength depending on the rod average burnup (e.g., weak at the BOL, moderate to strong around 30 MWd/kgU, and weak through the EOL), and weak correlations with the rest of input parameters.
- FGR: A strong inverse correlation with the grain radius, a moderate inverse correlation with the fuel density (or porosity) at BOL and weak relation through the EOL for the fuel density.
- Fuel elongation: A weak-to-moderate inverse correlation with the grain radius and fuel density depending on the burnup, and non-significant correlations with the rest of parameters.
- Max. fuel centerline temperature: A moderate-to-strong inverse correlation with the fuel density and negligible correlation with the rest of parameters.

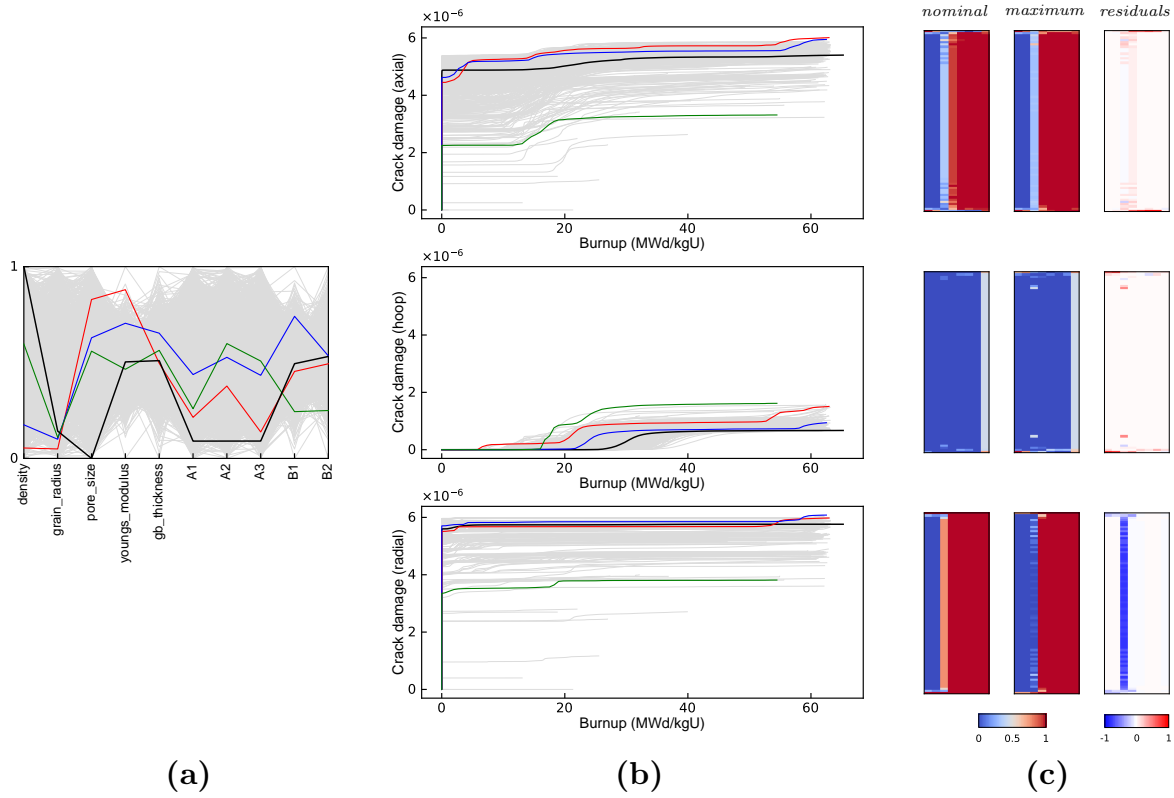


Fig. 18. The combination of perturbed input parameters (a) and the corresponding simulation results using the perturbed input parameters (b) for the doped fuel (LHS with  $N = 1024$ ). Gray lines indicate the perturbations and corresponding simulation results using these perturbed input parameters. Solid lines indicate the nominal parameter conditions and simulation results. Some combinations of the perturbed input parameters that yield maximum crack damage predictions are indicated in different colors than the gray, whose contour plots are shown in (c) at the EOL.

- Max. hoop stress: A strong-to-moderate inverse correlation with the grain radius and pore size.
- Plenum pressure: A moderate positive correlation with  $B_2$  at 10 MWd/kgU and a weak correlation through the EOL for  $B_2$ , a strong inverse correlation with the grain radius through the EOL, and a moderate inverse correlation with the fuel density up to 30 MWd/kgU.

From the analyses for both undoped (Figure 19) and doped (Figure 20) fuel rodlets, we obtained similar results between the selected QoIs and input parameters. This might be mainly due to utilization of similar models for both undoped and doped conditions in the simulations.

*Delta moment-independent analysis* (Borgonovo, 2007; Plischke et al., 2013) on model outputs is performed; we used the same LHS sampling with  $N = 1024$ . The results at various rod average burnups are shown for the selected eight QoIs; crack damage in axial, hoop, and radial directions, FGR, fuel elongation, max. fuel centerline temperature, max. hoop stress, and plenum pressure in Tables VIII–XV. The results are provided for both undoped and doped fuel rodlets. We chose the same color theme here

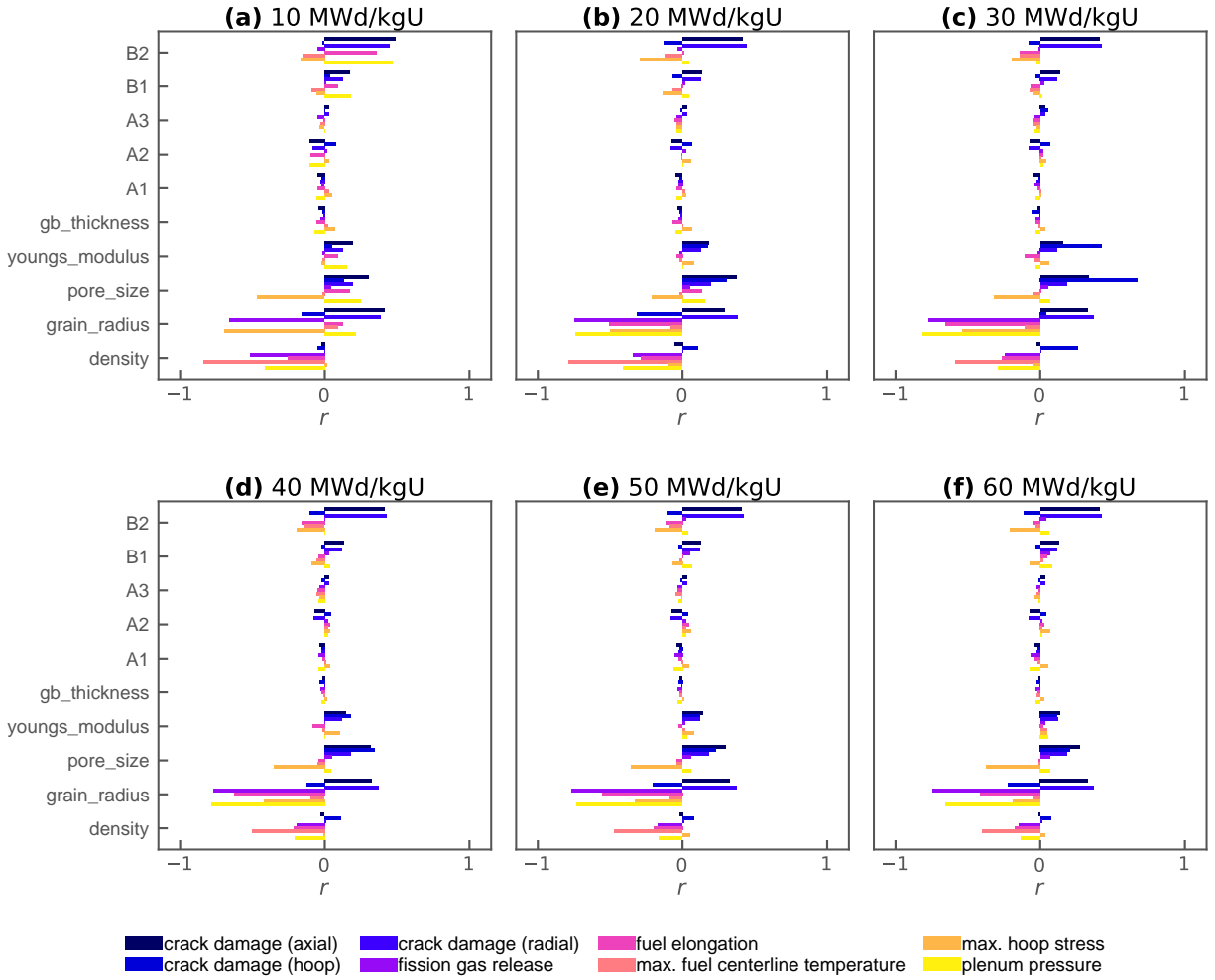


Fig. 19. Pearson correlation coefficients between QoIs (e.g., the crack damage indices, FGR, fuel elongation, max. fuel centerline temperature, max. hoop stress, and pressure) and the selected input parameters (e.g., density, grain radius, fabrication pore size, Youngs module multiplier, grain boundary thickness, and five model parameters of Equation 2) at a rod average burnup of 10, 20, 30, 40, 50, and 60 MWd/kgU in (a) through (f) for the undoped fuel rodlets.

as of the plots in both Figures 19 and 20 for each QoI. As far as interactions are concerned, one can also observe that  $\sum_{i=1}^n \delta_i \approx 1$  for ten model input parameters ( $n = 10$ ), in this case. The delta moment-independent analysis is performed using the SALib which outputs both delta indicator and first-order Sobol' sensitivity indices.

In summary, our observations from delta moment-independent and Sobol' analyses are listed below.

- *Crack damage in axial direction* (Table VIII): Grain radius is the most influential parameter, followed by  $B_2$  and pore size according to the delta indicator.  $B_2$  is the most influential parameter, followed



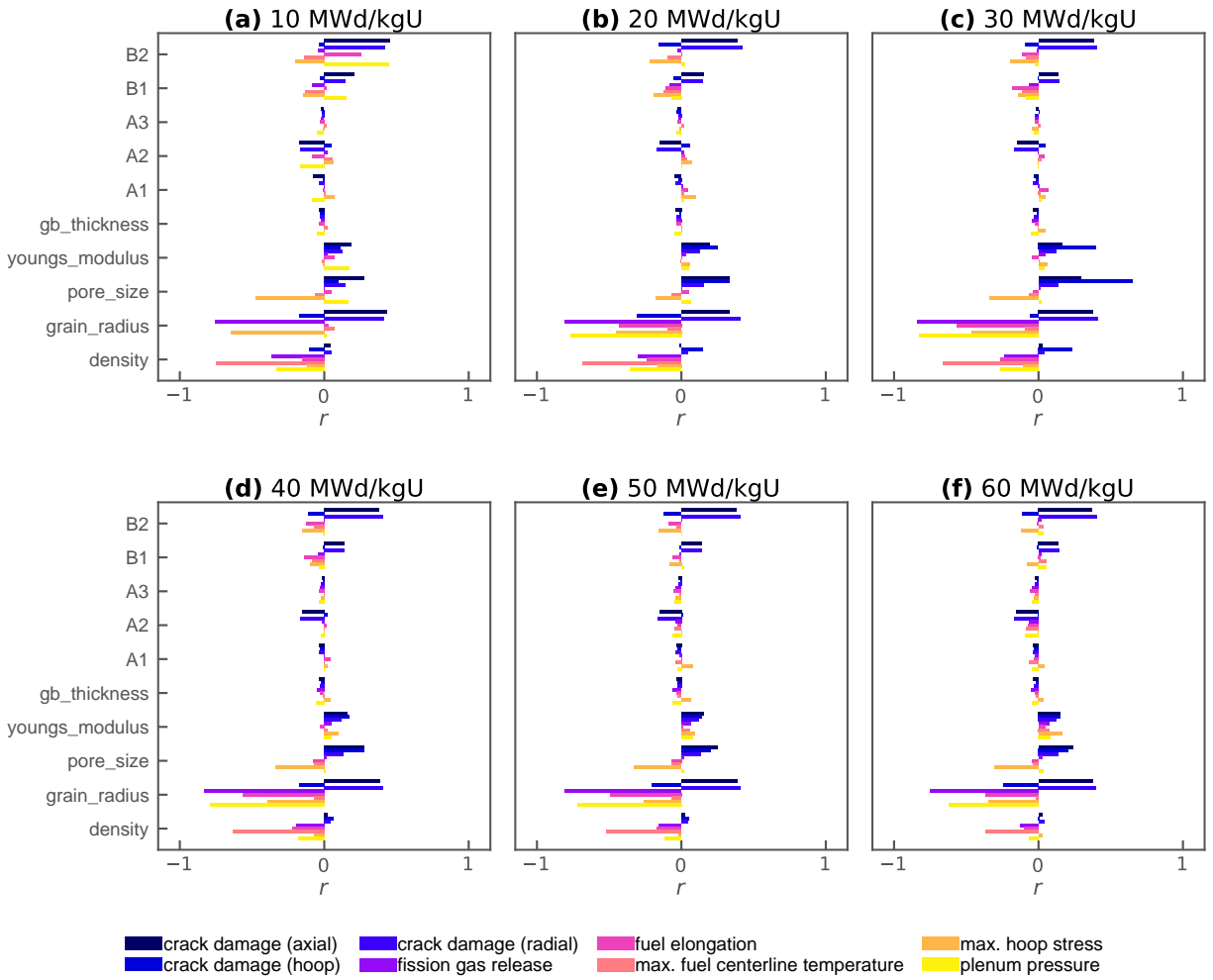


Fig. 20. Pearson correlation coefficients between QoIs (e.g., the crack damage indices, FGR, fuel elongation, max. fuel centerline temperature, max. hoop stress, and pressure) and the selected input parameters (e.g., density, grain radius, fabrication pore size, Youngs module multiplier, grain boundary thickness, and five model parameters of Equation 2) at a rod average burnup of 10, 20, 30, 40, 50, and 60 MWd/kgU in (a) through (f) for the doped fuel rodlets.

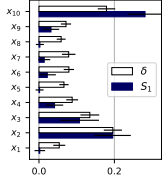
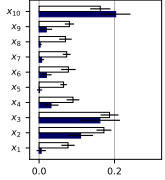
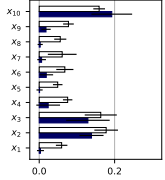
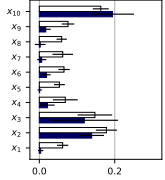
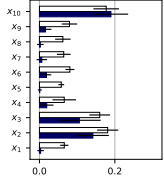
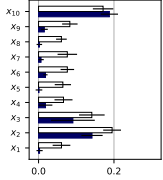
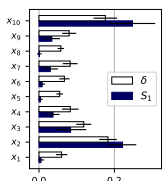
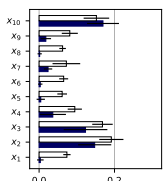
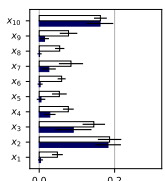
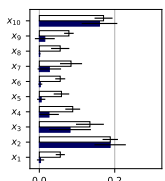
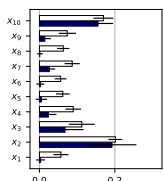
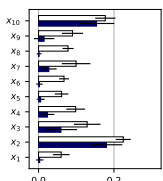
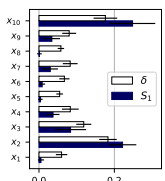
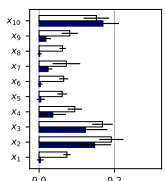
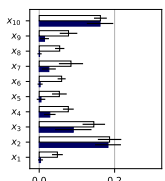
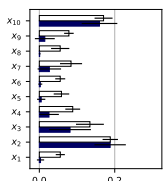
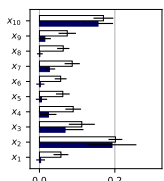
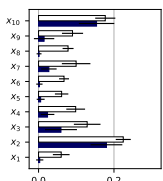
by grain radius and pore size according to the Sobol' sensitivity indices. Similar observations are valid for each fuel type from both sensitivity measures.

- *Crack damage in hoop direction* (Table IX): Grain radius is the most influential parameter except 20–30 MWd/kgU where the pore size becomes the most influential parameter according to the delta indicator. Relatively similar results are obtained for the Sobol' sensitivity indices as well. Similar observations are valid for each fuel type from both sensitivity measures.
- Crack damage in radial direction (Table X): Grain radius and  $B_2$  are influential parameters, according

to both delta indicator and Sobol' sensitivity indices. For the doped fuel, the grain radius becomes the most influential parameter and followed by  $B_2$ .

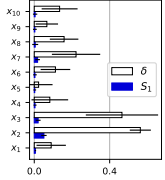
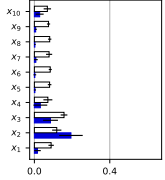
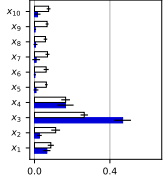
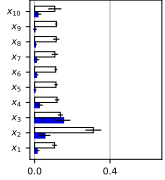
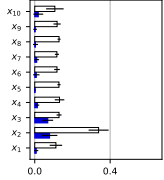
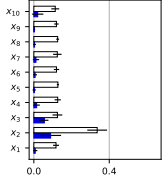
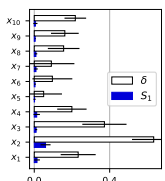
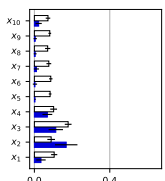
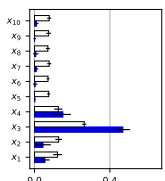
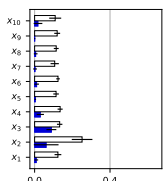
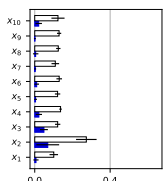
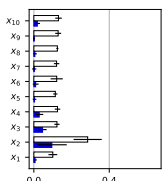
- FGR (Table XI): Grain radius is the most influential parameter, followed by fuel density (or porosity), according to both sensitivity measures. Similar observations are valid for each fuel type from both sensitivity measures.
- Fuel elongation (Table XII): Grain radius is the most influential parameter, according to both sensitivity measures. The grain radius is followed by fuel density and  $B_2$  at 10 MWd/kgU. The effect of  $B_2$  on the QoI becomes insignificant after 10 MWd/kgU, while effect of the fuel density diminishes through the EOL. Similar observations are valid for each fuel type from both sensitivity measures.
- Max. fuel centerline temperature (Table XIII): Fuel density is the most influential parameter according to both sensitivity measures. Similar observations are valid for each fuel type from both sensitivity measures.
- Max. hoop stress (Table XIV): Grain radius is the most influential parameter according to both sensitivity measures, followed by pore size up to 40 MWd/kgU. After 40 MWd/kgU, the pore size becomes the most influential parameter and followed by the grain radius. Similar observations are valid for each fuel type from both sensitivity measures.
- Plenum pressure (Table XV): Grain radius is the most influential parameter, according to both sensitivity measures, except at 10 MWd/kgU where fuel density, grain radius, and  $B_2$  have relatively similar influences on the QoI. Similar observations are valid for each fuel type from both sensitivity measures.

TABLE VIII. Delta moment-independent analysis of selected input parameters on the *crack damage in axial direction* for both undoped and doped fuel rodlets. The sensitivity measures are uncertainty importance measure,  $\delta$  and first-order Sobol' indices,  $S_1$ , which vary between zero and one. The larger the sensitivity measure, the more influential the parameter is. The LHS sampling is considered with  $N = 1024$ .

X	Y : Crack damage in axial direction											
	<i>Undoped fuel rodlets</i>											
	10 MWd/kgU	20 MWd/kgU	30 MWd/kgU	40 MWd/kgU	50 MWd/kgU	60 MWd/kgU	10 MWd/kgU	20 MWd/kgU	30 MWd/kgU	40 MWd/kgU	50 MWd/kgU	60 MWd/kgU
												
	$\delta$ $S_1$	$\delta$ $S_1$	$\delta$ $S_1$	$\delta$ $S_1$	$\delta$ $S_1$	$\delta$ $S_1$	$\delta$ $S_1$	$\delta$ $S_1$	$\delta$ $S_1$	$\delta$ $S_1$	$\delta$ $S_1$	$\delta$ $S_1$
$x_{10}$	0.1790	0.2813	0.1623	0.2031	0.1589	0.1925	0.1630	0.1939	0.1771	0.1896	0.1711	0.1878
$x_9$	0.0717	0.0319	0.0805	0.0191	0.0776	0.0180	0.0761	0.0171	0.0797	0.0161	0.0830	0.0153
$x_8$	0.0588	0.0025	0.0699	0.0028	0.0558	0.0026	0.0592	0.0024	0.0622	0.0023	0.0606	0.0021
$x_7$	0.0788	0.0140	0.0732	0.0067	0.0610	0.0064	0.0621	0.0063	0.0645	0.0063	0.0763	0.0066
$x_6$	0.0794	0.0221	0.0777	0.0192	0.0680	0.0187	0.0655	0.0192	0.0808	0.0187	0.0763	0.0183
$x_5$	0.0663	0.0017	0.0649	0.0012	0.0491	0.0010	0.0533	0.0010	0.0579	0.0009	0.0645	0.0011
$x_4$	0.0881	0.0414	0.0899	0.0316	0.0755	0.0238	0.0689	0.0214	0.0658	0.0194	0.0661	0.0182
$x_3$	0.1348	0.1074	0.1869	0.1612	0.1632	0.1292	0.1474	0.1193	0.1599	0.1059	0.1412	0.0911
$x_2$	0.1959	0.1957	0.1720	0.1100	0.1776	0.1387	0.1779	0.1389	0.1810	0.1417	0.1950	0.1418
$x_1$	0.0538	0.0022	0.0768	0.0055	0.0595	0.0033	0.0619	0.0035	0.0659	0.0031	0.0608	0.0027
	<i>Doped fuel rodlets</i>											
												
	$\delta$ $S_1$	$\delta$ $S_1$	$\delta$ $S_1$	$\delta$ $S_1$	$\delta$ $S_1$	$\delta$ $S_1$	$\delta$ $S_1$	$\delta$ $S_1$	$\delta$ $S_1$	$\delta$ $S_1$	$\delta$ $S_1$	$\delta$ $S_1$
$x_{10}$	0.1761	0.2482	0.1520	0.1695	0.1623	0.1613	0.1703	0.1596	0.1697	0.1554	0.1769	0.1539
$x_9$	0.0801	0.0343	0.0814	0.0179	0.0777	0.0141	0.0784	0.0146	0.0738	0.0144	0.0901	0.0147
$x_8$	0.0582	0.0011	0.0623	0.0015	0.0543	0.0009	0.0554	0.0010	0.0632	0.0011	0.0783	0.0013
$x_7$	0.0828	0.0300	0.0723	0.0238	0.0843	0.0255	0.0841	0.0266	0.0870	0.0263	0.0997	0.0273
$x_6$	0.0674	0.0085	0.0652	0.0031	0.0595	0.0025	0.0554	0.0026	0.0563	0.0024	0.0675	0.0022
$x_5$	0.0549	0.0038	0.0612	0.0044	0.0535	0.0048	0.0587	0.0050	0.0620	0.0054	0.0612	0.0056
$x_4$	0.0831	0.0373	0.0947	0.0364	0.0772	0.0281	0.0886	0.0256	0.0896	0.0238	0.0985	0.0238
$x_3$	0.1188	0.0838	0.1681	0.1231	0.1449	0.0904	0.1342	0.0815	0.1124	0.0679	0.1289	0.0594
$x_2$	0.1831	0.2217	0.1916	0.1474	0.1867	0.1825	0.1882	0.1878	0.2015	0.1925	0.2247	0.1801
$x_1$	0.0599	0.0053	0.0738	0.0033	0.0482	0.0035	0.0557	0.0032	0.0570	0.0030	0.0601	0.0031

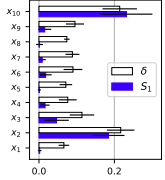
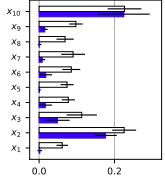
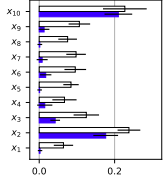
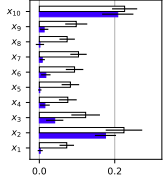
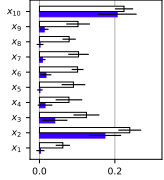
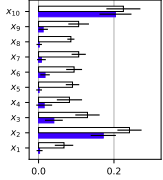
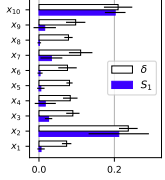
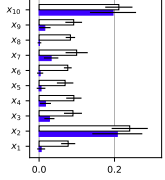
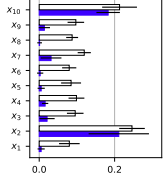
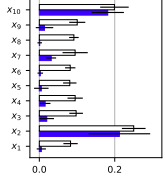
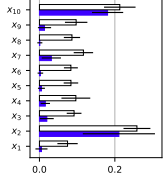
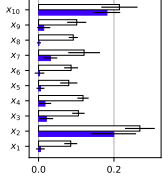
$X = \{x_i\}_{i=1}^{10} = \{\text{density, grain\_radius, pore\_size, youngs\_modulus, gb\_thickness, A1, A2, A3, B1, B2}\}$

TABLE IX. Delta moment-independent analysis of selected input parameters on the *crack damage in hoop direction* for both undoped and doped fuel rodlets. The sensitivity measures are uncertainty importance measure,  $\delta$  and first-order Sobol' indices,  $S_1$ , which vary between zero and one. The larger the sensitivity measure, the more influential the parameter is. The LHS sampling is considered with  $N = 1024$ .

X	Y : Crack damage in hoop direction											
	Undoped fuel rodlets											
	10 MWd/kgU	20 MWd/kgU	30 MWd/kgU	40 MWd/kgU	50 MWd/kgU	60 MWd/kgU						
												
	$\delta$ $S_1$	$\delta$ $S_1$	$\delta$ $S_1$	$\delta$ $S_1$	$\delta$ $S_1$	$\delta$ $S_1$						
$x_{10}$	0.1345	0.0045	0.0689	0.0281	0.0748	0.0159	0.1071	0.0181	0.1067	0.0188	0.1135	0.0206
$x_9$	0.0669	0.0032	0.0751	0.0069	0.0669	0.0034	0.1154	0.0018	0.1187	0.0019	0.1197	0.0023
$x_8$	0.1583	0.0050	0.0813	0.0028	0.0581	0.0054	0.1147	0.0040	0.1291	0.0040	0.1263	0.0040
$x_7$	0.2217	0.0177	0.0781	0.0079	0.0689	0.0089	0.1075	0.0104	0.1176	0.0109	0.1245	0.0113
$x_6$	0.1123	0.0037	0.0842	0.0025	0.0620	0.0021	0.1120	0.0103	0.1181	0.0083	0.1201	0.0067
$x_5$	0.0231	0.0027	0.0807	0.0029	0.0629	0.0080	0.1137	0.0019	0.1286	0.0017	0.1277	0.0022
$x_4$	0.0826	0.0041	0.0716	0.0316	0.1651	0.1641	0.1192	0.0256	0.1315	0.0141	0.1266	0.0147
$x_3$	0.4652	0.0206	0.1573	0.0855	0.2639	0.4676	0.1365	0.1541	0.1290	0.0694	0.1249	0.0557
$x_2$	0.5627	0.0513	0.1187	0.1940	0.1123	0.0262	0.3115	0.0550	0.3388	0.0790	0.3360	0.0890
$x_1$	0.0899	0.0059	0.0889	0.0163	0.0866	0.0656	0.1056	0.0133	0.1124	0.0080	0.1176	0.0073
	Doped fuel rodlets											
												
	$\delta$ $S_1$	$\delta$ $S_1$	$\delta$ $S_1$	$\delta$ $S_1$	$\delta$ $S_1$	$\delta$ $S_1$						
$x_{10}$	0.2178	0.0059	0.0722	0.0227	0.0781	0.0108	0.1092	0.0179	0.1233	0.0211	0.1309	0.0184
$x_9$	0.1622	0.0049	0.0817	0.0044	0.0749	0.0010	0.1198	0.0005	0.1292	0.0007	0.1290	0.0011
$x_8$	0.1559	0.0089	0.0706	0.0042	0.0711	0.0070	0.1147	0.0057	0.1250	0.0050	0.1248	0.0056
$x_7$	0.0907	0.0091	0.0766	0.0107	0.0780	0.0094	0.1066	0.0023	0.1092	0.0022	0.1206	0.0020
$x_6$	0.0961	0.0040	0.0870	0.0031	0.0717	0.0037	0.1242	0.0107	0.1299	0.0104	0.1212	0.0097
$x_5$	0.0498	0.0015	0.0835	0.0032	0.0755	0.0017	0.1138	0.0033	0.1212	0.0043	0.1139	0.0037
$x_4$	0.1996	0.0129	0.1021	0.0688	0.1263	0.1507	0.1353	0.0302	0.1370	0.0220	0.1255	0.0285
$x_3$	0.3722	0.0098	0.1792	0.1136	0.2642	0.4689	0.1329	0.0889	0.1217	0.0489	0.1226	0.0463
$x_2$	0.6337	0.0598	0.0891	0.1688	0.1285	0.0450	0.2518	0.0614	0.2737	0.0691	0.2855	0.0955
$x_1$	0.2330	0.0145	0.1051	0.0350	0.1220	0.0555	0.1237	0.0089	0.1011	0.0067	0.1006	0.0065

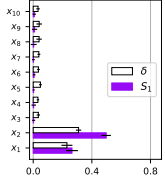
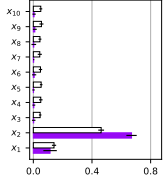
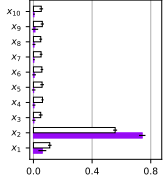
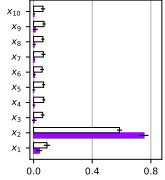
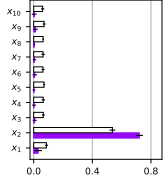
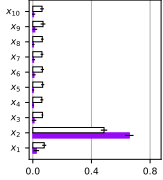
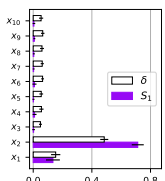
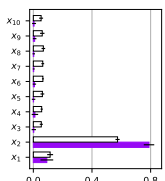
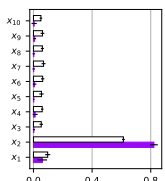
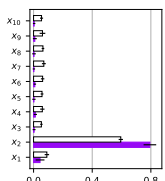
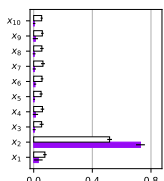
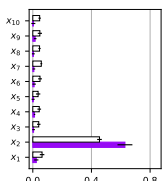
$X = \{x_i\}_{i=1}^{10} = \{\text{density, grain\_radius, pore\_size, youngs\_modulus, gb\_thickness, A1, A2, A3, B1, B2}\}$

TABLE X. Delta moment-independent analysis of selected input parameters on the *crack damage in radial direction* for both undoped and doped fuel rodlets. The sensitivity measures are uncertainty importance measure,  $\delta$  and first-order Sobol' indices,  $S_1$ , which vary between zero and one. The larger the sensitivity measure, the more influential the parameter is. The LHS sampling is considered with  $N = 1024$ .

X	Y : Crack damage in radial direction											
	<i>Undoped fuel rodlets</i>											
	10 MWd/kgU		20 MWd/kgU		30 MWd/kgU		40 MWd/kgU		50 MWd/kgU		60 MWd/kgU	
												
	$\delta$	$S_1$	$\delta$	$S_1$	$\delta$	$S_1$	$\delta$	$S_1$	$\delta$	$S_1$	$\delta$	$S_1$
$x_{10}$	0.2142	0.2322	0.2265	0.2247	0.2271	0.2099	0.2262	0.2080	0.2243	0.2061	0.2250	0.2040
$x_9$	0.0955	0.0153	0.0977	0.0150	0.1065	0.0130	0.0979	0.0127	0.1024	0.0126	0.1063	0.0122
$x_8$	0.0740	0.0015	0.0690	0.0014	0.0754	0.0016	0.0738	0.0016	0.0788	0.0017	0.0857	0.0017
$x_7$	0.0887	0.0087	0.0902	0.0084	0.0978	0.0078	0.1039	0.0078	0.1037	0.0077	0.1065	0.0075
$x_6$	0.0902	0.0178	0.0854	0.0178	0.0957	0.0172	0.0934	0.0173	0.1012	0.0173	0.0943	0.0172
$x_5$	0.0713	0.0010	0.0742	0.0011	0.0843	0.0011	0.0824	0.0012	0.0902	0.0013	0.0901	0.0014
$x_4$	0.0764	0.0162	0.0776	0.0164	0.0670	0.0147	0.0756	0.0148	0.0783	0.0148	0.0819	0.0149
$x_3$	0.1140	0.0467	0.1131	0.0487	0.1250	0.0424	0.1229	0.0408	0.1247	0.0407	0.1297	0.0406
$x_2$	0.2168	0.1846	0.2256	0.1762	0.2380	0.1764	0.2245	0.1755	0.2396	0.1738	0.2412	0.1717
$x_1$	0.0661	0.0019	0.0614	0.0019	0.0643	0.0022	0.0728	0.0024	0.0621	0.0025	0.0675	0.0027
	<i>Doped fuel rodlets</i>											
	10 MWd/kgU		20 MWd/kgU		30 MWd/kgU		40 MWd/kgU		50 MWd/kgU		60 MWd/kgU	
												
	$\delta$	$S_1$	$\delta$	$S_1$	$\delta$	$S_1$	$\delta$	$S_1$	$\delta$	$S_1$	$\delta$	$S_1$
$x_{10}$	0.2112	0.2022	0.2056	0.1961	0.2103	0.1829	0.2118	0.1815	0.2041	0.1807	0.2138	0.1813
$x_9$	0.0849	0.0152	0.0891	0.0152	0.0970	0.0137	0.0921	0.0137	0.0883	0.0134	0.0966	0.0137
$x_8$	0.0804	0.0009	0.0773	0.0010	0.0868	0.0011	0.0849	0.0011	0.0904	0.0010	0.0914	0.0011
$x_7$	0.1016	0.0329	0.1094	0.0319	0.1024	0.0314	0.1200	0.0315	0.1163	0.0315	0.1036	0.0313
$x_6$	0.0763	0.0029	0.0716	0.0028	0.0861	0.0025	0.0829	0.0025	0.0837	0.0025	0.0870	0.0025
$x_5$	0.0731	0.0050	0.0744	0.0052	0.0775	0.0053	0.0853	0.0052	0.0809	0.0053	0.0802	0.0051
$x_4$	0.0923	0.0167	0.0914	0.0168	0.1001	0.0157	0.1011	0.0154	0.0975	0.0156	0.1097	0.0170
$x_3$	0.0959	0.0255	0.0868	0.0274	0.0941	0.0209	0.0922	0.0197	0.0999	0.0196	0.1058	0.0206
$x_2$	0.2442	0.2116	0.2470	0.2074	0.2543	0.2111	0.2533	0.2123	0.2601	0.2107	0.2823	0.1994
$x_1$	0.0729	0.0055	0.0720	0.0055	0.0852	0.0051	0.0799	0.0053	0.0767	0.0053	0.0789	0.0049

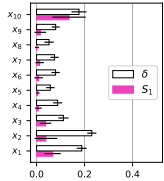
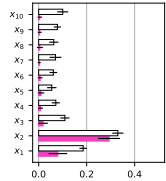
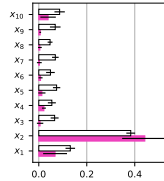
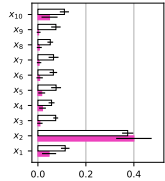
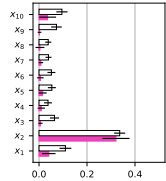
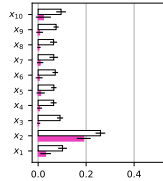
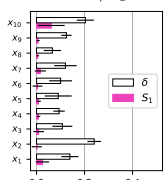
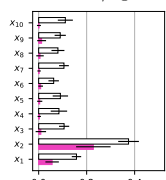
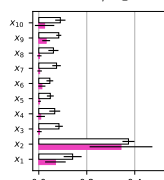
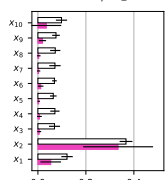
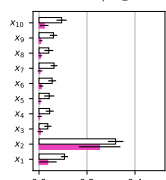
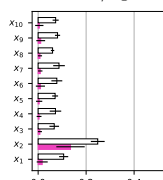
$X = \{x_i\}_{i=1}^{10} = \{\text{density, grain\_radius, pore\_size, youngs\_modulus, gb\_thickness, A1, A2, A3, B1, B2}\}$

TABLE XI. Delta moment-independent analysis of selected input parameters on the *fission gas release* for both undoped and doped fuel rodlets. The sensitivity measures are uncertainty importance measure,  $\delta$  and first-order Sobol' indices,  $S_1$ , which vary between zero and one. The larger the sensitivity measure, the more influential the parameter is. The LHS sampling is considered with  $N = 1024$ .

X	Y : Fission gas release											
	Undoped fuel rodlets											
	10 MWd/kgU	20 MWd/kgU	30 MWd/kgU	40 MWd/kgU	50 MWd/kgU	60 MWd/kgU	10 MWd/kgU	20 MWd/kgU	30 MWd/kgU	40 MWd/kgU	50 MWd/kgU	60 MWd/kgU
												
	$\delta$	$S_1$	$\delta$	$S_1$	$\delta$	$S_1$	$\delta$	$S_1$	$\delta$	$S_1$	$\delta$	$S_1$
$x_{10}$	0.0330	0.0074	0.0508	0.0051	0.0534	0.0037	0.0645	0.0026	0.0612	0.0037	0.0631	0.0058
$x_9$	0.0408	0.0091	0.0553	0.0101	0.0605	0.0104	0.0714	0.0114	0.0712	0.0124	0.0698	0.0139
$x_8$	0.0401	0.0033	0.0452	0.0032	0.0499	0.0038	0.0636	0.0045	0.0644	0.0040	0.0648	0.0033
$x_7$	0.0386	0.0014	0.0439	0.0023	0.0522	0.0030	0.0668	0.0045	0.0642	0.0054	0.0627	0.0057
$x_6$	0.0355	0.0064	0.0488	0.0056	0.0576	0.0048	0.0586	0.0056	0.0634	0.0070	0.0654	0.0081
$x_5$	0.0492	0.0028	0.0535	0.0014	0.0592	0.0016	0.0687	0.0014	0.0708	0.0016	0.0674	0.0018
$x_4$	0.0323	0.0035	0.0507	0.0035	0.0617	0.0036	0.0695	0.0027	0.0650	0.0023	0.0616	0.0026
$x_3$	0.0351	0.0026	0.0466	0.0026	0.0495	0.0033	0.0624	0.0047	0.0655	0.0069	0.0656	0.0088
$x_2$	0.3093	0.4977	0.4626	0.6698	0.5573	0.7419	0.5858	0.7535	0.5368	0.7206	0.4858	0.6585
$x_1$	0.2300	0.2646	0.1412	0.1142	0.1115	0.0605	0.0915	0.0394	0.0870	0.0303	0.0780	0.0240
	Doped fuel rodlets											
												
	$\delta$	$S_1$	$\delta$	$S_1$	$\delta$	$S_1$	$\delta$	$S_1$	$\delta$	$S_1$	$\delta$	$S_1$
$x_{10}$	0.0539	0.0049	0.0531	0.0050	0.0510	0.0050	0.0543	0.0039	0.0544	0.0033	0.0467	0.0036
$x_9$	0.0650	0.0078	0.0609	0.0090	0.0617	0.0085	0.0607	0.0086	0.0590	0.0115	0.0482	0.0161
$x_8$	0.0599	0.0040	0.0684	0.0029	0.0690	0.0027	0.0641	0.0030	0.0560	0.0032	0.0460	0.0035
$x_7$	0.0617	0.0028	0.0644	0.0026	0.0609	0.0021	0.0701	0.0022	0.0633	0.0042	0.0580	0.0073
$x_6$	0.0639	0.0085	0.0653	0.0074	0.0629	0.0078	0.0618	0.0087	0.0570	0.0091	0.0493	0.0090
$x_5$	0.0548	0.0019	0.0617	0.0016	0.0547	0.0023	0.0577	0.0024	0.0507	0.0028	0.0363	0.0022
$x_4$	0.0561	0.0091	0.0569	0.0109	0.0598	0.0116	0.0598	0.0120	0.0597	0.0120	0.0440	0.0117
$x_3$	0.0494	0.0028	0.0544	0.0032	0.0534	0.0033	0.0534	0.0036	0.0542	0.0037	0.0405	0.0053
$x_2$	0.4845	0.7130	0.5745	0.7889	0.6134	0.8215	0.5949	0.7934	0.5178	0.7282	0.4548	0.6284
$x_1$	0.1533	0.1345	0.1146	0.0920	0.0972	0.0607	0.0907	0.0442	0.0765	0.0317	0.0632	0.0239

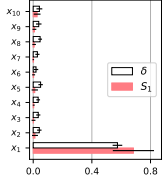
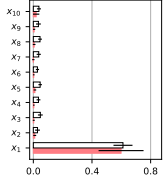
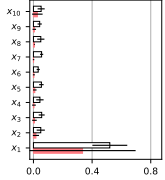
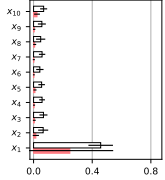
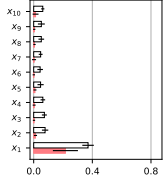
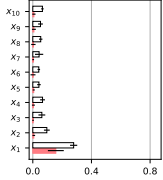
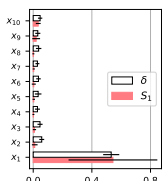
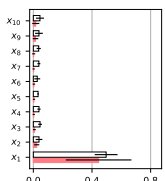
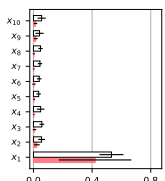
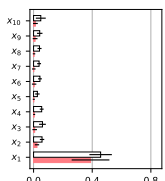
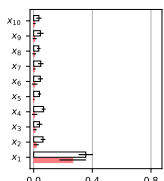
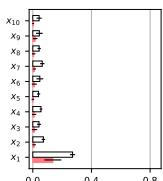
$X = \{x_i\}_{i=1}^{10} = \{\text{density, grain\_radius, pore\_size, youngs\_modulus, gb\_thickness, A1, A2, A3, B1, B2}\}$

TABLE XII. Delta moment-independent analysis of selected input parameters on the *fuel elongation* for both undoped and doped fuel rodlets. The sensitivity measures are uncertainty importance measure,  $\delta$  and first-order Sobol' indices,  $S_1$ , which vary between zero and one. The larger the sensitivity measure, the more influential the parameter is. The LHS sampling is considered with  $N = 1024$ .

X	Y : Fuel elongation											
	Undoped fuel rodlets											
	10 MWd/kgU		20 MWd/kgU		30 MWd/kgU		40 MWd/kgU		50 MWd/kgU		60 MWd/kgU	
												
	$\delta$	$S_1$	$\delta$	$S_1$	$\delta$	$S_1$	$\delta$	$S_1$	$\delta$	$S_1$	$\delta$	$S_1$
$x_{10}$	0.1768	0.1353	0.1004	0.0044	0.0869	0.0388	0.1104	0.0485	0.0954	0.0359	0.0956	0.0217
$x_9$	0.0797	0.0156	0.0781	0.0044	0.0686	0.0060	0.0750	0.0032	0.0728	0.0022	0.0749	0.0062
$x_8$	0.0521	0.0019	0.0631	0.0052	0.0470	0.0046	0.0516	0.0058	0.0384	0.0039	0.0644	0.0035
$x_7$	0.0751	0.0128	0.0701	0.0024	0.0690	0.0022	0.0652	0.0049	0.0395	0.0078	0.0652	0.0084
$x_6$	0.0794	0.0086	0.0612	0.0063	0.0486	0.0074	0.0645	0.0073	0.0516	0.0057	0.0714	0.0043
$x_5$	0.0574	0.0054	0.0547	0.0099	0.0743	0.0129	0.0758	0.0159	0.0535	0.0150	0.0655	0.0106
$x_4$	0.0880	0.0077	0.0716	0.0077	0.0544	0.0213	0.0570	0.0191	0.0376	0.0095	0.0646	0.0061
$x_3$	0.1119	0.0380	0.1093	0.0183	0.0661	0.0055	0.0742	0.0084	0.0645	0.0058	0.0913	0.0024
$x_2$	0.2303	0.0393	0.3301	0.2937	0.3833	0.4421	0.3743	0.4002	0.3363	0.3208	0.2596	0.1902
$x_1$	0.1884	0.0674	0.1855	0.0800	0.1314	0.0679	0.1139	0.0466	0.1100	0.0409	0.1018	0.0313
	Doped fuel rodlets											
												
	$\delta$	$S_1$	$\delta$	$S_1$	$\delta$	$S_1$	$\delta$	$S_1$	$\delta$	$S_1$	$\delta$	$S_1$
$x_{10}$	0.2036	0.0612	0.1112	0.0010	0.0898	0.0242	0.0984	0.0351	0.0942	0.0219	0.0730	0.0048
$x_9$	0.1245	0.0063	0.0899	0.0123	0.0833	0.0308	0.0755	0.0191	0.0603	0.0076	0.0809	0.0108
$x_8$	0.0662	0.0047	0.0804	0.0056	0.0610	0.0026	0.0724	0.0035	0.0408	0.0055	0.0601	0.0077
$x_7$	0.1205	0.0157	0.1054	0.0018	0.0741	0.0035	0.0711	0.0030	0.0625	0.0040	0.0870	0.0089
$x_6$	0.1003	0.0041	0.0626	0.0083	0.0462	0.0128	0.0689	0.0117	0.0548	0.0091	0.0779	0.0094
$x_5$	0.0903	0.0084	0.0905	0.0044	0.0481	0.0033	0.0641	0.0034	0.0424	0.0039	0.0708	0.0042
$x_4$	0.0939	0.0081	0.0845	0.0025	0.0665	0.0081	0.0709	0.0064	0.0444	0.0029	0.0722	0.0039
$x_3$	0.1076	0.0087	0.1060	0.0091	0.0842	0.0022	0.0692	0.0055	0.0367	0.0052	0.0671	0.0075
$x_2$	0.2405	0.0014	0.3746	0.2279	0.3739	0.3427	0.3673	0.3343	0.3192	0.2525	0.2485	0.1350
$x_1$	0.1391	0.0246	0.1576	0.0561	0.1411	0.0693	0.1214	0.0535	0.1060	0.0363	0.1064	0.0169

$X = \{x_i\}_{i=1}^{10} = \{\text{density, grain\_radius, pore\_size, youngs\_modulus, gb\_thickness, A1, A2, A3, B1, B2}\}$

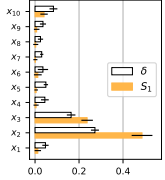
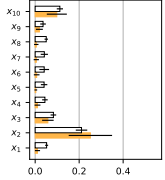
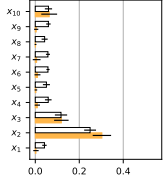
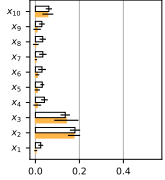
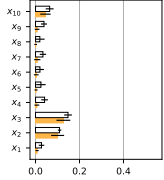
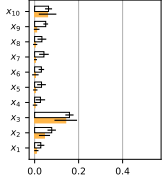
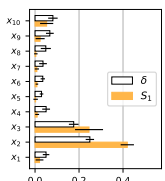
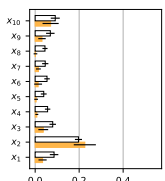
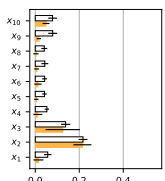
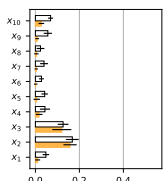
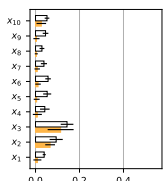
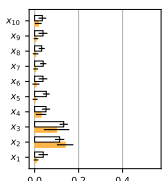
TABLE XIII. Delta moment-independent analysis of selected input parameters on the *maximum fuel centerline temperature* for both undoped and doped fuel rodlets. The sensitivity measures are uncertainty importance measure,  $\delta$  and first-order Sobol' indices,  $S_1$ , which vary between zero and one. The larger the sensitivity measure, the more influential the parameter is. The LHS sampling is considered with  $N = 1024$ .

X	Y : Maximum fuel centerline temperature											
	Undoped fuel rodlets											
	10 MWd/kgU	20 MWd/kgU	30 MWd/kgU	40 MWd/kgU	50 MWd/kgU	60 MWd/kgU	10 MWd/kgU	20 MWd/kgU	30 MWd/kgU	40 MWd/kgU	50 MWd/kgU	60 MWd/kgU
												
	$\delta$ $S_1$	$\delta$ $S_1$	$\delta$ $S_1$	$\delta$ $S_1$	$\delta$ $S_1$	$\delta$ $S_1$						
$x_{10}$	0.0421	0.0266	0.0382	0.0192	0.0525	0.0265	0.0687	0.0235	0.0620	0.0128	0.0657	0.0075
$x_9$	0.0376	0.0082	0.0347	0.0053	0.0425	0.0059	0.0566	0.0040	0.0522	0.0036	0.0524	0.0074
$x_8$	0.0471	0.0062	0.0456	0.0055	0.0501	0.0059	0.0486	0.0076	0.0519	0.0055	0.0540	0.0039
$x_7$	0.0286	0.0008	0.0368	0.0001	0.0556	0.0007	0.0581	0.0018	0.0475	0.0024	0.0430	0.0025
$x_6$	0.0192	0.0028	0.0281	0.0027	0.0326	0.0028	0.0429	0.0018	0.0440	0.0009	0.0410	0.0013
$x_5$	0.0504	0.0106	0.0466	0.0108	0.0542	0.0092	0.0550	0.0096	0.0470	0.0087	0.0419	0.0061
$x_4$	0.0339	0.0034	0.0351	0.0033	0.0442	0.0035	0.0580	0.0031	0.0626	0.0030	0.0664	0.0040
$x_3$	0.0345	0.0020	0.0477	0.0027	0.0561	0.0068	0.0675	0.0049	0.0729	0.0020	0.0617	0.0015
$x_2$	0.0415	0.0120	0.0286	0.0096	0.0499	0.0169	0.0655	0.0155	0.0778	0.0122	0.0957	0.0068
$x_1$	0.5745	0.6834	0.6114	0.5984	0.5208	0.3349	0.4578	0.2475	0.3709	0.2164	0.2786	0.1570
	Doped fuel rodlets											
												
	$\delta$ $S_1$	$\delta$ $S_1$	$\delta$ $S_1$	$\delta$ $S_1$	$\delta$ $S_1$	$\delta$ $S_1$						
$x_{10}$	0.0471	0.0341	0.0452	0.0167	0.0556	0.0142	0.0492	0.0125	0.0356	0.0045	0.0431	0.0023
$x_9$	0.0313	0.0201	0.0384	0.0151	0.0416	0.0157	0.0419	0.0104	0.0457	0.0068	0.0445	0.0159
$x_8$	0.0370	0.0012	0.0367	0.0025	0.0483	0.0031	0.0405	0.0031	0.0347	0.0040	0.0434	0.0060
$x_7$	0.0287	0.0036	0.0378	0.0023	0.0447	0.0017	0.0377	0.0014	0.0483	0.0043	0.0646	0.0108
$x_6$	0.0359	0.0039	0.0268	0.0039	0.0394	0.0033	0.0435	0.0038	0.0454	0.0069	0.0480	0.0102
$x_5$	0.0338	0.0039	0.0325	0.0045	0.0357	0.0039	0.0259	0.0015	0.0392	0.0003	0.0392	0.0006
$x_4$	0.0291	0.0016	0.0385	0.0029	0.0492	0.0032	0.0554	0.0040	0.0675	0.0066	0.0559	0.0090
$x_3$	0.0465	0.0085	0.0459	0.0072	0.0574	0.0074	0.0607	0.0077	0.0398	0.0092	0.0424	0.0115
$x_2$	0.0582	0.0104	0.0388	0.0231	0.0553	0.0235	0.0579	0.0234	0.0636	0.0173	0.0722	0.0089
$x_1$	0.5320	0.5438	0.4966	0.4454	0.5320	0.4207	0.4574	0.3885	0.3554	0.2665	0.2712	0.1367

$X = \{x_i\}_{i=1}^{10} = \{\text{density, grain\_radius, pore\_size, youngs\_modulus, gb\_thickness, A1, A2, A3, B1, B2}\}$

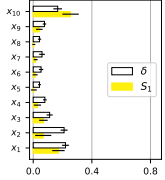
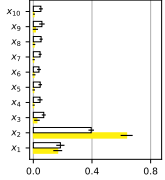
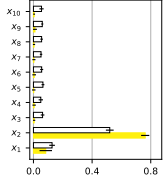
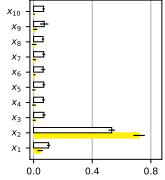
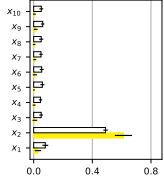
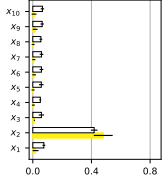
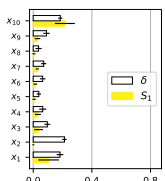
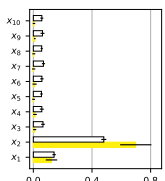
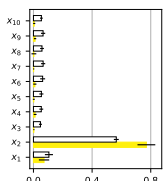
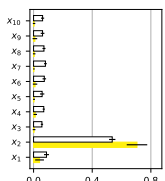
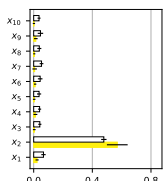
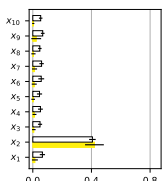


TABLE XIV. Delta moment-independent analysis of selected input parameters on the *maximum hoop stress* for both undoped and doped fuel rodlets. The sensitivity measures are uncertainty importance measure,  $\delta$  and first-order Sobol' indices,  $S_1$ , which vary between zero and one. The larger the sensitivity measure, the more influential the parameter is. The LHS sampling is considered with  $N = 1024$ .

X	Y : Maximum hoop stress											
	Undoped fuel rodlets											
	10 MWd/kgU		20 MWd/kgU		30 MWd/kgU		40 MWd/kgU		50 MWd/kgU		60 MWd/kgU	
												
	$\delta$	$S_1$	$\delta$	$S_1$	$\delta$	$S_1$	$\delta$	$S_1$	$\delta$	$S_1$	$\delta$	$S_1$
$x_{10}$	0.0836	0.0409	0.1123	0.0984	0.0600	0.0633	0.0612	0.0567	0.0643	0.0450	0.0632	0.0588
$x_9$	0.0360	0.0074	0.0358	0.0192	0.0597	0.0042	0.0296	0.0078	0.0385	0.0073	0.0504	0.0091
$x_8$	0.0248	0.0032	0.0504	0.0050	0.0425	0.0012	0.0334	0.0019	0.0197	0.0006	0.0330	0.0025
$x_7$	0.0303	0.0016	0.0417	0.0052	0.0576	0.0061	0.0339	0.0024	0.0338	0.0080	0.0423	0.0039
$x_6$	0.0359	0.0126	0.0411	0.0069	0.0578	0.0101	0.0301	0.0088	0.0202	0.0033	0.0307	0.0033
$x_5$	0.0493	0.0049	0.0407	0.0029	0.0506	0.0028	0.0314	0.0085	0.0246	0.0024	0.0313	0.0031
$x_4$	0.0446	0.0047	0.0443	0.0105	0.0589	0.0093	0.0411	0.0085	0.0412	0.0061	0.0263	0.0018
$x_3$	0.1640	0.2368	0.0830	0.0578	0.1169	0.1185	0.1357	0.1407	0.1477	0.1267	0.1583	0.1415
$x_2$	0.2723	0.4865	0.2107	0.2511	0.2492	0.3029	0.1800	0.1756	0.1093	0.1005	0.0777	0.0448
$x_1$	0.0473	0.0127	0.0521	0.0106	0.0417	0.0030	0.0242	0.0018	0.0272	0.0071	0.0280	0.0078
	Doped fuel rodlets											
	10 MWd/kgU		20 MWd/kgU		30 MWd/kgU		40 MWd/kgU		50 MWd/kgU		60 MWd/kgU	
												
	$\delta$	$S_1$	$\delta$	$S_1$	$\delta$	$S_1$	$\delta$	$S_1$	$\delta$	$S_1$	$\delta$	$S_1$
$x_{10}$	0.0827	0.0528	0.0900	0.0702	0.0773	0.0489	0.0697	0.0271	0.0586	0.0264	0.0352	0.0165
$x_9$	0.0664	0.0231	0.0670	0.0311	0.0763	0.0162	0.0603	0.0081	0.0421	0.0042	0.0351	0.0061
$x_8$	0.0505	0.0036	0.0474	0.0014	0.0405	0.0031	0.0249	0.0046	0.0248	0.0035	0.0312	0.0044
$x_7$	0.0361	0.0083	0.0504	0.0147	0.0431	0.0065	0.0385	0.0038	0.0395	0.0077	0.0445	0.0048
$x_6$	0.0320	0.0085	0.0527	0.0135	0.0453	0.0125	0.0308	0.0013	0.0588	0.0115	0.0369	0.0059
$x_5$	0.0260	0.0027	0.0403	0.0044	0.0432	0.0047	0.0412	0.0061	0.0457	0.0052	0.0480	0.0023
$x_4$	0.0474	0.0095	0.0558	0.0076	0.0518	0.0115	0.0437	0.0166	0.0468	0.0083	0.0552	0.0294
$x_3$	0.1768	0.2455	0.0845	0.0368	0.1336	0.1249	0.1227	0.1202	0.1403	0.1142	0.1307	0.0996
$x_2$	0.2507	0.4195	0.2084	0.2258	0.2171	0.2142	0.1657	0.1576	0.0966	0.0663	0.1162	0.1387
$x_1$	0.0529	0.0204	0.0871	0.0336	0.0547	0.0145	0.0471	0.0099	0.0356	0.0085	0.0420	0.0066

$X = \{x_i\}_{i=1}^{10} = \{\text{density, grain\_radius, pore\_size, youngs\_modulus, gb\_thickness, A1, A2, A3, B1, B2}\}$

TABLE XV. Delta moment-independent analysis of selected input parameters on the *plenum pressure* for both undoped and doped fuel rodlets. The sensitivity measures are uncertainty importance measure,  $\delta$  and first-order Sobol' indices,  $S_1$ , which vary between zero and one. The larger the sensitivity measure, the more influential the parameter is. The LHS sampling is considered with  $N = 1024$ .

X	Y : Plenum pressure											
	Undoped fuel rodlets											
	10 MWd/kgU	20 MWd/kgU	30 MWd/kgU	40 MWd/kgU	50 MWd/kgU	60 MWd/kgU	10 MWd/kgU	20 MWd/kgU	30 MWd/kgU	40 MWd/kgU	50 MWd/kgU	60 MWd/kgU
												
	$\delta$ $S_1$	$\delta$ $S_1$	$\delta$ $S_1$	$\delta$ $S_1$	$\delta$ $S_1$	$\delta$ $S_1$	$\delta$ $S_1$	$\delta$ $S_1$	$\delta$ $S_1$	$\delta$ $S_1$	$\delta$ $S_1$	$\delta$ $S_1$
$x_{10}$	0.1670	0.2547	0.0515	0.0046	0.0551	0.0046	0.0681	0.0030	0.0520	0.0050	0.0655	0.0089
$x_9$	0.0771	0.0417	0.0586	0.0143	0.0603	0.0105	0.0728	0.0110	0.0614	0.0135	0.0638	0.0160
$x_8$	0.0433	0.0040	0.0530	0.0049	0.0557	0.0039	0.0645	0.0045	0.0513	0.0034	0.0551	0.0024
$x_7$	0.0601	0.0167	0.0462	0.0026	0.0519	0.0032	0.0696	0.0059	0.0501	0.0073	0.0595	0.0071
$x_6$	0.0538	0.0131	0.0386	0.0044	0.0561	0.0050	0.0659	0.0060	0.0547	0.0080	0.0590	0.0089
$x_5$	0.0429	0.0045	0.0469	0.0030	0.0648	0.0022	0.0699	0.0017	0.0593	0.0017	0.0580	0.0018
$x_4$	0.0796	0.0286	0.0457	0.0024	0.0501	0.0046	0.0670	0.0029	0.0470	0.0027	0.0513	0.0039
$x_3$	0.1119	0.0694	0.0712	0.0245	0.0623	0.0048	0.0706	0.0047	0.0512	0.0082	0.0586	0.0110
$x_2$	0.2106	0.0684	0.3948	0.6365	0.5205	0.7623	0.5332	0.7202	0.4901	0.6121	0.4184	0.4803
$x_1$	0.2201	0.1721	0.1845	0.1665	0.1271	0.0840	0.1029	0.0449	0.0792	0.0292	0.0754	0.0190
	Doped fuel rodlets											
												
	$\delta$ $S_1$	$\delta$ $S_1$	$\delta$ $S_1$	$\delta$ $S_1$	$\delta$ $S_1$	$\delta$ $S_1$	$\delta$ $S_1$	$\delta$ $S_1$	$\delta$ $S_1$	$\delta$ $S_1$	$\delta$ $S_1$	$\delta$ $S_1$
$x_{10}$	0.1847	0.2159	0.0580	0.0044	0.0542	0.0053	0.0616	0.0035	0.0365	0.0017	0.0538	0.0033
$x_9$	0.0906	0.0291	0.0625	0.0099	0.0658	0.0113	0.0613	0.0090	0.0461	0.0146	0.0677	0.0234
$x_8$	0.0365	0.0054	0.0570	0.0033	0.0583	0.0031	0.0710	0.0042	0.0384	0.0042	0.0480	0.0044
$x_7$	0.0716	0.0283	0.0690	0.0022	0.0661	0.0014	0.0808	0.0022	0.0535	0.0066	0.0599	0.0118
$x_6$	0.0643	0.0140	0.0586	0.0086	0.0627	0.0096	0.0733	0.0102	0.0442	0.0101	0.0575	0.0098
$x_5$	0.0382	0.0063	0.0555	0.0020	0.0541	0.0024	0.0585	0.0030	0.0368	0.0034	0.0457	0.0025
$x_4$	0.0651	0.0319	0.0578	0.0112	0.0535	0.0113	0.0696	0.0116	0.0403	0.0117	0.0521	0.0116
$x_3$	0.0962	0.0367	0.0659	0.0092	0.0477	0.0029	0.0571	0.0035	0.0420	0.0039	0.0493	0.0071
$x_2$	0.2131	0.0011	0.4808	0.6984	0.5650	0.7703	0.5366	0.7053	0.4785	0.5701	0.4065	0.4204
$x_1$	0.1827	0.1055	0.1416	0.1237	0.1055	0.0722	0.0881	0.0409	0.0668	0.0232	0.0655	0.0143

$X = \{x_i\}_{i=1}^{10} = \{\text{density, grain\_radius, pore\_size, youngs\_modulus, gb\_thickness, A1, A2, A3, B1, B2}\}$

## V. HALDEN IFA-677.1 AND IFA-716.1

This section presents the BISON simulation and comparisons of the predictions to the available experimental data of fuel centerline temperature, FGR, rod internal pressure, and/or fuel stack elongation for Halden IFA-677.1 and IFA-716.1 Rods in Section V-A and Section V-B, respectively. These results contribute to the assessment of BISON for the analysis of  $\text{UO}_2$  and chromia ( $\text{Cr}_2\text{O}_3$ )-doped  $\text{UO}_2$  fueled light-water reactor (LWR) rods. These assessment cases are made available in the BISON assessment database as a part of the present milestone and another Nuclear Energy Advanced Modeling and Simulation (NEAMS) milestone by Singh et al. (2022).

### A. Halden IFA-677.1 Rods 1 and 5

The High Initial Rating Test Integrated Fuel Assembly (IFA)-677.1 (Jošek, 2008; Jenssen, 2010) was performed in the Halden Reactor Project with the aim to investigate the performance of modern fuels subjected to high initial rating with respect to thermal behavior, dimensional changes (densification and swelling), FGR and pellet-clad mechanical interaction (PCMI). The test rig contained six rods supplied by Westinghouse, Framatome ANP and GNF. Two of the rods contained  $\text{UO}_2$  fuel doped with  $\text{Cr}_2\text{O}_3$  and  $\text{Al}_2\text{O}_3$ . All rods were instrumented with pressure transducers, fuel centerline thermocouples (TCs) in both ends and fuel stack elongation detectors, in addition to a cladding extensometer on one of the rods. The test assembly was loaded in the Halden reactor in December 2004, and it completed six cycles of irradiation under Halden Boiling Water Reactor (HBWR) conditions in September 2007, achieving a rig average burnup of  $\sim 26.3$  MWd/kgOX.

#### 1) Test Description

The IFA-677.1 rig contained a single cluster of six rods with an active fuel length of about 400 mm and an initial fuel enrichment of about 4.95%. IFA-677.1 Rod 1 contained doped  $\text{UO}_2$  fuel with 900 ppm  $\text{Cr}_2\text{O}_3$  and 200 ppm  $\text{Al}_2\text{O}_3$ , meanwhile Rod 5 contained doped  $\text{UO}_2$  fuel with 500 ppm  $\text{Cr}_2\text{O}_3$  and 200 ppm  $\text{Al}_2\text{O}_3$ . The doped fuel has both higher density and larger grain size than standard  $\text{UO}_2$ . The main characteristics of Rods 1 and 5 are summarized in Table XVI.

#### 2) Operating Conditions and Irradiation History

The test rig was operated under standard HBWR conditions, i.e., natural circulation at a coolant pressure of 34 bar and saturation temperature of  $\sim 235^\circ\text{C}$ , experiencing 842 full power days of accumulated operation. The final average assembly burnup is 31.8 MWd/kgOX (Baurens, 2016). The average linear heat rates (LHRs) were kept below the FGR threshold during the first six irradiation cycles, and an assembly average burnup of 17 MWd/kgOX was reached by the end of this period. Later, the LHR was elevated slowly to bring the fuel temperature above the FGR threshold to study the FGR performance. The power level was later kept close to the FGR threshold.

#### 3) Material and Behavioral Models

The following material and behavioral models for  $\text{UO}_2$  fuel were used: (i) HALDEN model is chosen to compute temperature- and burnup-dependent thermal properties via `UO2Thermal`; (ii) MATPRO and LLS-informed (Equation 2) models are chosen to compute fuel creep mechanical behavior via `UO2CreepUpdate`; (iii) isotropic elastic mechanical behavior via `UO2ElasticityTensor`; (iv) relocation strains, relocation activation threshold power set to 5 kW/m, via `UO2RelocationEigenstrain`; (v) MATPRO model for fuel thermal expansion via `UO2ThermalExpansionMATPROEigenstrain`; (vi) expansion due to solid and gaseous swelling via `UO2VolumetricSwellingEigenstrain`;

TABLE XVI. Fabrication characteristics of IFA-677.1 Rods 1 and 5

	Rod 1	Rod 5
Cladding material	Zry-4	Zry-4
Fuel material	doped UO <sub>2</sub>	doped UO <sub>2</sub>
Fill gas	He	He
Total rod length (mm)	456.0	459.5
Total active fuel stack length (mm)	398.6	403.5
Drilled active section length, <i>top</i> (mm)	109.2	111.0
Drilled active section length, <i>bottom</i> (mm)	109.7	111.1
Pellet inner diameter, <i>drilled sections</i> (mm)	1.8	1.8
Pellet outer diameter (mm)	9.13	9.13
Diametral gap ( $\mu\text{m}$ )	170	170
Cladding thickness (mm)	0.725	0.725
Cladding outer diameter (mm)	10.75	10.75
Free volume ( $\text{cm}^3$ )	5.34	5.26
Fill gas pressure (MPa)	1.35	1.35
Fuel Cr <sub>2</sub> O <sub>3</sub> content (ppm)	900	500
Fuel Al <sub>2</sub> O <sub>3</sub> content (ppm)	200	200
Fuel U-235 enrichment (%)	4.94	4.94
Initial fuel density ( $\text{kg/m}^3$ )	10690	10700
Fuel average grain radius ( $\mu\text{m}$ )	28.0	22.5

and (vii) FGR model, `Sifgrs` with the combined gaseous swelling model (Pastore et al., 2015) via `UO2VolumetricSwellingEigenstrain`. In addition, the following settings were adopted that are specific to Cr<sub>2</sub>O<sub>3</sub>-doped UO<sub>2</sub> fuel analysis:

- Specific option for the lattice diffusion coefficient of fission gas atoms in the SIFGRS FGR and swelling model. The diffusion coefficient for UO<sub>2</sub> is scaled with a temperature-dependent correction developed at LANL (Cooper et al., 2018). This correction accounts for the increased diffusivity in Cr<sub>2</sub>O<sub>3</sub>-doped UO<sub>2</sub> relative to standard UO<sub>2</sub>. This is associated with a higher uranium vacancy concentration in doped fuel.
- Cr<sub>2</sub>O<sub>3</sub>-doped UO<sub>2</sub> is characterized by a larger grain size than standard UO<sub>2</sub>. In contrast to enhanced diffusivity, the larger grain radius tends to reduce FGR due to the associated larger intra-granular diffusion distance for gas atoms to travel before reaching the grain boundaries. The reported average grain radius for IFA-677.1 Rod 1 is 28 $\mu\text{m}$  and Rod 5 is 22.5 $\mu\text{m}$  (Jošek, 2008; Jenssen, 2010). Accordingly, this value has been set for the fission gas model, which in turn utilizes it in the fission gas atom diffusion calculation. The grain radius is used in the fuel creep model as well.
- A total densification in the MATPRO densification model of 0.09%. This is consistent with the experimental indications (Jošek, 2008; Jenssen, 2010) and with the lower densification expected in Cr<sub>2</sub>O<sub>3</sub>-doped UO<sub>2</sub> relative to standard UO<sub>2</sub>.

The following material and behavioral models were used for the Zircaloy-4 cladding: (i) isotropic thermal properties of Zircaloy are computed via `ZryThermal`; (ii) mechanical creep and elastic deformation behavior are computed via `ZryCreepLimbackHoppeUpdate` and `ZryElasticityTensor`;

(iii) ESCORE model is chosen to compute the volumetric swelling due to irradiation exposure via `ZryIrradiationGrowthEigenstrain`; (iv) MATPRO model is chosen to compute the thermal expansion of Zircaloy via `ZryThermalExpansionMATPROEigenstrain`; and (v) EPRI/KWU/C-E model is chosen to compute the waterside oxidation of the Zircaloy cladding via `ZryOxidation`.

#### 4) Boundary and operating conditions

The average LHR history for Rods 1 and 5 are illustrated in Figure 21, based on the Halden data. A modification to the average linear heat rate is required based on the information provided in (Weisenak, 2019). An approximate 2% reduction in the average linear power is applied to the power after a burnup of approximately 14.5 MWd/kgU and lasting until the end of the irradiation. This reduction the power occurred due to changes in the reactor environment near the IFA-667.1 rig. A second change was also applied to the axial profile including a reduction in power at the bottom (1.5%) and top (3.5%) power nodes, a slight increase at the upper and lower TCs (2.6%), and a larger increase at the middle power node (4.3%).

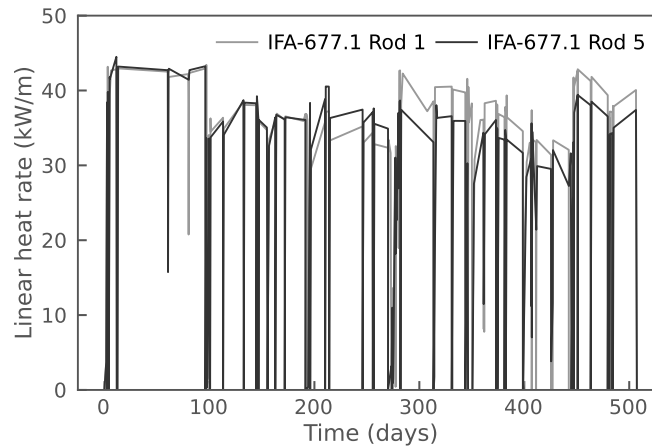


Fig. 21. Average LHR history used as input for the simulation of IFA-677.1 Rods 1 and 5. The Halden raw data were condensed using the Fuel Rod Analysis ToolBox (Lassmann et al., 2015).

The thermal boundary conditions at the cladding outer surface were determined using BISON's coolant channel model. The coolant inlet temperature history was determined from the Halden raw data and supplied to BISON as a time-dependent input. Coolant flow conditions were taken from Organisation for Economic Co-operation and Development (OECD) HRP (2005). The Jens-Lottes heat transfer correlation, which is recommended for Halden HBWR conditions, was applied.

#### 5) Results & Discussion

**Fuel centerline temperature.** The calculated fuel centerline temperature at the location of the upper fuel TC as a function of the irradiation time is shown for IFA-677.1 Rod 1 in Figure 22(a) and IFA-677.1 Rod 5 in Figure 23(a). The calculated temperature predictions are compared to the online measured data. An underprediction of the measured temperature of up to approximately 100 K is observed for the first three cycles of irradiation. Such a discrepancy corresponds to a relative error of  $\sim 7\%$ , which is within the uncertainties due to the measured power that was used as an input for performing the calculation. The BISON calculation matches the experimental data well for the fourth and fifth cycle of irradiation.

For the sixth cycle, an overprediction of  $\sim 100$  K is observed. The difference in the behavior between the early and late periods of the irradiation may be associated with gap closure which occurred around the beginning of the fourth cycle. Gap closure leads to solid contact between the fuel and cladding. Modeling heat transfer across this solid-solid interface gap involves complex physics and may require further refinement (Toptan et al., 2019, 2020). The calculated and measured fuel centerline temperatures at the lower TC location are shown in Figure 22(d). This additional comparison confirms the behavior observed for the temperature prediction at the upper TC location, with an under prediction of up to  $\sim 100$  K for the first three irradiation cycles, a very close prediction during the first and fourth cycles, and an over prediction during the last cycle.

The BISON-predicted results, using both MATPRO and LLS-informed creep models, are relatively similar to each other against the measured data. However, the discrepancy between the model predictions and measured data tends to become more pronounced at higher burnup rates. The temperature residuals between the numerical solutions using Equation 2 and the MATPRO model are plotted in Figure 24(a,d) for both IFA-677.1 Rods 1 and 5. For the temperature predictions at both lower and upper TC positions, the BISON-predicted temperatures using the LLS-informed creep model are about  $\sim 40$  K higher than those obtained using the MATPRO creep model through the EOL, and  $\sim 20$  K lower during early irradiation cycles.

*Plenum pressure.* The time evolution of plenum (or rod internal) pressure calculated by BISON is compared to the experimental data from the pressure transducer in IFA-677.1 Rod 1 in Figure 22(b) and Rod 5 in Figure 23(b). Prediction is accurate for the first three cycles of irradiation, although a moderate overprediction of the rod inner pressure is observed. Starting from the fourth cycle, BISON underpredicts the rod pressure. Discrepancies are partly attributed to the inaccuracies in the calculation of the plenum temperature. The use of LLS-informed creep model in BISON yields a difference of up to  $\sim 0.2$  MPa and  $\sim 0.1$  MPa (see Figure 24(b)) between the predictions and measured data for the IFA-677.1 Rod 1 and Rod 6, respectively.

*Fission gas release.* The calculated FGR as a function of the rod average burnup is shown in Figure 22(c) for IFA-677.1 Rod 1 and Figure 23(c) for IFA-677.1 Rod 5 along with the measured data, which are inferred from the inner rod pressure online measurement (Jošek, 2008). FGR is predicted accurately during the first  $\sim 17$  MWd/kgU. After that, FGR is underpredicted, with the calculated value at the EOL being 8% and the experimental value being 22%. The underprediction is consistent with the tendency to under predict the fuel temperature, as FGR is mainly temperature driven. However, a discrepancy of up to a factor of three can be considered acceptable, in view of the inherent modeling uncertainties for FGR (Pastore et al., 2015). The use of LLS-informed creep model in BISON yields a difference of up to  $\sim 2\%$  and  $\sim 1\%$  (see Figure 24(c)) in the FGR predictions for IFA-677.1 Rod 1 and Rod 6, respectively. This difference against the MATPRO model is in the positive direction for the measured data.

*Fuel stack elongation.* The fuel stack elongation predictions as a function of the irradiation time is shown for IFA-677.1 Rod 1 in Figure 22(e) and IFA-677.1 Rod 5 in Figure 23(e). The BISON-predicted fuel stack elongation results are compared to the measured data for each rod. An overprediction of the measured elongation of up to approximately 5 mm is observed through the EOL. The use of LLS-informed creep model yields 1 mm improvement in the fuel elongation predictions for IFA-677.1 Rod 1 as compared to the MATPRO model, while non-negligible difference is observed for IFA-677.1 Rod 5.

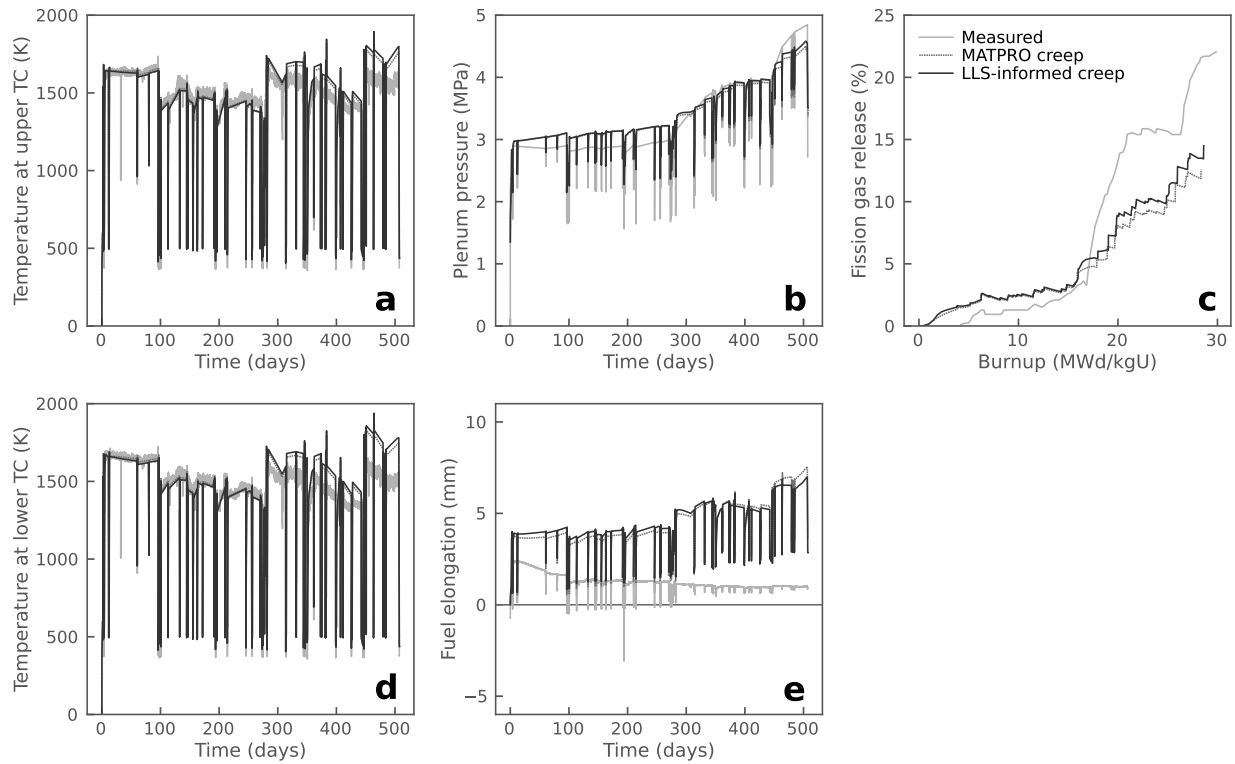


Fig. 22. Comparison of predicted and measured data for Halden IFA677.1 Rod 1: (a) temperature at lower TC location, (b) temperature at upper TC location, (c) fission gas release, (d) plenum pressure, and (e) fuel stack elongation. BISON predictions are obtained using the default MATPRO model and the LLS-informed model from LANL (Galvin et al., 2022).

### B. Halden IFA-716.1 Rods 1 and 6

The IFA-716.1 test (Tverberg, 2014; Baurens, 2016) was performed at the Halden Reactor Project with the aim to study the fuel performance of  $\text{Cr}_2\text{O}_3$ -doped  $\text{UO}_2$  and large grain  $\text{UO}_2$  with respect to FGR, swelling and densification. The very high temperature region was already covered by the high initial rating test IFA-677.1 (Jošek, 2008); therefore, IFA-716.1 was operated at lower power such that the fuel temperature is below the FGR threshold during the initial power cycles. The test rig contained six rods supplied by AREVA and ULBA. Two of the rods contained  $\text{UO}_2$  fuel doped with  $\text{Cr}_2\text{O}_3$ . All rods were instrumented with pressure transducers, fuel centerline TCs on the upper end and fuel stack elongation detectors, in addition to a cladding extensometer for one of the rods. The test assembly was loaded in the Halden reactor in January 2010 and completed six cycles of irradiation under HBWR conditions in May 2015, achieving a rig average burnup of  $\sim 31.8$  MWd/kgOX.

#### 1) Test Description

The IFA-716.1 rig contained a single cluster of six rods with an active fuel length of about 400 mm and initial enrichment of about 4.9%. IFA-716.1. Rod 1 contained doped  $\text{UO}_2$  fuel with 1580 ppm  $\text{Cr}_2\text{O}_3$ , and Rod 6 contained doped  $\text{UO}_2$  fuel with 1050 ppm  $\text{Cr}_2\text{O}_3$ . The doped fuel has larger grain size compared

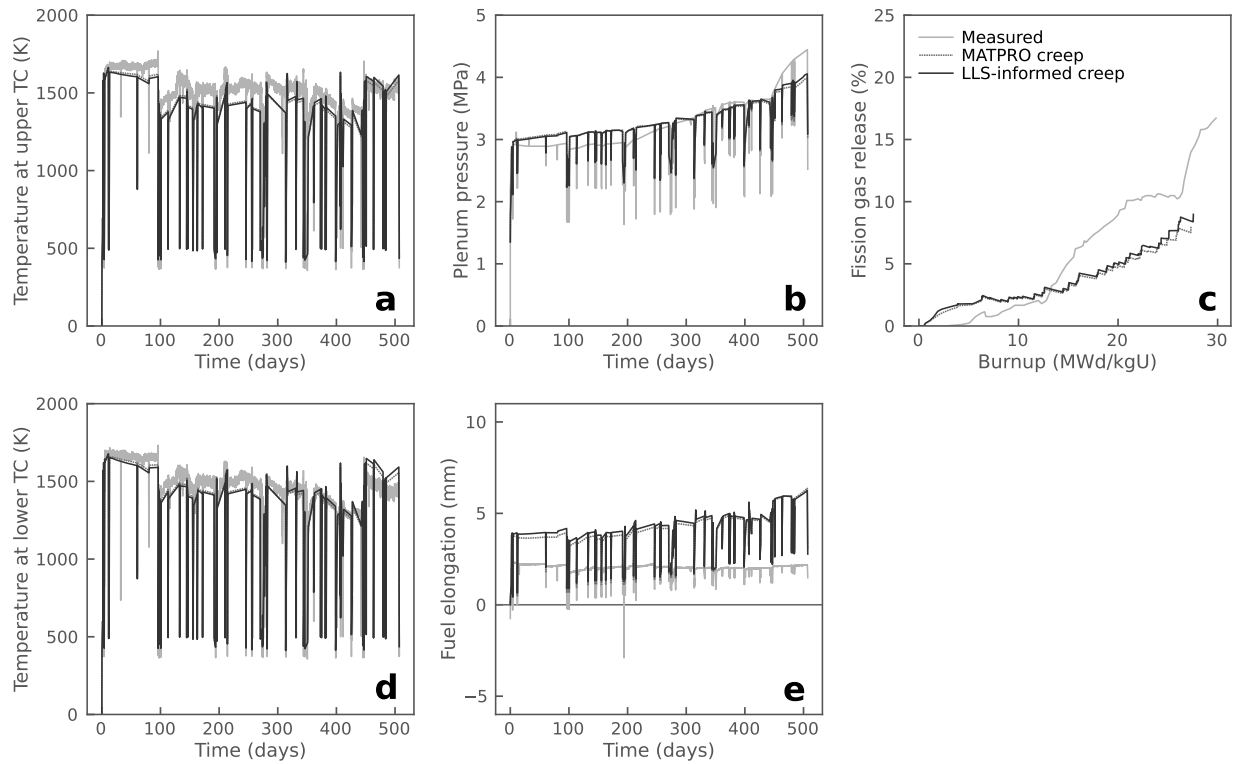


Fig. 23. Comparison of predicted and measured data for Halden IFA677.1 Rod 5: (a) temperature at lower TC location, (b) temperature at upper TC location, (c) fission gas release, (d) plenum pressure, and (e) fuel stack elongation. BISON predictions are obtained using the default MATPRO model and the LLS-informed model from LANL (Galvin et al., 2022).

to standard  $\text{UO}_2$  fuel. The main characteristics of Rods 1 and 6 are summarized in Table XVII.

### 2) Operating Conditions and Irradiation History

The test rig was operated under standard HBWR conditions, i.e., natural circulation at a coolant pressure of 34 bar and saturation temperature of  $\sim 235^\circ\text{C}$ , experiencing 842 full power days of accumulated operation. The final average assembly burnup is 31.8 MWd/kgOX (Baurens, 2016). The average LHR were kept below the FGR threshold during the first six irradiation cycles, and an assembly average burnup of 17 MWd/kgOX was reached by the end of this period. Later, the average LHR was elevated slowly to bring the fuel temperature above the FGR threshold to study the FGR performance. The power level was later kept close to the FGR threshold.

### 3) Material and Behavioral Models

The following material and behavioral models for  $\text{UO}_2$  fuel were used: (i) Halden model is chosen to compute temperature and burnup-dependent thermal properties via `UO2Thermal`; (ii) MATPRO model is chosen to compute fuel creep mechanical behavior via `UO2CreepUpdate`; (iii) a strain calculator via `ComputeIsotropicElasticityTensor`; (iv) relocation strains, relocation activation threshold power set to 5 kW/m via `UO2RelocationEigenstrain`; (v) thermal expansion with a constant via



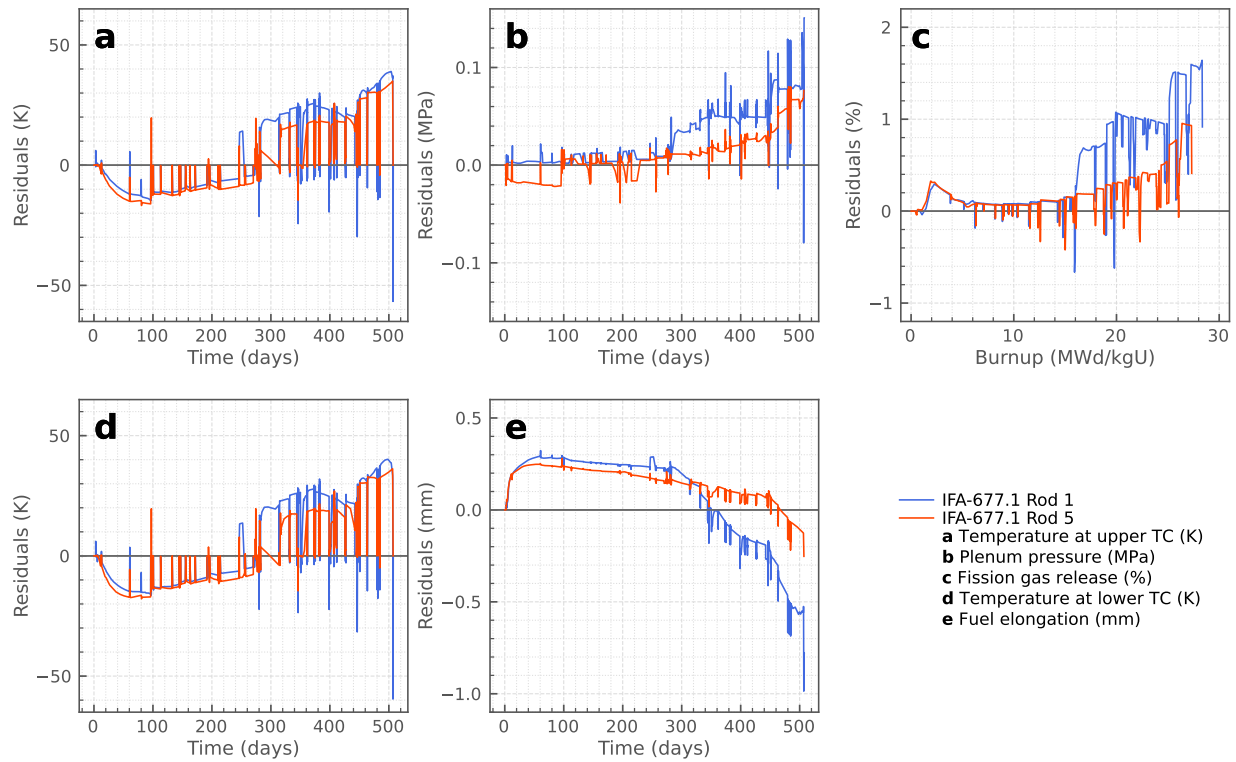


Fig. 24. Residuals for (a) temperature at the upper TC locations, (b) plenum pressure, (c) fission gas release, (d) temperature at the lower TC locations, and (e) fuel elongation are computed between the BISON predictions using LLS-informed creep model and MATPRO creep model, for the Halden IFA-677.1 Rods 1 and 5.

ComputeThermalExpansionEigenstrain; (vi) volumetric expansion due to solid and gaseous swelling via UO2VolumetricSwellingEigenstrain; and (vii) FGR model, Sifgrs with the gaseous swelling model (Pastore et al., 2015) via UO2VolumetricSwellingEigenstrain. In addition, the following settings were adopted that are specific to Cr<sub>2</sub>O<sub>3</sub>-doped UO<sub>2</sub> fuel analysis:

- Specific option for the lattice diffusion coefficient of fission gas atoms in the SIFGRS FGR and swelling model. The diffusion coefficient for Cr<sub>2</sub>O<sub>3</sub>-doped UO<sub>2</sub> is derived from the atomistic simulation developed at LANL (Cooper et al., 2021). This correction accounts for the increased diffusivity in Cr<sub>2</sub>O<sub>3</sub>-doped UO<sub>2</sub> relative to standard UO<sub>2</sub>. This is associated with a higher uranium vacancy concentration in doped fuel.
- Cr<sub>2</sub>O<sub>3</sub>-doped UO<sub>2</sub> is characterized by a larger grain size than standard UO<sub>2</sub>. In contrast to the enhanced diffusivity, the larger grain radius tends to reduce FGR due to the associated larger intra-granular diffusion distance for gas atoms to travel before reaching the grain boundaries. The reported average grain radius for IFA-716.1 is 35μm for Rod 1 and 29.5μm for Rod 6 (Tverberg, 2014; Baurens, 2016). Accordingly, this value has been set for the fission gas model, which in turn utilizes it in the fission gas atom diffusion calculation. The grain radius is used in the fuel creep model as well.

TABLE XVII. Fabrication characteristics of IFA-716.1 Rods 1 and 6

	Rod 1	Rod 6
Cladding material	Zry-4	Zry-4
Fuel material	doped UO <sub>2</sub>	doped UO <sub>2</sub>
Fill gas	He	He
Total active fuel stack length (mm)	399.5	399.3
Pellet inner diameter, <i>drilled sections</i> (mm)	1.8	1.8
Pellet outer diameter (mm)	9.12	9.12
Diametral gap (μm)	180	180
Cladding thickness (mm)	0.725	0.725
Cladding outer diameter (mm)	10.75	10.75
Free volume (cm <sup>3</sup> )	5.80	6.0
Fill gas pressure (MPa)	1.0	1.0
Fuel Cr <sub>2</sub> O <sub>3</sub> content (ppm)	1580	1050
Fuel U-235 enrichment (%)	4.90	4.89
Initial fuel density (kg/m <sup>3</sup> )	10500	10530
Fuel average grain radius (μm)	35.0	29.5

- A total densification in the MATPRO densification model of 0.15%. This is consistent with the experimental indications (Tverberg, 2014; Baurens, 2016) and with the lower densification expected in Cr<sub>2</sub>O<sub>3</sub>-doped UO<sub>2</sub> relative to standard UO<sub>2</sub>.

The following material and behavioral models were used for the Zircaloy-4 cladding: (i) isotropic thermal properties of Zircaloy are computed via `ZryThermal`; (ii) mechanical creep and elastic deformation behavior via `ZryCreepLimbackHoppeUpdate` and `ZryElasticityTensor`; (iii) MATPRO model for computation of the thermal expansion via `ZryThermalExpansionMATPROEigenstrain`; (iv) ESCORE model is chosen to compute the volumetric swelling due to irradiation exposure via `ZryIrradiationGrowthEigenstrain`; and (v) EPRI/KWU/C-E model for the waterside oxidation of the Zircaloy cladding via `ZryOxidation`.

#### 4) Boundary and Operating Conditions

Average LHR history for Rod 1 and Rod 6 are illustrated in Figure 25. The thermal boundary conditions at the cladding outer surface were determined using BISON's internal coolant channel model. The coolant inlet temperature history was determined from the Halden raw data and supplied to BISON as a time-dependent input. Coolant flow conditions were taken from OECD HRP (2005). The Jens-Lottes heat transfer correlation, which is recommended for Halden HBWR conditions, was applied.

#### 5) Results & Discussion

*Fuel centerline temperature.* The calculated fuel centerline temperature at the location of the upper fuel TC for IFA-716.1 Rod 1 and Rod 6 as a function of the irradiation time are respectively shown in Figures 26(a) and 27(a), and compared to the online measured data. An underprediction of the measured temperature of up to approximately 150 K is observed throughout the irradiation for both rods using the base case setup. Such discrepancy is attributed by Singh et al. (2022) to overestimation of fuel thermal expansion therefore underestimated gap thickness, as well as too small fuel densification. The use of either

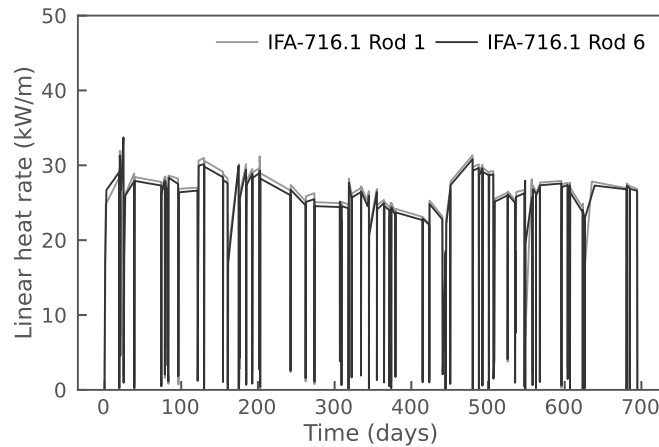


Fig. 25. Average LHR history used as input for the simulation of IFA-716.1 Rods 1 and 6. The Halden raw data were condensed using the Fuel Rod Analysis ToolBox (Lassmann et al., 2015).

LLS-informed or MATPRO creep models does not significantly enhance the temperature predictions for both rods.

*Fission gas release.* The calculated FGR as a function of the rod average burnup are shown in Figures 26(b) and 27(b) for Rod 1 and Rod 6 respectively along with the measured data (which are inferred from the inner rod pressure measurement). With both setups, BISON predicts an earlier FGR onset than the online measurement, and the estimated FGR is lower than the measured data. With the base case setup, FGR is underestimated by  $\sim 4\%$  primarily due to underestimated fuel temperature, as FGR is temperature-sensitive. With the corrected setup, discrepancy between the measured and predicted FGR becomes much smaller ( $\sim 1.5\%$ ), which is more acceptable considering the relatively large inherent uncertainty related with FGR predictions (Pastore et al., 2015). It is also worth pointing out that the measured FGR is derived from the change of rod internal pressure, while the pressure sensor was reported with failure after 625 full power days ( $\sim 26$  MWd/kgU) for Rod 1. Therefore, measured FGR after 625 full power days should not be used for the purpose of validation for Rod 1. Similarly, the use of either LLS-informed or MATPRO creep models does not significantly enhance the fission gas release predictions for both rods.

*Plenum pressure.* In Figures 26(c) and 27(c), the time evolution of rod internal pressure calculated by BISON are compared to the measured data from the pressure transducers in IFA-716.1 Rod 1 and Rod 6. With the base case setup, the rod internal pressure is underestimated by  $\sim 0.15$  MPa for the first three irradiation cycles. As previously pointed out, the pressure transducer in Rod 1 failed during the last cycle, causing the sharp increase of the measured data towards the EOL. Underestimation of the rod internal pressure in the last three cycles is most likely due to underestimated fuel elongation. Similarly, the use of either LLS-informed or MATPRO creep models do not significantly enhance the rod internal pressure predictions for both rods.

*Fuel stack elongation.* The calculated fuel stack elongation history is compared to the experimental data from the fuel elongation detector in IFA-716.1 Rod 1 in Figure 26(d) and IFA-716.1 Rod 6 in

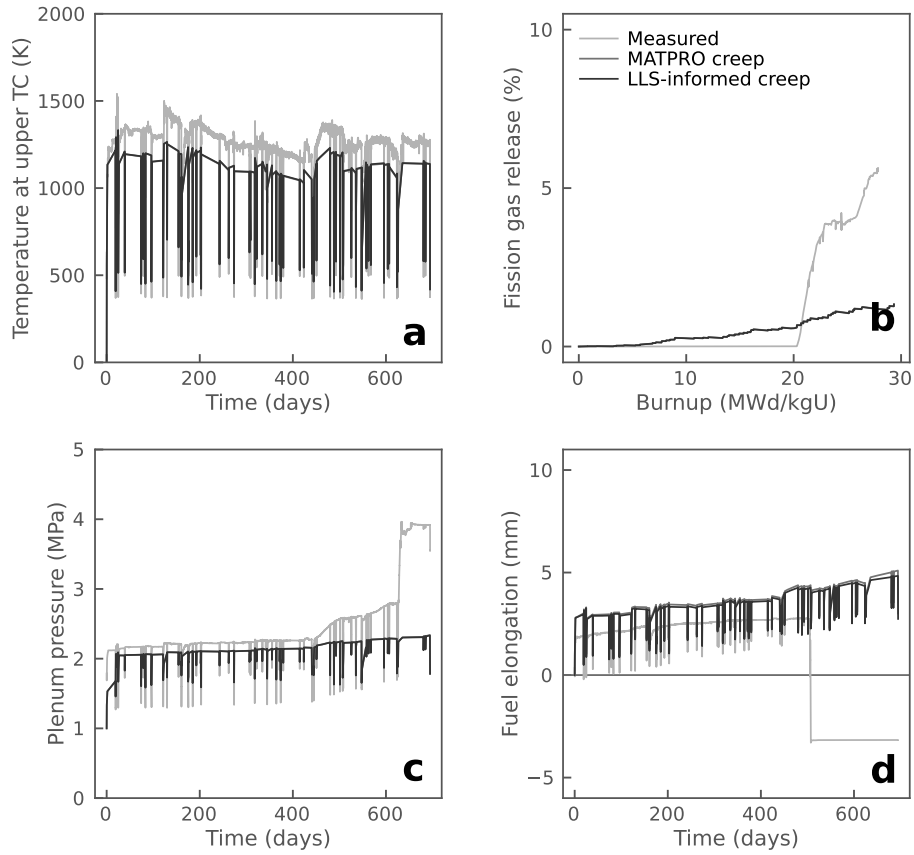


Fig. 26. Comparison of predicted and measured data for Halden IFA-716.1 Rod 1: (a) temperature at upper TC location, (b) fission gas release, (c) rod internal pressure, and (d) fuel stack elongation. BISON predictions are obtained using the default MATPRO model and the LLS-informed model from LANL (Galvin et al., 2022).

Figure 27(d). Malfunctioning of the elongation detector was reported for both Rod 1 and Rod 6 during the later cycles, causing the flat lines towards the EOL. With the base case setup, a systematic overprediction of the fuel elongation rate over time is observed in the BISON calculation. With the corrected setup, the simulated fuel elongation matches well with measured data for the initial cycles, but tends to be greater than measured data during later cycles. Similar to previous QoIs, the use of either LLS-informed or MATPRO creep models does not significantly enhance the fuel stack elongation predictions for both the rods. The difference in these predictions between both models is up to 0.25 mm.

## VI. CONCLUSION

In this study, our efforts mainly focused on enhancing BISON's modeling capabilities for accident tolerant fuel (ATF) fuels to provide an improved prediction of the fuel thermo-mechanical behavior. The new modeling capabilities (see Section II) that were made available in BISON are:

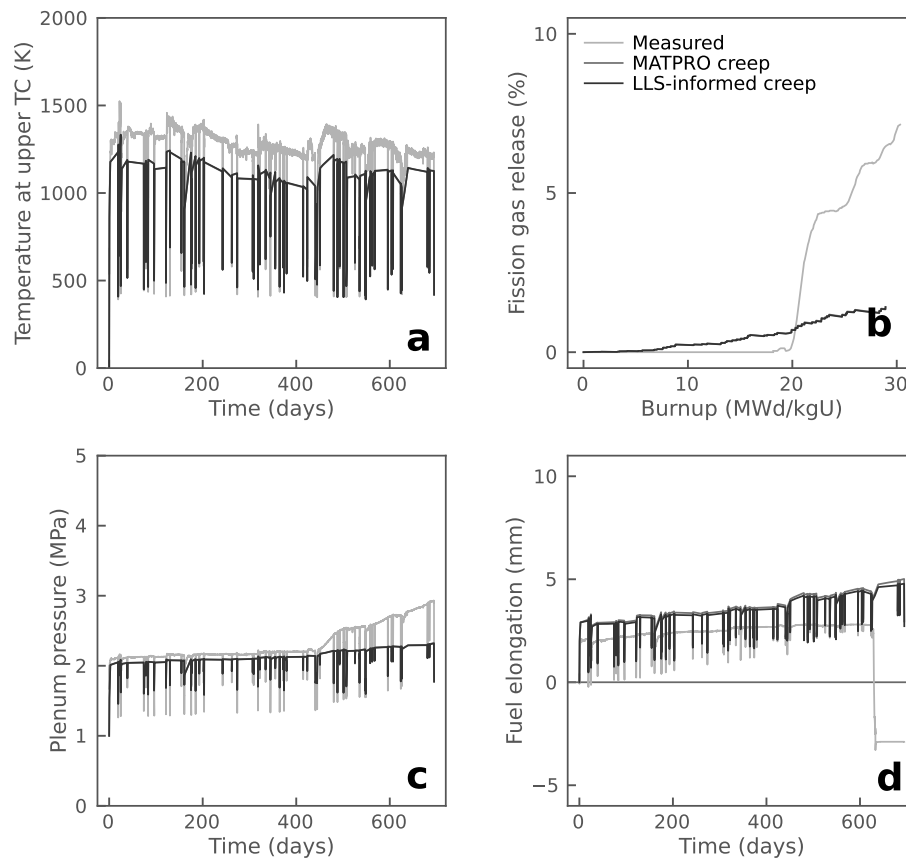


Fig. 27. Comparison of predicted and measured data for Halden IFA-716.1 Rod 6: (a) temperature at upper TC location, (b) fission gas release, (c) rod internal pressure, and (d) fuel stack elongation. BISON predictions are obtained using the default MATPRO model and the LLS-informed model from LANL (Galvin et al., 2022).

- A new tensile strength model for  $\text{UO}_2$  fuel was incorporated in the code, in which the tensile strength is a function of the microstructure effects such as grain size, fabrication pore size, and porosity. Prior to this study, a constant tensile strength value was considered in the numerical simulations.
- A new LLS-informed creep model for  $\text{UO}_2$  fuel was developed by Galvin et al. (2022) of LANL and assessed in this study. Prior to this study, the default MATPRO creep model (see Appendix A) was used, which does not take into the grain boundary thickness, but takes into account fuel density and O/M differently than the new model.

This study explored the physical interpretations of the implemented methods and fully exercised these capabilities in the sensitivity analysis and validation activities in this report. Here is a brief summary of the work performed in this study:

- These two new models were exercised in a 2D-RZ demonstration problem for both undoped and doped fuel rodlets. The code predictions from these tests were compared against the previous approaches (e.g., constant tensile strength, the default MATPRO creep model) to investigate the

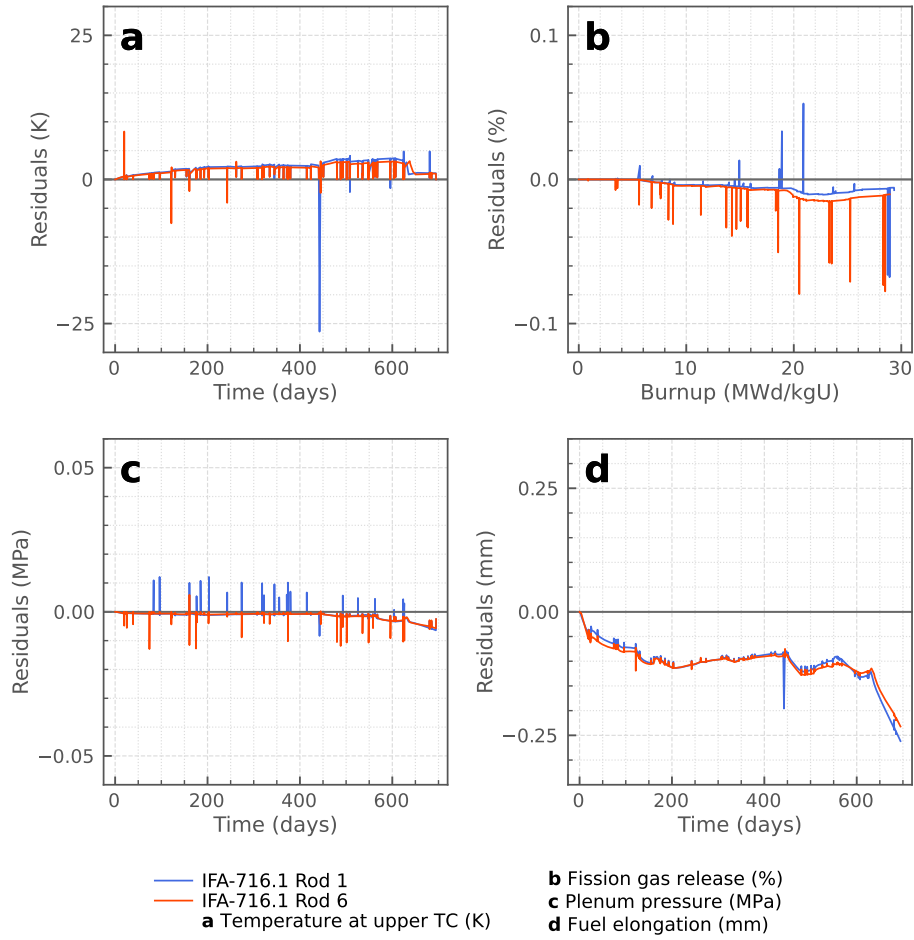


Fig. 28. The residuals for (a) temperature at the upper TC locations, (b) fission gas release, (c) plenum pressure, and (d) fuel elongation are computed between the BISON predictions using LLS-informed creep model (Equation 2) and MATPRO creep model, for the Halden IFA-716.1 Rods 1 and 6.

impact of these models on the thermo-mechanical behavioral changes.

- *Impact of tensile strength on the predictions* was evaluated in Section III-A by comparing the code predictions using the new tensile strength model and AFC-measured tensile strength values (83.2 MPa for the undoped fuel; 103.1 MPa for the doped fuel) from Gamble and Cooper (2021). For the undoped fuel, the code-predicted tensile strength varies between 90 and 120 MPa via the implemented model, which is slightly larger at the BOL than 83.2 MPa and approaches to the AFC-measured value towards the EOL. For the doped fuel, the code-predicted tensile strength varies between 60 and 80 MPa via the implemented model, which is significantly lower than 103.1 MPa and degrades to 60 MPa at the EOL. The crack damage behavior differentiated based on the computed tensile strengths. Note that the crack damage is inversely proportional to the

tensile strength.

- *Impact of creep modeling on the predictions* was evaluated in Section III-B by comparing the code predictions using the new LLS-informed and the default MATPRO creep models. For the undoped fuel, local crack damage behavior differentiated significantly in each direction depending on the rod average burnup: (i) less cracking at low burnup rates and more cracking with the new model through the EOL in the axial direction; (ii) insignificant differences in the crack damage in the hoop direction except towards the top fuel rod where the use of new model yields a larger damage; and (iii) less cracking at the top and bottom of fuel rod locations while more cracking through the center of fuel rod with the use of new model in the radial direction. For the doped fuel, the crack damage differentiated more in the axial direction and negligibly small differences in both hoop and radial directions, using the new creep modeling option.
- Sensitivity analyses were performed at a component level in which we investigated the effects of model input parameters on its output and at a system level in which we investigated the effects of various uncertainties in input parameters on the integral responses. For the former, we employed analyses for the tensile strength and LLS-informed creep models. For the latter, we employed analyses for a 2D-RZ application. To perform these studies, we used STM, Dakota, and SALib software packages and applied the following sensitivity measures; Pearson correlation coefficients, Morris sensitivity measures, Sobol' indices, and delta moment-independent sensitivity indicator.
  - *For the tensile strength model*, three parameters ( $p$ ,  $P$ , and  $G$ ) of the model were perturbed according to the uncertainties obtained from Oguma (1982). From the Pearson analysis, all three parameters were found inversely proportional to the tensile strength and fabrication pore size  $P$  was found the most influential. Similarly,  $P$  was found the most influential parameter on the tensile strength from the Sobol' analysis,
  - *For the LLS-informed creep model*, five fitting parameters ( $A_1$ ,  $A_2$ ,  $A_3$ ,  $B_1$ , and  $B_2$ ) of the model were perturbed according to the uncertainties provided by LANL. From the Pearson analysis,  $B$  terms were found to be the most influential parameters and inversely proportional with the creep rate while  $A$  terms were found to be directly proportional. Similarly, Sobol' analysis supported this finding in which  $B$  terms were found to be influential and  $A$  terms were found to have negligible effects on the creep rate. These analyses were performed at a fixed irradiation temperature and fission rate. Later, temperatures and fission rates were also varied and Sobol' analyses were repeated for the creep model:  $B_1$  became the most influential parameter as temperatures were varied at a fixed fission rate, and  $B_2$  became the most influential parameter as fission rates were varied at a fixed temperature.
  - *For the 2D-RZ application*, we performed analyses for both undoped and doped fuel rodlets under normal operating conditions using the Pearson correlation coefficients and delta moment-independent sensitivity indicator as sensitivity measures. The results were provided for various rod average burnups. Here, we only provided the SA results for the crack damage, see Section IV-C3 for SA results on other QoIs.

From the Pearson analysis: (i)  $B_2$  and grain radius had a moderate positive relation and pore size had a weak-to-moderate positive relation with the crack damage in axial and radial directions, for both fuel types; (ii) Youngs modulus and pore size exhibited positive relation (weak relation at BOL, moderate-to-strong relation around 30 MWd/kgU, and weak relation through the EOL)

with the crack damage in hoop direction, for both fuel types.

From the delta moment-independent analysis: (i) grain radius was the most influential parameter for the crack damage in axial direction and followed by  $B_2$  and pore size, for both fuel rodlets; (ii) grain radius was the most influential parameter except 20-30 MWd/kgU where the pore size became the most influential on the crack damage in hoop direction, for both fuel rodlets; (iii) grain radius and  $B_2$  were the most influential parameters on the crack damage in radial direction for the undoped fuel rodlets while the grain radius was the most influential parameter for the doped fuel rodlets.

For both undoped and doped fuel rodlets, we obtained relatively similar results between selected QoIs and input parameters, which might be mainly due to utilization of similar models for both fuel type conditions in the simulations.

- As a combination of efforts in this project and another NEAMS project by Singh et al. (2022), Halden IFA-677.1 (Rods 1 and 5) and IFA-716.1 (Rods 1 and 6) were added to the BISON assessment suite. These IFA rods are made of doped  $\text{UO}_2$  fuels. Integral responses such as fuel centerline temperature, fission gas release, rod internal pressure, and fuel stack elongation were evaluated in the assessment of BISON predictions against the measured data. With the new atomistic creep model, a  $\pm 50$  K difference on the temperature, up to 0.15 MPa difference on the plenum pressure, up to 2% difference on the FGR, and up to 1 mm difference on the fuel elongation predictions were observed for Halden IFA-677.1 Rods 1 and 5. Meanwhile, negligible differences on the code predictions were observed for Halden IFA-716.1 Rods 1 and 6. Note that the selected Halden cases were exposed up to 30 MWd/kgU, the future work should focus on assessing the model at burnups greater than 30 MWd/kgU.

The work presented here expands BISON's ATF modeling capabilities for doped  $\text{UO}_2$  fuels and its validation test suite.



## REFERENCES

- B. M. Adams, W. J. Bohnhoff, K. R. Dalbey, M. S. Ebeida, J. P. Eddy, M. S. Eldred, G. Geraci, R. W. Hooper, P. D. Hough, K. T. Hu, J. D. Jakeman, M. Khalil, K. A. Maupin, J. A. Monschke, E. M. Ridgway, A. A. Rushdi, J. A. Stephens, L. P. Swiler, D. M. Vigil, T. M. Wildey, and J. G. Winokur. Dakota, a multilevel parallel object-oriented framework for design optimization, parameter estimation, uncertainty quantification, and sensitivity analysis: Version 6.11 user's manual. Sandia Report SAND2014-4633, SNL, July 2014. updated November 2019.
- C. M. Allison, G. A. Berna, R. Chambers, E. W. Coryell, K. L. Davis, D. L. Hagrman, D. T. Hagrman, N. L. Hampton, J. K. Hohorst, R. E. Mason, M. L. McComas, K. A. McNeil, R. L. Miller, C. S. Olsen, G. A. Reymann, and L. J. Siefken. SCDAP/RELAP5/MOD3.1 Code Manual, Volume IV: MATPRO-A library of materials properties for light-water-reactor accident analysis. Tech. Rep. NUREG/CR-6150, EGG-2720, Idaho National Engineering Laboratory (INEL), 1993.
- T. Barani, D. Pizzocri, G. Pastore, L. Luzzi, and J. D. Hales. Isotropic softening model for fuel cracking in BISON. *Nucl. Eng. Des.*, 342:257–263, 2019. doi:10.1016/j.nucengdes.2018.12.005.
- B. Baurens. In-pile results from the fission gas release mechanisms study in IFA-716 after final unloading. Tech. Rep. HWR-1161, OECD Halden Reactor Project, April 2016.
- E. Borgonovo. A new uncertainty importance measure. *Reliab. Eng. Syst.*, 92(6):771–784, 2007. doi:10.1016/j.res.2006.04.015.
- G. E. P. Box and M. E. Muller. A note on the generation of random normal deviates. *Ann. Math. Stat.*, 29(2):610–611, 1958. doi:10.1214/aoms/1177706645.
- D. Brucklacher and W. Dienst. Creep behavior of ceramic nuclear fuels under neutron irradiation. *J. Nucl. Mater.*, 42(3):285–296, 1972. doi:10.1016/0022-3115(72)90079-7.
- D. Brucklacher, W. Dienst, and F. Thummler. Creep behavior of oxide fuels under neutron irradiation, Paper 251. In *Proceedings REAKTORTAGUNG 1973 des Deutschen Atomforums/KTG held in Karlsruhe*, pages 413–416, Apr 10-13 1973.
- F. Campolongo, J. Cariboni, and A. Saltelli. An effective screening design for sensitivity analysis of large models. *Environ. Model. Softw.*, 22(10):1509–1518, 2007. doi:10.1016/j.envsoft.2006.10.004.
- M. W. D. Cooper, C. R. Stanek, and D. A. Andersson. The role of dopant charge state on defect chemistry and grain growth of doped  $\text{UO}_2$ . *Acta Mater.*, 150:403–413, 2018. doi:10.1016/j.actamat.2018.02.020.
- M. W. D. Cooper, G. Pastore, C. Matthews Y. Che, A. Forslund, C. R. Stanek, T. Tverberg K. Shirvan, K. A. Gamble, B. Mays, and D. A. Andersson. Fission gas diffusion and release for  $\text{Cr}_2\text{O}_3$ -doped  $\text{UO}_2$ : From the atomic to the engineering scale. *J. Nucl. Mater.*, 545:152590, 2021. doi:10.1016/j.jnucmat.2020.152590.
- W. Dienst. Irradiation induced creep of ceramic materials. *J. Nucl. Mater.*, 65:1–8, 1977. doi:10.1016/0022-3115(77)90035-6.
- C. O. T. Galvin, A. Chakraborty, D. A. Andersson, L. Capolungo, and M. W. D. Cooper. Development of a creep model informed by lower-length scale simulations to simulate creep in doped  $\text{UO}_2$ . Tech. Rep. LANL-22/, Materials Science and Technology Division, LANL, Los Alamos, NM United States, 7 2022.
- K. Gamble and A. Toptan. FY21 BISON BWR fuel modeling capability: Sensitivity analysis during normal operation. Tech. Rep. INL/LTD-21-62647, INL, Idaho Falls, ID United States, 4 2021.
- K. A. Gamble and M. W. D. Cooper. Multiscale modeling of  $\text{Cr}_2\text{O}_3$ -doped  $\text{UO}_2$  creep and fracture.

- Tech. Rep. INL/EXT-21-64733, INL, Idaho Falls, ID United States, 9 2021.
- K. A. Gamble, T. W. Knight, E. Roberts, J. D. Hales, and B. W. Spencer. Mechanistic verification of empirical  $\text{UO}_2$  fuel fracture models. *J. Nucl. Mater.*, 556:153163, 2021. doi:10.1016/j.jnucmat.2021.153163.
- D. L. Hagrman and G. A. Reymann. MATPRO-Version 11: A handbook of materials properties for use in the analysis of light water reactor fuel rod behavior. Tech. rep., INEL, 2 1979.
- J. Herman and W. Usher. SALib: An open-source Python library for sensitivity analysis. *J. Open Source Softw.*, 2(9), 2017. doi:10.21105/joss.00097.
- H. K. Jenssen. PIE report on six  $\text{UO}_2$  fuel rods irradiated in IFA-677 high initial rating test. Tech. Rep. HWR-968, OECD Halden Reactor Project, March 2010.
- R. Jošek. The high initial rating test IFA-677: Final report on in-pile results. Tech. Rep. HWR-872, OECD Halden Reactor Project, April 2008.
- K. Lassmann, A. Schubert, J. van de Laar, and P. Van Uffelen. The 'Fuel Rod Analysis ToolBox': A general program for preparing the input of a fuel rod performance code. *Ann. Nucl. Energy*, 81: 332–335, 2015. doi:10.1016/j.anucene.2015.03.012.
- A. T. Mai, W. F. Lyon, R. O. Montgomery, and R. S. Dunham. An evaluation of the MATPRO fuel creep model using the FALCON fuel analysis code. *Trans. Am. Nucl. Soc.*, 102:888–889, 2010.
- OECD HRP. Data Sheet / IFA-677.1. Tech. Rep. QA-F-702, OECD Halden Reactor Project, 2005.
- M. Oguma. Microstructure effects on fracture strength of  $\text{UO}_2$  fuel pellets. *J. Nucl. Sci. Technol.*, 19 (12):1005–1014, 1982. doi:10.1080/18811248.1982.9734249.
- G. Pastore and A. Toptan. Fresh fuel properties: Ceramic compounds. In Ehud Greenspan, editor, *Encyclopedia of Nuclear Energy*, pages 343–355. Elsevier, Oxford, 2021. doi:10.1016/B978-0-12-819725-7.00099-4.
- G. Pastore, L. P. Swiler, J. D. Hales, S. R. Novascone, D. M. Perez, B. W. Spencer, L. Luzzi, P. Van Uffelen, and R.L. Williamson. Uncertainty and sensitivity analysis of fission gas behavior in engineering-scale fuel modeling. *J. Nucl. Mater.*, 456:398–408, 2015. doi:10.1016/j.jnucmat.2014.09.077.
- C. J. Permann, D. R. Gaston, D. Andrs, R. W. Carlsen, F. Kong, A. D. Lindsay, J. M. Miller, J. W. Peterson, A. E. Slaughter, R. H. Stogner, and R. C. Martineau. MOOSE: Enabling massively parallel multiphysics simulation. *SoftwareX*, 11:100430, 2020. doi:10.1016/j.softx.2020.100430.
- J. S. Perrin. Effect of irradiation on creep of  $\text{UO}_2\text{-PuO}_2$ . *J. Nucl. Mater.*, 42(1):101–104, 1 1972. doi:10.1016/0022-3115(72)90013-X.
- E. Plischke, E. Borgonovo, and C. L. Smith. Global sensitivity measures from given data. *European Journal of Operational Research*, 226(3):536–550, 2013. doi:10.1016/j.ejor.2012.11.047.
- K. Sakai. The fuel creep test IFA-701: Results after four irradiation cycles. Tech. Rep. HWR-1039, OECD Halden Reactor Project, 2013.
- K. Sakai, H. Hanakawa, and T. Tverberg. Investigation of fission induced creep of  $\text{UO}_2$  and Cr-doped fuel in IFA-701. Tech. Rep. HWR-1006, OECD Halden Reactor Project, 2011.
- A. Saltelli. Making best use of model evaluations to compute sensitivity indices. *Computer Physics Communications*, 145(2):280–297, 2002. doi:10.1016/S0010-4655(02)00280-1.
- G. Singh et al. Implementation of assessment cases on accident tolerant fuel in BISON. Tech. rep., INL, Idaho Falls, ID United States, 9 2022.
- A. A. Solomon. Radiation induced creep of  $\text{UO}_2$ . *J. Am. Ceram. Soc.*, 56(3):164–171, 1973. doi:10.1111/j.1151-2916.1973.tb15435.x.
- B. W. Spencer, H. Huang, J. D. Hales, and J. Dolbow. Discrete modeling of early-life thermal fracture

- in ceramic nuclear fuel. In *Proceedings of Water Reactor Fuel Performance Meeting/Top Fuel/LWR Fuel Performance Meeting (WRFPM 2014)*, Sendai (Japan), 9 2014. URL <https://www.osti.gov/biblio/1177218>.
- R. Szoke and T. Tverberg. Update on in-pile results from the fuel creep test IFA-701. Tech. Rep. HWR-1092, OECD Halden Reactor Project, 2014.
- A. Toptan, D. J. Kropaczek, and M. N. Avramova. Gap conductance modeling i: Theoretical considerations for single- and multi-component gases in curvilinear coordinates. *Nucl. Eng. Des.*, 353:110283, 2019. doi:10.1016/j.nucengdes.2019.110283.
- A. Toptan, J. D. Hales, R. L. Williamson, S. R. Novascone, G. Pastore, and D. J. Kropaczek. Modeling of gap conductance for LWR fuel rods applied in the BISON code. *Journal of Nuclear Science and Technology*, 57(8):963–974, 2020. doi:10.1080/00223131.2020.1740808.
- T. Tverberg. Update on the in-pile results from the fission gas release mechanisms study in IFA-716. Technical Report HWR-1090, OECD Halden Reactor Project, September 2014.
- W. Weisenak. Modifications to IFA-677 data conversion. Tech. Rep. HWR-1263, OECD Halden Reactor Project, 2019.
- R. L. Williamson, J. D. Hales, S. R. Novascone, G. Pastore, K. A. Gamble, B. W. Spencer, W. Jiang, S. A. Pitts, A. Casagrande, D. Schwen, A.X. Zabriskie, A. Toptan, R. Gardner, C. Matthews, W. Liu, and H. Chen. BISON: A flexible code for advanced simulation of the performance of multiple nuclear fuel forms. *Nucl. Technol.*, 207(7):954–980, 2021. doi:10.1080/00295450.2020.1836940.

## APPENDIX A MATPRO CREEP MODEL

A model for combined secondary thermal creep and irradiation creep of UO<sub>2</sub> fuel is available, with the creep rate modeled as a function of time, temperature, effective stress, density, grain size, fission rate, and O/M. The constitutive relation is taken from the MATPRO FCREEP material model (Allison et al., 1993; Pastore and Toptan, 2021) and given as:

$$\dot{\epsilon} = \frac{A_1 + A_2 \dot{F}}{(A_3 + D)G^2} \sigma \exp\left(\frac{-Q_1}{RT}\right) + \frac{A_4}{(A_6 + D)} \sigma^{4.5} \exp\left(\frac{-Q_2}{RT}\right) + A_7 \dot{F} \sigma \exp\left(\frac{-Q_3}{RT}\right) \quad (\text{A.1})$$

where  $\dot{\epsilon}$  is the creep rate (s<sup>-1</sup>),  $\sigma$  is the effective (Mises) stress (Pa),  $T$  is the temperature (K),  $D$  is the fuel density (percent of theoretical),  $G$  is the grain size ( $\mu\text{m}$ ),  $\dot{F}$  is the volumetric fission rate (fissions/m<sup>3</sup>-s),  $Q_i$  are the activation energies (J/mol), and  $R$  is the universal gas constant (8.3145 J/mol-K).

The first term in Equation A.1 represents diffusional thermal creep and is applicable to low stress and low temperature conditions. The second term in Equation A.1 represents thermal dislocation or power-law creep and is applicable to high stress and high temperature conditions. Note that irradiation creep is included in both the first and third terms, as both are functions of the fission rate ( $\dot{F}$ ). Irradiation enhances normal diffusional thermal creep (at elevated temperatures) as indicated in the first term. Irradiation creep also occurs at lower temperatures where thermal creep is not active, and is accounted for by the third term in Equation A.1. Material constants for the thermal creep terms are listed in Table A.1. The activation energies for the thermal creep terms ( $Q_1$  and  $Q_2$ ) are strongly dependent upon the fuel O/M  $x$  and, in MATPRO, are defined using the Arrhenius type relations as tabulated in Table A.1.

TABLE A.1. Parameters used in the UO<sub>2</sub> thermal creep model

$Q_1$ (J/mol)			$Q_2$ (J/mol)			$f(x)$	
$74,829f(x) + 301,762$			$83,143f(x) + 469,191$			$\frac{1}{\exp\left(\frac{-20}{\log(x-2)} - 8\right) + 1}$	
$A_1$	$A_2$	$A_3$	$A_4$	$A_6$	$A_7$	$Q_3$	Description
0.3919	$1.3100 \times 10^{-19}$	-87.7	$2.0391 \times 10^{-25}$	-90.5	$\frac{7.78 \times 10^{-37}}{3.7226 \times 10^{-35}}$	0 2617*R	MATPRO-Halden model Original MATPRO model

**Transitional stress** In MATPRO, a transition stress is defined to govern the transition between the first (low stress) and second (high stress) regions. When the applied stress is larger than the transition stress, the applied stress is used in the power-law relation and the transition stress is used in the linear creep relation. When the applied stress is lower than the transition stress, the applied stress is used in the linear relation and the power-law contribution is zero. Mai et al. (2010) investigated the MATPRO transition approach in comparison to experimental data and concluded that a better fit to the data could be achieved by simply ignoring the transition stress and applying both the low and high stress terms in all cases. This approach has been adopted in BISON.

**MATPRO-Halden model** The low temperature irradiation creep (third term in Equation A.1) requires further discussion. As the equation indicates, the original MATPRO formulation included exponential temperature dependence in this term. After a careful review of the MATPRO documentation and supporting literature, it is clear that this temperature dependency was based on a single experimental study (Brucklacher et al., 1973) involving a very limited number of experiments. Additionally, this early study

specified a relatively narrow applicability range for the correlation ( $523 < T(K) < 773$ ), which was not enforced in the MATPRO implementation. Several other studies, both early (Brucklacher and Dienst, 1972; Perrin, 1972; Solomon, 1973; Dienst, 1977) and more recent (Sakai et al., 2011; Sakai, 2013; Szoke and Tverberg, 2014), did not observe temperature dependency for low temperature irradiation creep, but reported creep rate variation as a function of only stress and fission rate. The most extensive data for irradiation creep of  $\text{UO}_2$  has been generated at the Halden Research Reactor, resulting in the following correlation (Sakai, 2013):  $\dot{\epsilon}_{\text{irr}} = A_7 \dot{F} \sigma$  with  $A_7 = 7.78 \times 10^{-37}$  (equivalent to  $Q_3 = 0$  in Equation A.1 with a modified  $A_7$  value).

The default model in BISON, which is referred to as the MATPRO-Halden model, replaces the third term in Equation A.1, thus removing temperature dependency. Note that the temperature dependent formulation can still be specified simply by providing the original MATPRO material constants (given in Table A.1) as input parameters to the code.